



GRADO EN INGENIERÍA EN TECNOLOGÍAS INDUSTRIALES

TRABAJO FIN DE GRADO

IMPLEMENTATION OF A CONTROLLER HARDWARE-IN-THE-LOOP TESTBED FOR DISTRIBUTED COORDINATION AND CONTROL ARCHITECTURES

Autor: Alejandro Mayoral Iglesias

Director: Alejandro Domínguez García

Declaro, bajo mi responsabilidad, que el Proyecto presentado con el título
Implementation of a controller hardware-in-the-loop testbed for distributed coordination
and control architectures

en la ETS de Ingeniería - ICAI de la Universidad Pontificia Comillas en el
curso académico 2019/20 es de mi autoría, original e inédito y

no ha sido presentado con anterioridad a otros efectos.

El Proyecto no es plagio de otro, ni total ni parcialmente y la información que ha sido
tomada de otros documentos está debidamente referenciada.

Fdo.: Alejandro Mayoral Iglesias

Fecha: 19/ 05/ 2020



Autorizada la entrega del proyecto

EL DIRECTOR DEL PROYECTO



Fdo.: Alejandro D. Dominguez-Garcia

Fecha: 04/ 06/ 2020



GRADO EN INGENIERÍA EN TECNOLOGÍAS INDUSTRIALES

TRABAJO FIN DE GRADO

IMPLEMENTATION OF A CONTROLLER HARDWARE-IN-THE-LOOP TESTBED FOR DISTRIBUTED COORDINATION AND CONTROL ARCHITECTURES

Autor: Alejandro Mayoral Iglesias

Director: Alejandro Domínguez García

ACKNOWLEDGMENTS

I wish to express my deepest gratitude to Olaoluwapo Ajala, and Prof. A. Dominguez-Garcia. Without whom this thesis would not be possible. For all the support and help they both gave me at all times, and the infinite patience that they had with me.

Also, the rest of the team involved in the project: D.Begara, P.Samper, N. Siddartha...

Finally, I would like to express my gratitude with the University of Illinois at Urbana-Champaign, for treating their exchange students the way they do, and for the incredible year we spent there.

I felt part of the Illini family from the beginning, and I will definitely always feel part of it.

Once an Illini, always an Illini...

IMPLEMENTATION OF A CONTROLLER HARDWARE-IN-THE-LOOP TESTBED FOR DISTRIBUTED COORDINATION AND CONTROL ARCHITECTURES

Autor: Mayoral Iglesias, Alejandro.

Supervisor: Dominguez-Garcia, Alejandro

Entidad Colaboradora: University of Illinois at Urbana-Champaign

RESUMEN DEL PROYECTO

La Universidad de Illinois está desarrollando un software para el control distribuido de 'microgrids'. Esta tesis se centrará en el desarrollo de un banco de pruebas para 'microgrids'. En proyectos futuros el control distribuido que está siendo desarrollado por la universidad, será probado en este banco de pruebas.

Uno de los mayores problemas de las 'microgrids' hoy en día, es el elevado coste de desarrollo que requieren. Esto es debido principalmente a dos cosas. En primer lugar, no hay suficientes modelos normalizados por lo que cada 'microgrid' debe ser desarrollada de cero. En segundo lugar, la única opción para probar una 'microgrid' en tiempo real y con una fidelidad elevada es utilizar infraestructura eléctrica real. Este banco de pruebas pretende ser adaptable a múltiples topologías de 'microgrids'. En esta tesis se implementarán los modelos de inversor P-Q, inversor V-F y Microturbina en Typhoon HIL

Palabras Clave: Microgrid, Banshee, Simulaciones HIL

1. Introducción

En los últimos años, se está produciendo un crecimiento exponencial de las Fuentes de energía distribuida (FED). Estas fuentes, son demasiado pequeñas para ser controladas por la red. Sin embargo, si se conectan muchas FED con el apropiado sistema de control, pueden ser controladas por la red, e incluso ofrecer servicios de regulación. Esta agrupación de FED mencionada anteriormente es lo que conocemos como 'microgrid'. El importante crecimiento en las FED implica por tanto un importante crecimiento de las 'microgrids'

Uno de los principales problemas de las 'microgrids' es como ya se ha comentado en el resumen del proyecto, el elevado coste de desarrollo. Mediante el uso de este banco de pruebas se podría abaratar el coste de desarrollo y también se evitaría el riesgo de dañar equipamiento eléctrico costoso. El principal objetivo de esta tesis es presentar un banco de pruebas que ofrezca tanto una simulación en tiempo real como una excelente fidelidad de los modelos. La tecnología utilizada para conseguir estos dos objetivos es la simulación "Hardware-in-the-loop" (HIL).

2. Definición del Proyecto

Este proyecto es parte de otro más grande en la Universidad de Illinois. La universidad está desarrollando un software para el control distribuido de microgrids. El banco de pruebas presentado en esta tesis será usado para evaluar el rendimiento de dicho control. Sin embargo, este no es el único objetivo de este banco de pruebas, el objetivo también

es crear un banco capaz de adaptarse fácilmente a todas las topologías de ‘microgrids’ de manera que pueda ser utilizado para el desarrollo de múltiples ‘microgrids’.

En esta tesis se presentará el banco de pruebas y se implementaran los modelos individuales necesarios para su creación. Se implementarán en Typhoon HIL los modelos de inversor P-Q, inversor V-F y Microturbina.

3. Descripción del Modelo

Tal y como se ha mencionado antes, en esta tesis se implementarán los modelos individuales de las FED necesarias para la creación de la red de distribución Banshee. Una vez implementada la red Banshee, deberían implementarse mas modelos para hacer el banco de pruebas mas fácilmente adaptable

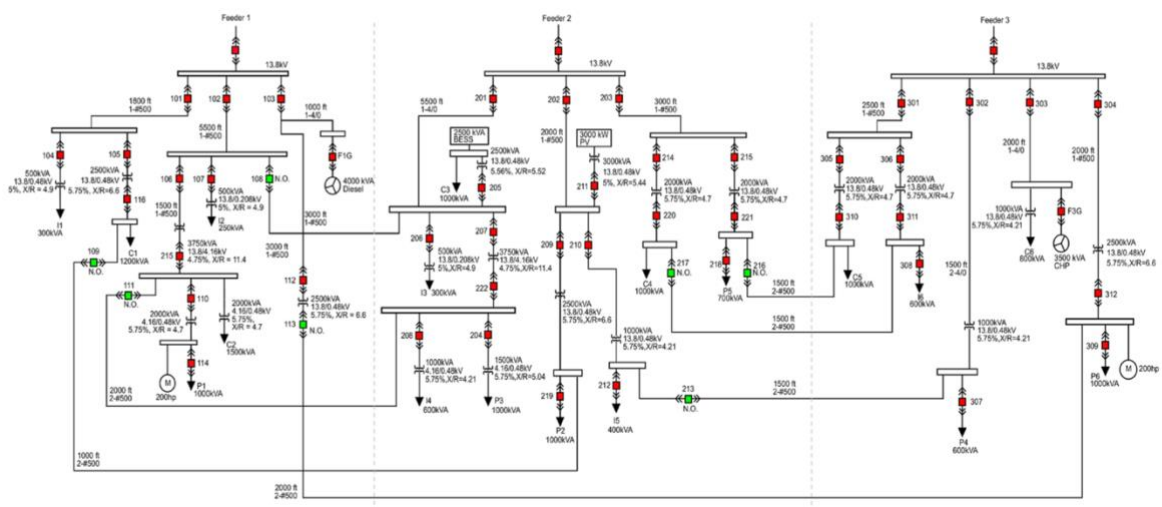


Figura 1 – Esquema de la Red de distribución Banshee [3]

4. Resultados

En este apartado se presentarán los resultados del inversor P-Q para dar al lector una idea general del formato de los resultados presentados en esta tesis. Los resultados de otros modelos tienen el mismo formato que este.

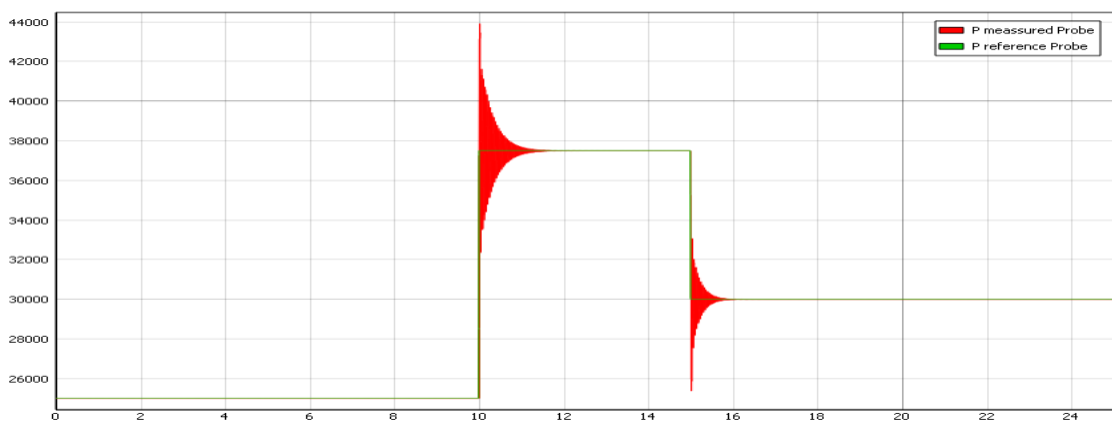


Figura 2– Power Output-Reference Power Grid-Feeding inverter HOM

5. Conclusión y Sigüientes Pasos

Durante el desarrollo de este proyecto han ido apareciendo numerosos problemas relacionados con Typhoon HIL. Los modelos previamente implementados en Simulink no funcionaban al ser implementados en Typhoon HIL. Uno de los principales problemas fue que Typhoon HIL tiene limitaciones resolviendo algunos tipos de sistemas no lineares como por ejemplo las cargas de potencia constante o los "Algebraic loops" formados en los modelos de orden reducido. Durante la implementación de los modelos, se ha ido buscando soluciones o alternativas a estas limitaciones del software de Typhoon HIL. De esta manera, los modelos mas importantes ya han sido implementados en esta tesis, y también se han comentado los problemas que han ido surgiendo durante la implementación, con el objetivo de evitárselos a alguien implementando un nuevo modelo en Typhoon HIL

Aunque Typhoon HIL tiene todavía mucho margen de mejora, es la empresa líder en simulaciones HIL, y las simulaciones HIL son la forma mejor, mas barata y mas rápida de probar una 'microgrid'. También se ha llevado a cabo un análisis económico que respalda esta afirmación y deja claro cual es el potencial de esta tecnología.

En esta tesis como ya se ha dicho, se han implementado los modelos individuales de las FED necesarias para la creación de la 'microgrid' Banshee. Los siguientes pasos se podrían dividir en dos.

1. Implementación de la red Banshee: Esta parte consiste en juntar los modelos implementados para formar la red Banshee. Antes de esto es necesaria la implementación de algunos modelos de cargas. Una vez implementada la red Banshee, se probará en la misma el software para el control distribuido desarrollado por la universidad
2. Implementación de nuevos modelos: Tal y como se ha dicho antes, este banco de pruebas debe ser lo mas adaptable que se pueda. La forma de conseguir esto es implementando numerosos modelos de manera que el banco sirva para 'microgrids', aunque estas contengan FED que no han sido implementadas en esta tesis. Se debería intentar añadir periódicamente nuevos modelos que se vayan considerando relevantes con el tiempo

6. Referencias

- [1] Alejandro D. Dominguez-Garcia. "Controller Hardware-in-the-Loop Testbed for Distributed Coordination and Control Architectures". ECE University of Illinois at Urbana-Champaign.
- [2] Olaoluwapo Ajala "A hierarchy of microgrid models with some applications" University of Illinois at Urbana-Champaign, 2018 <http://hdl.handle.net/2142/102828>
- [3] Reynaldo Salcedo, "Banshee distribution network benchmark and prototyping platform for hardware-in-the-loop integration of microgrid and device controllers" IET Journals March 2019

IMPLEMENTATION OF A CONTROLLER HARDWARE-IN-THE-LOOP TESTBED FOR DISTRIBUTED COORDINATION AND CONTROL ARCHITECTURES

Author: Mayoral Iglesias, Alejandro.

Supervisor: Dominguez-Garcia, Alejandro

Collaborating Entity: University of Illinois at Urbana-Champaign

ABSTRACT

The University of Illinois is developing a distributed control architecture for microgrids. This thesis will focus on the development of a testbed that will be available to test microgrid's features. In future projects, this distributed control architecture software will be tested with this testbed.

One of the main problems of microgrids these days is the cost of testing and development since almost every microgrid has a different topology and DER distribution. With the creation of this Testbed, microgrids can be tested without the risk of damaging expensive material, since until now the only way to test a microgrid in real-time and obtaining high-fidelity is by testing the microgrid with the real electrical infrastructure. This testbed pretends to be usable for most microgrid configurations. In this thesis the models of a grid-feeding inverter, grid-forming inverter, and microturbine were implemented into Typhoon HIL.

Keywords: Microgrid, Banshee, HIL simulations

1. Introduction

In the last years, there has been an incredible growth of DERs (Distributed Energy Resources). These resources are too small to be controlled by the grid. However, if many DERs are connected with the appropriate control architecture, the main grid can control them together and they can offer regulation services to the grid. This aggrupation of DERs mentioned before is what we call a microgrid. The incredible growth of DERs implies also an incredible growth of microgrids.

The main problem of microgrids is their cost of development. In order to test the microgrid's features in real-time and with high-fidelity, the only alternative is to test the microgrid with the real electrical equipment. In this thesis, a microgrid testbed will be presented. The objective is to reduce the cost of development of microgrids and to use this testbed to evaluate the performance of the distributed control architecture for microgrids that is being developed by the University of Illinois. The technology that will allow this real-time simulation and ultra-high fidelity is the Hardware-In-The-Loop simulations (HIL)

2. Project Definition

This project is part of a larger project at the University of Illinois. The university is developing a distributed control architecture. The testbed presented in this thesis will be used to evaluate the performance of the control. However, the testbed not only will be used for that purpose. The testbed created will be easily adaptable to many microgrid

topologies and DERs distribution. The testbed will consist in implementing the Banshee distribution network into Typhoon HIL.

In this thesis, the testbed will be presented, and the most important models will be implemented into Typhoon HIL. The high-order models of a grid-feeding inverter, grid-forming inverter, and a microturbine will be implemented into Typhoon HIL

3. Model Description

In this thesis the individual models of the DERs that appear on the Banshee model were implemented into Typhoon HIL, however, the next steps will be connecting these models together to form the Banshee network. When this is done, more models should be implemented in order to increase the adaptability of the testbed

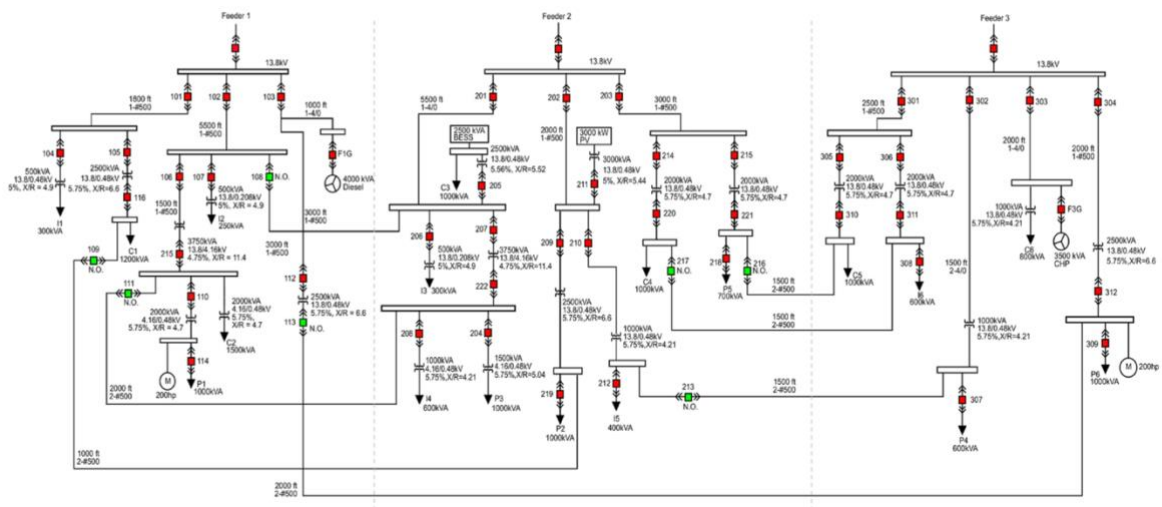


Figure 1 – Banshee Distribution Network Scheme [3]

4. Results

In this section, the results of the grid-feeding inverter models will be presented to give the reader an overview of how the results look like. The results of the other models will have the same format as this one

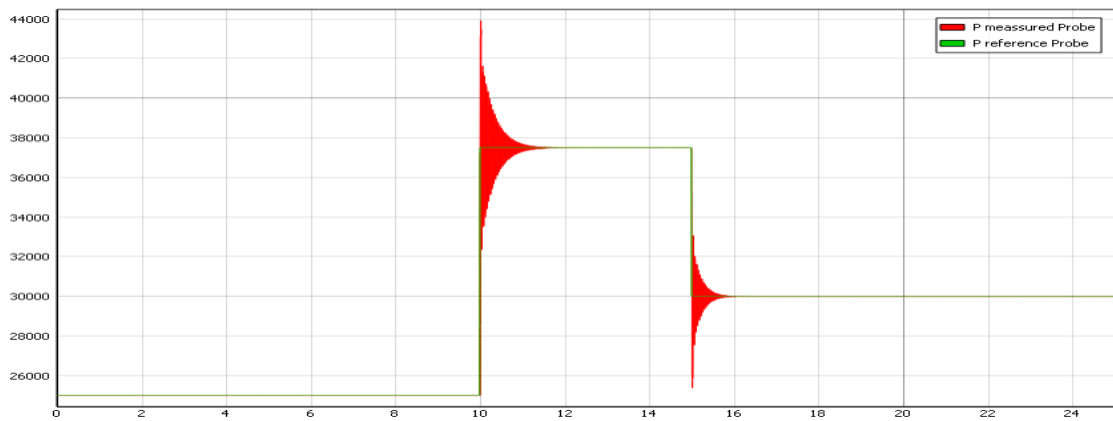


Figure 2– Power Output-Reference Power Grid-Feeding inverter HOM

5. Conclusions and Further Steps

Many problems were faced when implementing the equations of the models into Typhoon HIL. Most models that worked when they were implemented into Simulink did not work when they were implemented into Typhoon. The biggest problem faced was caused because Typhoon HIL can't handle some kind of non-linearities, for example, the constant power load, and the algebraic loops formed on the reduced-order models. These problems mentioned above slowed down the process of development of the testbed, however, solutions and alternatives were found in order to solve the problems that appeared. This way, now that the models are already implemented, and the problems faced were presented in this thesis, it should be easier to develop and create new testbeds

Even though Typhoon HIL has room for improvement in many aspects, because of the problems mentioned before and some others that appeared. Hardware-in-the-loop simulations are the best, cheapest, and fastest way to test microgrids. An economic analysis was performed in the thesis, and the results showed up the incredible potential of HIL simulations.

Also, The University of Illinois will test the distributed control architecture for microgrids that they are developing with this testbed.

In this thesis, the most important models of the Banshee model were implemented and are ready to be connected all together, however, the further steps should be divided into two steps

3. Implementation of the Banshee distribution network: this part will only consist of connecting together all the models implemented, However, some load models might need to be implemented first. When the testbed is ready, the distributed control architecture mentioned before will be tested
4. Implementation of new models: As it was said, this testbed should be adaptable to as many microgrids topologies as possible. The way of achieving this adaptability would be having implemented many models of not so common elements, to be constantly incorporating them into the testbed.

6. References

- [1] Alejandro D. Dominguez-Garcia. "*Controller Hardware-in-the-Loop Testbed for Distributed Coordination and Control Architectures*". ECE University of Illinois at Urbana-Champaign.
- [2] Olaoluwapo Ajala "A *hierarchy of microgrid models with some applications*" University of Illinois at Urbana-Champaign, 2018 <http://hdl.handle.net/2142/102828>
- [3] Reynaldo Salcedo, "Banshee distribution network benchmark and prototyping platform for hardware-in-the-loop integration of microgrid

Index

CHAPTER 1. INTRODUCTION	2
1.1 PROJECT MOTIVATION	2
1.2 THE PROJECT	4
CHAPTER 2. TECHNOLOGY DESCRIPTION	6
2.1 MICROGRIDS.....	6
2.1.1 <i>Grid-Connected mode</i>	8
2.1.2 <i>Islanded Mode</i>	9
2.2 CONTROL ARCHITECTURES.....	10
2.2.1 <i>Centralized Architecture</i>	11
2.2.2 <i>Distributed Architecture</i>	12
2.3 BANSHEE DISTRIBUTION NETWORK	13
2.4 TYPHOON HIL.....	14
2.5 DIRECT-QUADRATURE-ZERO TRANSFORMATION.....	16
CHAPTER 3. ECONOMIC ANALYSIS	18
STEP 1: COST REDUCTION ESTIMATION	22
STEP 2 INVESTMENT ANALYSIS	23
CHAPTER 4. MODEL IMPLEMENTATION	26
4.1 THE NETWORK MODEL	26
4.2 GRID-FEEDING INVERTER	27
4.2.1 <i>Introduction</i>	27
4.2.2 <i>Topology and controls</i>	29
4.2.3 <i>Parameter and Variables definition</i>	31
4.2.4 <i>Reduced-Order Model</i>	32
4.2.5 <i>High-Order Model</i>	37
4.3 GRID-FORMING INVERTER	42
4.3.1 <i>Introduction</i>	42
4.3.2 <i>Topology and controls</i>	44
4.3.3 <i>Parameter and Variables Definition</i>	47
4.3.4 <i>Reduced-Order Model</i>	49
4.3.5 <i>High-Order Model</i>	53

4.4 MICROTURBINE V-F	59
4.4.1 Introduction	59
4.4.2 Topology and controls	60
4.4.3 Parameter and Variables Definition	63
4.4.4 Reduced-Order Model	65
4.4.5 High-Order Model.....	70
CHAPTER 5. CONCLUDING REMARKS & FURTHER STEPS	76
5.1 CONCLUDING REMARKS	76
5.2 FURTHER STEPS	78
APPENDIX I. INVERTER MODELS.....	80
1. GRID-FEEDING INVERTER	81
1.1 EQUATIONS	81
1.2 CODES.....	82
1.3 MODEL SCHEMES.....	85
1.4 RESULTS	86
2. GRID-FORMING INVERTER	87
2.1 EQUATIONS	87
2.2 CODES	90
2.3 MODEL SCHEMES.....	90
2.4 RESULTS	91
APPENDIX II. MICROTURBINE MODEL.....	94
1.1 EQUATIONS	94
1.1.1 Damper winding Model	95
1.1.2 Stator Windings and Short Transmission Line.....	95
1.1.3 Excitation System Model.....	96
1.1.4 Governor Model	97
1.2 MODEL SCHEMES.....	97
APPENDIX III. SUSTAINABLE DEVELOPMENT GOALS	98
GOAL 7: AFFORDABLE AND CLEAN ENERGY	99
QUANTIFIABLE IMPACT.....	101
REFERENCES.....	102

Figure Index

FIGURE 1.1 DER INCREASE IN THE US	2
FIGURE 1.2 SCHEMATIC OF THE CONTROLLER HARDWARE-IN-THE-LOOP TESTBED [1]	5
FIGURE 2.1 MICROGRID GENERAL SCHEME [4].....	6
FIGURE 2.1.1 GRID-CONNECTED MODE SCHEME [5].....	8
FIGURE 2.1.2 ISLANDED MODE SCHEME [5].....	9
FIGURE 2.2.1 CENTRALIZED ARCHITECTURE SCHEME.....	11
FIGURE 2.2.2 CENTRALIZED ARCHITECTURE SCHEME.....	12
FIGURE 2.3.1 FIDELITY COMPARISON [9].....	13
FIGURE 2.4.1 TYPHOON HIL HARDWARE DEVICE [10]	14
FIGURE 2.4.2 SCHEMATIC EDITOR [10]	15
FIGURE 2.5 DQ0 TRANSFORMATION COMPONENTS [3].....	17
FIGURE 3.1 DERs COMPOSITION BY MARKET SEGMENT [12]	20
FIGURE 3.2 COST DISTRIBUTION BY COMPONENT [12]	21
FIGURE 3.3 CASH FLOW DIAGRAM	24
FIGURE 4.1.1.1 SHORT TRANSMISSION LINE MODEL [8]	26
FIGURE 4.2.1.1 INVERTER SCHEME 1	27
FIGURE 4.2.1.2 INVERTER SCHEME 2	28
FIGURE 4.2.1.3 LCL FILTER REPRESENTATION [2]	28
FIGURE 4.2.2.1 GRID-FEEDING INVERTER CONTROL TOPOLOGY SCHEME [2].....	29
FIGURE 4.2.2.2 PLL CONTROL SCHEME [6]	30
FIGURE 4.2.2.3 CASCADE CONTROL SCHEME [7]	30
FIGURE 4.2.4.2.1 P MEASURED VS P REFERENCE PLOT.....	35
FIGURE 4.2.4.2.2 Q MEASURED VS Q REFERENCE PLOT.....	35
FIGURE 4.2.5.3.1 P MEASURED VS P REFERENCE PLOT	39
FIGURE 4.2.5.3.2 Q MEASURED VS Q REFERENCE PLOT	39
FIGURE 4.2.5.3.3 FREQUENCY PLOT.....	40
FIGURE 4.2.5.3.4 P RMSE – Q RMSE PLOT	40
FIGURE 4.3.1.1 MODEL SCHEME 1.....	42
FIGURE 4.3.2.1 GRID-FEEDING INVERTER CONTROL TOPOLOGY SCHEME [2].....	44
FIGURE 5.2.2.2 SIMPLIFIED INVERTER CONTROL SCHEME [11]	45
FIGURE 5.2.2.3 INVERTER CONTROL SCHEME [11]	46

FIGURE 4.3.4.2.1 INVERTERS 1 AND 2 FREQUENCY (Hz)	50
FIGURE 4.3.4.2.2 VOLTAGE 1 AND VOLTAGE 2 (P.U).....	51
FIGURE 4.3.4.2.3 TOTAL P AND Q INJECTED (P.U)	51
FIGURE 4.3.5.3.1 LOAD VOLTAGE	56
FIGURE 4.3.5.3.2 INVERTER’S VOLTAGE	56
FIGURE 4.3.5.3.3 INVERTER’S FREQUENCY	57
FIGURE 4.3.5.3.4 TOTAL P AND Q	57
FIGURE 4.4.2.1 DAMPER WINDINGS SCHEME [14]	60
FIGURE 4.4.2.3 IEE DC1 EXCITER SCHEME [15].....	61
FIGURE 4.4.2.4. DEGOV1 SCHEME [16].....	62
FIGURE 4.4.4.1.1 REDUCED-ORDER MODEL 2 EXCITATION SYSTEM EQUATIONS [2].....	66
FIGURE 4.4.4.1.2 REDUCED-ORDER MODEL 2 GOVERNOR AND PRIMER MOVER EQUATIONS [2]	66
FIGURE 4.4.4.2.1 FREQUENCY PLOT	67
FIGURE 4.4.4.2.2 GENERATOR’S VOLTAGE PLOT	67
FIGURE 4.4.4.2.3 LOAD’S VOLTAGE PLOT.....	68
FIGURE 4.4.4.2.4 POWER CONSUMED BY THE LOAD	68
FIGURE 4.4.5.3.1 SYNCHRONOUS GENERATOR’S FREQUENCY	72
FIGURE 4.4.5.3.2 SYNCHRONOUS GENERATOR’S VOLTAGE	72
FIGURE 4.4.5.3.3 SYNCHRONOUS GENERATOR’S ACTIVE POWER	73
FIGURE 4.4.5.3.4 LOAD’S VOLTAGE	73
FIGURE 5.1 FURTHER STEPS.....	78
FIGURE 3.3.1 GRID-FEEDING INVERTER HO MODEL.....	85
FIGURE 1.3.2 NODE 1	85
FIGURE 1.4.1 ACCUMULATED ACTIVE POWER RMSE	86
FIGURE 1.4.2 NODE 1 VOLTAGE PLOT.....	86
FIGURE 2.3.1 MICROGRID SCHEME.....	90
FIGURE 2.3.2. INVERTER 1 SCHEME.	91
FIGURE 2.4.1 INVERTER 1 VOLTAGE.....	92
FIGURE 2.4.2 INVERTER 2 VOLTAGE.....	92
FIGURE 2.4.3 ACTIVE POWER GENERATED BY EACH INVERTER.....	93
FIGURE 2.4.4 REACTIVE POWER GENERATED BY EACH INVERTER	93
FIGURE 1.2 MICROGRID MODEL SCHEME	97
FIGURE 1 SUSTAINABLE DEVELOPMENT GOALS.....	98

Table Index

Grid-Feeding Inverter

TABLE 4.2.3.1: PARAMETERS	31
TABLE 4.2.3.2: VARIABLES	32
TABLE 4.2.5.2 : PARAMETERS USED	38

Grid-Forming Inverter

TABLE 4.3.3.1 : PARAMETERS.....	47
TABLE 4.3.3.2: VARIABLES	48
TABLE 4.3.5.2 : PARAMETERS USED	54

Microturbine

TABLE 4.4.3.1: PARAMETERS	63
TABLE 4.4.3.2: VARIABLES	64
TABLE 4.4.5.2: PARAMETERS USED	71



UNIVERSIDAD PONTIFICIA COMILLAS
ESCUELA TÉCNICA SUPERIOR DE INGENIERÍA (ICAI)
GRADO EN INGENIERÍA EN TECNOLOGÍAS INDUSTRIALES

CHAPTER 1. INTRODUCTION

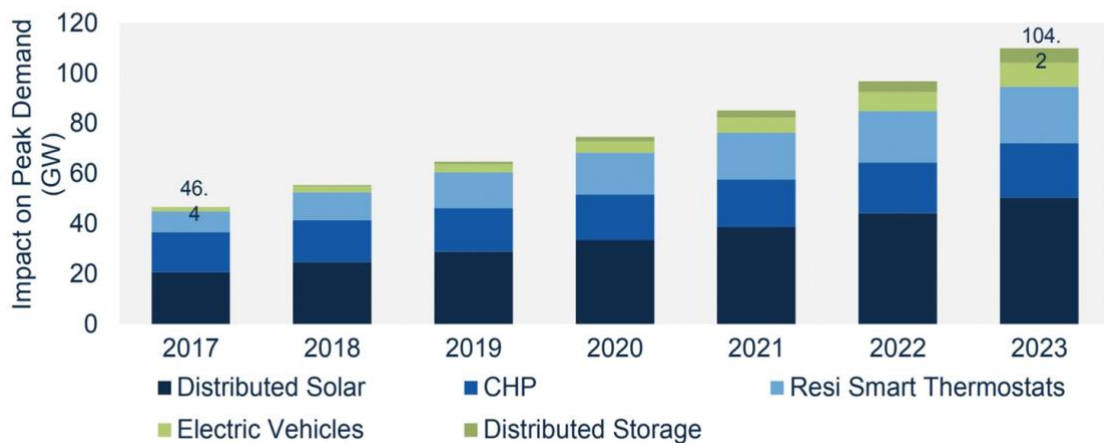
1.1 PROJECT MOTIVATION

In the last years, renewable energy has experienced incredible growth. Distributed energy resources that from now on will be referred to as DER, are getting more efficient and competitive with time. Actually, every microgrid is controlled by a centralized control architecture. In the following pages, a new and more reliable alternative will be presented: The distributed control.

The Electric Power Industry was designed as a high scale industry based on centralized generation and control. The cost of fossil fuels and the concern with climate change has increased the distributed renewable energy resources being present at the electric power grid (as shown in graph 1.1).

US DER and Connected Devices Impact Expected to More Than Double from 46 GW to 104 GW

US DER and Connected Device Impact on Peak Potential, 2017-2023



Source: GTM Research and Department of Energy

Figure 1.1 DER increase in the US

We can see in the graph that the amount of distributed resources will experience a growth of about 226.5% in the US and just in 7 years.

As mentioned before, the grid and the control systems were not designed to control small-scale distributed energy resources (DER). This is why there is a need for a new type of grid and control architectures that will be able to handle this new reality of the electric grid.

In the past years, we have experienced the growth and development of a new kind of grid, the “microgrid”, capable of assuming some of the new needs of the electric power industry. In relation to the control architecture, there is a need for a new control that can be used in microgrids and that can adapt to the DER needs. A group of DER and loads in a microgrid is seen from the grid as a single entity, this meaning that the microgrid can provide regulation services, and that it can be easily controlled by the grid.

There is an obvious need of microgrid development. The problem is that developing new microgrids is expensive. First of all, because of the cost of testing the microgrid. The only solution in order to test the microgrid in real-time and with ultra-high fidelity is to use the real components, this producing the risk of damaging really expensive material. Also, there are not enough normalized models adaptable to all topologies.

The University of Illinois is developing a distributed control architecture designed to control microgrids. The idea is that the software will be as general as possible, making it easier to be used in many topologies. Also, The University of Illinois is developing a microgrid Testbed in order to test microgrids and reduce the cost of microgrid developments. Which in fact, is the purpose of this thesis.

This software will have a direct impact on many of the Sustainable Development Goals (SDG):

- **1 No poverty:** As it is easily adaptable to different topologies, it can be used for places where there is no access to the grid, with the installation of DER
- **7 Affordable and clean energy:** Distributed energy resources are mainly renewable and non-polluting resources.

It will also have an impact on many other SDG

A software- hardware in the loop is being used to test the software. This Software-Hardware called Typhoon HIL allows testing the software using high fidelity models. By using this software, the initial investment necessary to test the software is reduced considerably. Also, the risk of damaging expensive material is eliminated.

1.2 THE PROJECT

The University of Illinois has started a research project in the creation of a distributed control scheme for microgrids. They started with the project named: “*Controller Hardware-in-the-Loop Testbed for Distributed Coordination and Control Architectures*”. This project is led by the University of Illinois Professor Alejandro Dominguez Garcia.

This is a really ambitious project. the university of Illinois is working with other world-class universities such as MIT to develop this project. As mentioned before, nowadays it is not possible to test software or equipment on microgrids without working with the actual network components. Some simulations can be done by computer programs, but fidelity, accuracy, and most important, real-time simulation will be lost. This is why Ultra-High-fidelity models of various components have been developed. The way to use these high-fidelity models without having the issue that computer programs have, is by implementing them into Typhoon HIL, which will be presented afterward in *Chapter 2.4*. In fact, this is what this thesis is going to be about: implementing the Ultra-High-Fidelity models on the Typhoon HIL hardware devices.

As a brief introduction to microgrids (will be explained in more detail in *Chapter 2.3*), a microgrid has two layers:

- **Physical Layer:** Electrical Infrastructure: Generation, distribution...
- **Cyber Layer:** Hardware and software for communications and control.

A new lab was created by the university, where the testbed has been implemented. The following Hardware devices are used to simulate the nodes and equipment:

- **Typhoon HIL Hardware:** Simulates in real-time the DER resources and equipment.
- **Open DSS Software:** To simulate the infinite network
- **Lower-Level Controller:** Texas instruments boards are used to simulate the Lower level Controls such as Governor, Frequency Droop...
- **Cyber-Nodes:** Each of them has an Arduino with the control software implemented

The following Schematic represents the functioning of the System

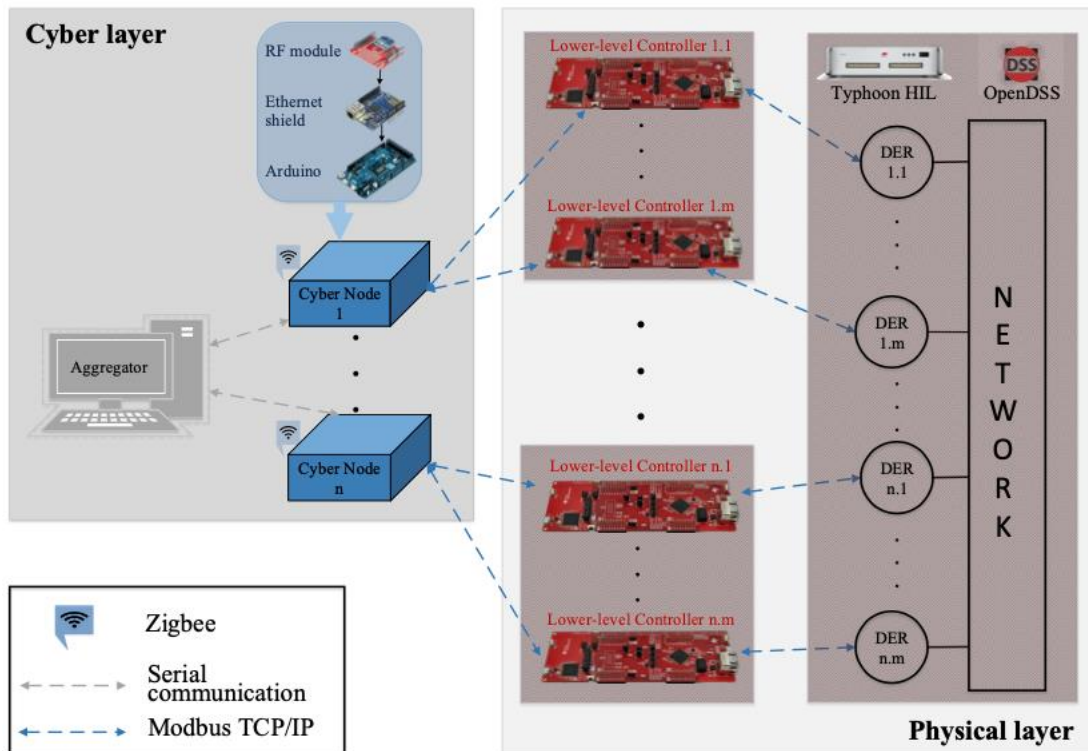


Figure 1.2 Schematic of the Controller Hardware-in-the-Loop Testbed [1]

This project when finished plans not only to develop a distributed control architecture for microgrids, it plans to offer a highly compatible software that can be easily extrapolated to other microgrid configurations. This will lower significantly the cost inherent in the development of microgrids and hopefully will help to the creation of new microgrids.

But not only the distributed control architecture will help microgrids to be more cost-effective and robust. Also, the Hardware-In-The-Loop Testbed will definitely help develop new microgrids. This is because to test the reliability as many other features if high fidelity is required the only alternative is testing with the actual hardware with the risk of damaging expensive material. This testbed, which is the purpose of this thesis, will be easily adaptable and can simplify the development and testing of microgrids. The high-Order Model Equations presented in [2] will be implemented into Typhoon HIL which is a Hardware-In-The-Loop simulation device (Will be presented in Chapter 2.4)

CHAPTER 2. TECHNOLOGY DESCRIPTION

2.1 MICROGRIDS

A microgrid can be defined as: A local energy grid with control capabilities. There are many elements that can be connected to a microgrid, but some of the most important are: PV systems, Electric Vehicles, Fuel Cells, and Residential Storage for example. They have two main modes of operation that will be described in detail afterward:

- **Grid-Connected Mode**
- **Islanded Mode**

The power system is facing a gradual depletion of fossil fuels, also the new regulations are limiting the emissions of power plants. This and many other things make microgrids an incredible opportunity for development. microgrids from a grid point of view are beneficial, the microgrids and all the DERs connected are treated as a controlled system and not just as a regular load node.



Figure 2.1 microgrid General Scheme [4]

microgrids have a central controller (at least until the Distributed Control Architecture is developed) this controller has the following objectives:

- Maintaining Voltage and Frequency to reference values
- Ensure Energy Optimization
- Make sure power Exchange with the grid is as expected

It is really important to have efficient and reliable microgrids since there is an enormous increase in distributed renewable energy resources and Electric cars. The main grid is not properly prepared to control these small DER connected all over the grid. This is because the electric system was designed for central generation on big power plants, not for DER. This DERs are too small to provide frequency regulation services, but combining many of them together in a microgrid this regulation and control services are available

A microgrid could be perceived as a way of updating the old Transmission network and making it more intelligent and efficient overall.

Also, microgrids are really useful to take energy to places where the distribution network is not available to get. But not only this, as the microgrids are available to work on islanded mode, even if the network goes down the microgrid should be available to continue its operation. There have been cases when the whole network failed but a microgrid was available to maintain the load to its consumer.

There are microgrids constantly operating in islanded mode such as: Military Ships and places where the network is not available to get. But usually, the microgrid is working in grid-connected mode either injecting or consuming power and if the network fails the microgrid automatically disconnects itself and enters islanded-mode.

Another important consideration is that when operating in islanded mode, DER should be available to provide the loads the required power and also provide regulation to the microgrid so that constant power and frequency are achieved.

2.1.1 GRID-CONNECTED MODE

In this mode, the microgrid is viewed as a single entity. The network is significantly larger than the microgrid, so the voltage and the frequency are fixed by the network. The microgrid only exchanges active and reactive power with the grid. The entire entity is referred to as an aggregator and operates the DERs connected.

microgrids also provide frequency regulation for the main grid. The network sends a regulation signal and the microgrids offer frequency regulation by changing the power reference. The microgrid always tries to make its $ACE=0$; so that the power exchanged with the network is the desired and the frequency is close to reference.

This is the way that most of the microgrids are working on . The inverters on this mode should be in grid-feeding mode (just injecting the active and reactive power desired). There is also the possibility that microgrids are interconnected with each other.

The control objectives change when working on grid-connected mode and islanded mode on grid-connected mode, usually, the microgrid is working on grid-connected mode until there is a problem. In this case, the “Switch” will open, and the microgrid will be in islanded mode

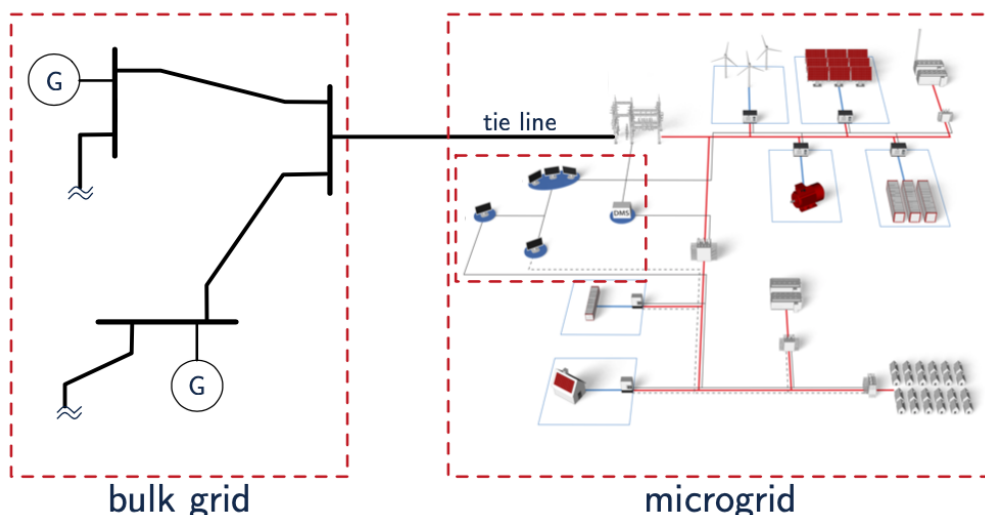


Figure 2.1.1 Grid-Connected Mode Scheme [5]

2.1.2 ISLANDED MODE

This is the mode that usually arrives when a fault occurs. For example, if the grid goes out some essential buildings that need to have electric power at all times have microgrids that are available to supply this power in the case of a grid failure. One curiosity of the microgrids operating in islanded mode, is that nuclear power plants have microgrids to ensure that the cooling system has constant energy supply, in fact, the Chernobyl disaster was a failed islanding test. It was a test to see how fast could the microgrid could start the power supply when the grid was off. But also, as mentioned before there are some cases where the microgrid is constantly operating in Islanded mode such as military ships or places where the network is not accessible

The microgrid has to now feed all the loads. The inverters (in case there are) should now be working on grid-forming mode, this is because frequency and voltage are not fixed by the network anymore. Inverters and DERs should set and keep the voltage and frequency to the reference values. The control objectives have changed from controlling the power exchange with the grid in grid-connected mode to Regulating voltage and frequency and making sure that they both are close to nominal values in order to protect the electrical infrastructure.

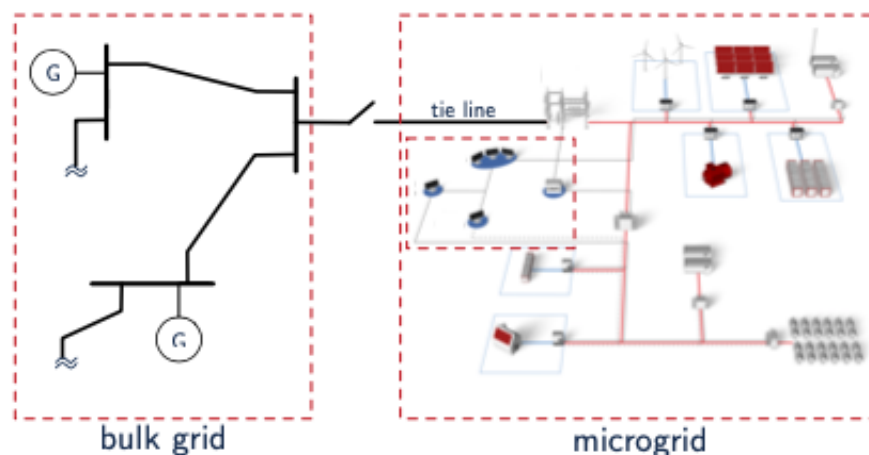


Figure 2.1.2 Islanded Mode Scheme [5]

2.2 CONTROL ARCHITECTURES

Control architectures can vary their objectives, part 2.2 will focus on the control architectures for microgrids.

As introduced in part 2.1 microgrids have two modes of operation. But first of all, why do we need controls in a microgrid? The controls in a microgrid have to deal with changing loads and generation capabilities. Most DERs depend on the climatological conditions, for example, a solar farm can't choose how much power to inject, or, a wind farm's power generation directly depends on the wind speed. The control has to ensure that the voltage and frequency are always close to nominal values, and also that all the loads are fed with the required power. Depending on the mode of operation, the objectives of the controller change. In both cases, the control has to ensure that all the loads in the microgrid are constantly fed with the required power.

- **Grid-Connected Mode:** In this mode of operation, as the microgrid is connected to the main grid and the grid is considered infinite compared with the microgrid, Voltage and frequency are fixed by the network. Then the control has two variables less to regulate. In this case, the grid communicates with the control device and sends some reference power requests to the microgrid. The control has to make sure that the power exchange with the grid is as expected, this is done by reorganizing the power generation in all DERs. In this mode the controls objective should be making its $ACE=0$;
- **Islanded Mode:** In this mode, the microgrid is no longer connected with the main grid, this meaning that the voltage and frequency are not fixed anymore. Voltage and frequency need to be regulated by the controller. They both should be close to nominal values at all times to avoid equipment damage. In islanded mode, the control should be similar to the one in the main grid, with the objectives of making frequency and voltage errors close to zero. This objective is the same as supplying the active and reactive power to all loads required constantly since the Active power is directly related to the frequency and reactive power with voltage.

To sum up, the control objectives are:

1. Making the generation match the demand constantly.
2. Executing an economic dispatch and making sure that the system is generating at the lowest cost.
3. Granting good quality energy being supplied:
 - Constant frequency and close to nominal.
 - Constant voltage and close to nominal.

2.2.1 CENTRALIZED ARCHITECTURE

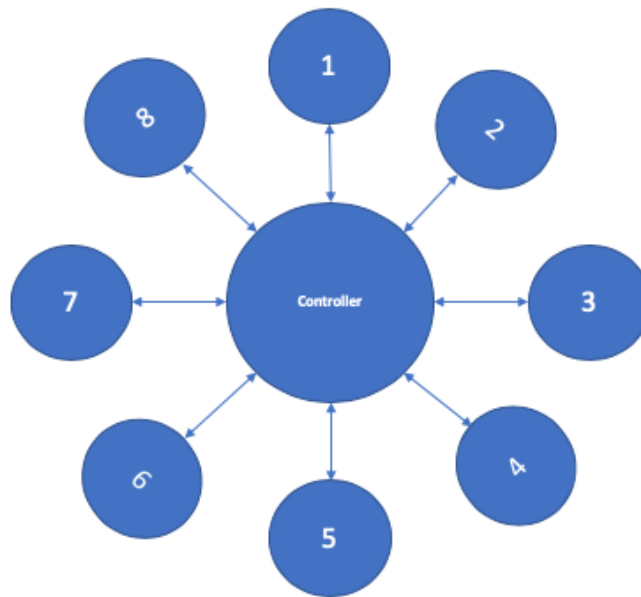


Figure 2.2.1 Centralized Architecture Scheme

The centralized control architecture requires direct communication between each generation resource and the central processor. Since all the decisions are made by the central processor, all the generation resources must be constantly connected with the processor. If there is any kind of communication problem between a node and the central controller, that node will not be able to provide adequate regulation in order to stabilize the system.

The fact that all the nodes are sending and receiving information from the same control node, makes this control fast and simple. Also, this control is more expensive than the distributed

The centralized control architecture is subject to a single point of failure.

2.2.2 DISTRIBUTED ARCHITECTURE

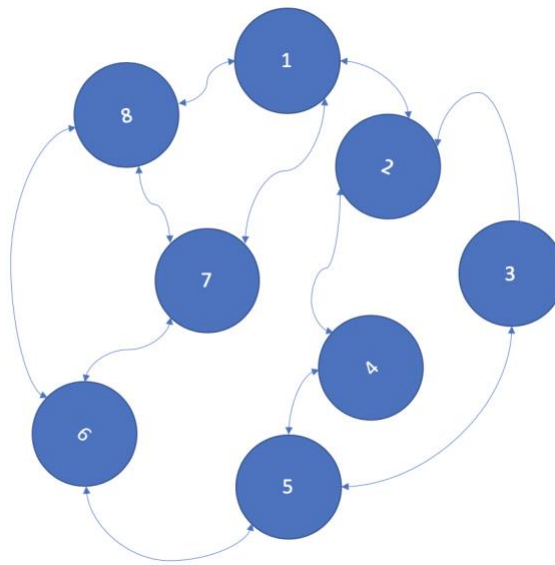


Figure 2.2.2 Centralized Architecture Scheme

In the distributed control there are many control nodes connected with each other. Now there are many computational nodes. This control is more adequate to control DER. Also, this control is in line with our objective of the project which is reducing the cost of microgrid developments. It requires less infrastructural upgrades compared with the centralized, which means that it is exactly what is needed to control a microgrid. (the cost of adding or eliminating a DER is much lower since this control is easily adaptable.)

The distributed control architecture has a big advantage in comparison with the centralized controller. It is more reliable; this is because the system can continue its normal operation even if one node has gone out of service. The price we have to pay to obtain this extra reliability is a slower response because all the nodes need to compute the algorithm and reach consensus between them.

2.4 TYPHOON HIL

Typhoon HIL is the market leader in Hardware-In-The-Loop simulation devices. Their devices offer an ultra-high-fidelity real-time Hardware in the Loop (HIL) platform. But first of all, what is Hardware-In-The-Loop simulations? HIL simulation requires a device that exactly replicates the dynamics of all the electric components in real-time, this way the microgrid can be simulated in real-time.

Typhoon HIL has both Hardware and Software.

1. **Hardware:** Typhoon HIL provided the university of Illinois some hardware devices. They simulate in real-time and with Ultra-High-Fidelity all the models implemented. In the case of this thesis, the models of a Grid-Feeding inverter, Grid-Forming Inverter, and Microturbine are implemented into the device. Just to give an idea of the cost of the Device, the prices start at 30.000\$ for academic use and the basic model.

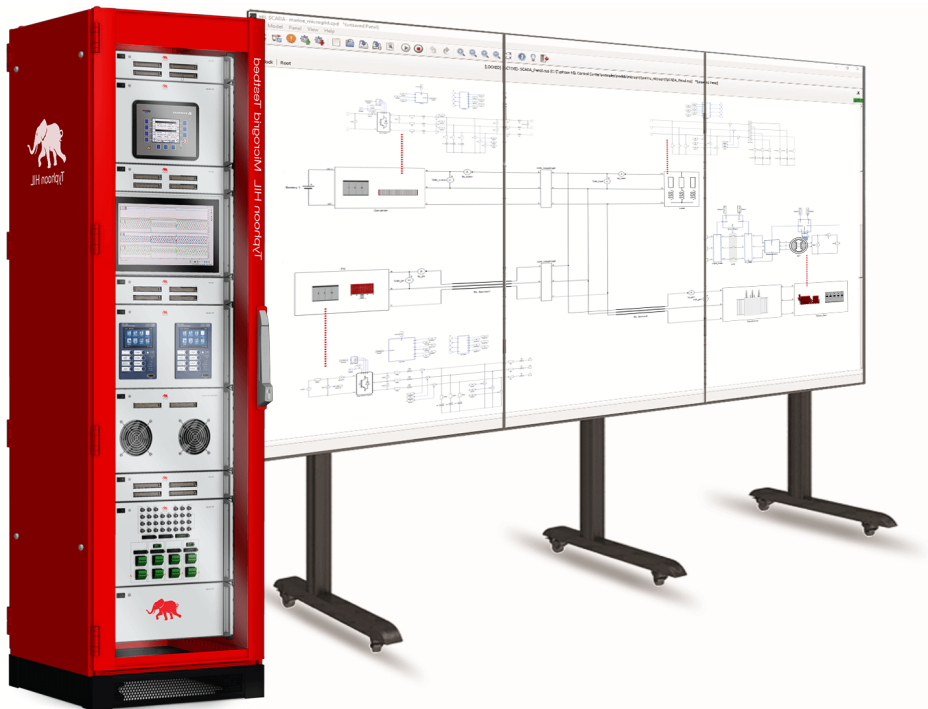


Figure 2.4.1 Typhoon HIL hardware device [10]

2. **Software:** Also, Typhoon HIL has some applications that help the user to implement models into the hardware device. There is a main application called Typhoon HIL Control Center. Also, inside the control center are some applications, the two most important will be presented below:

- **Schematic Editor:** This is the app that is used to implement the models. Models can be created in the schematic editor and when finished they can be uploaded to de hardware device to start HIL simulations. Although the schematic editor is really similar to Simulink, it has some important differences especially in the processing that sometimes make models that work in Simulink fail in Typhoon HIL (This was one of the problems we faced)

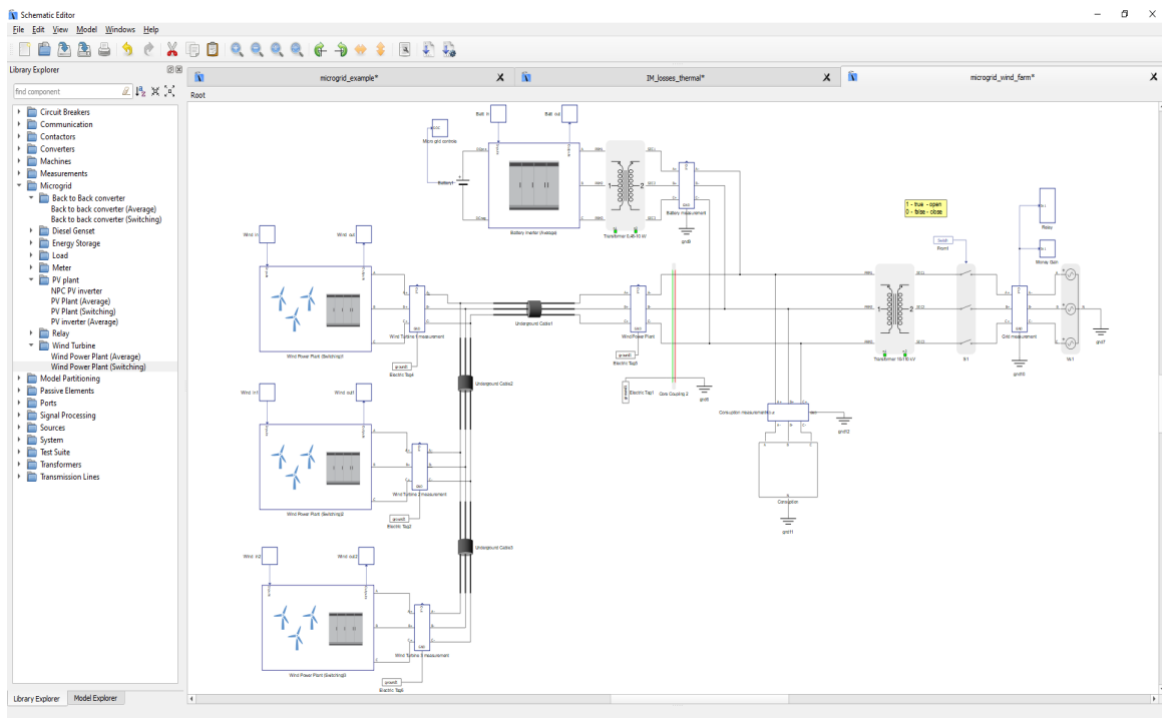


Figure 2.4.2 Schematic Editor [10]

- **HIL SCADA:** This is a graphical interface that allows to monitor and manage the desired variables in real-time simulations. It is really useful to monitor and make changes during the real-time HIL simulations. Also, it is completely configurable in all senses.

2.5 DIRECT-QUADRATURE-ZERO TRANSFORMATION

In this section, the Parks qd0 Transformation method will be presented. The difference with the regular qd0 Transformation method is that the axis are changed.

All the equations that will be implemented from the document [2]. Are given in qd0 bases for the simplicity of the controls. Basically, the transformation is just a tensor that rotates the reference frame of a three-phase system into a moving reference system that moves synchronously. We denote $\alpha(t)$ as *the angular position reference* of a rotating frame at an arbitrary angular velocity $\omega(t)$. Let the vector $f_{qd0[\alpha(t)]}$ be defined as:

$$f_{qd0[\alpha(t)]} = [f_{q[\alpha(t)]} \quad f_{d[\alpha(t)]} \quad f_{0[\alpha(t)]}]^T$$

And the vector

$$f_{abc}(t) = [f_a(t) \quad f_b(t) \quad f_c(t)]^T$$

Also, the matrix $K_1(\alpha(t))$ so that the following equation verifies:

$$f_{qd0[\alpha(t)]} = K_1(\alpha(t)) f_{abc}(t)$$

$$K_1(\alpha(t)) := \frac{2}{3} \begin{bmatrix} \cos(\alpha(t)) & \cos(\alpha(t) - \frac{2\pi}{3}) & \cos(\alpha(t) + \frac{2\pi}{3}) \\ \sin(\alpha(t)) & \sin(\alpha(t) - \frac{2\pi}{3}) & \sin(\alpha(t) + \frac{2\pi}{3}) \\ \frac{1}{2} & \frac{1}{2} & \frac{1}{2} \end{bmatrix}$$

$$\alpha(t) = \int_0^t \omega(\tau) d\tau + \alpha(0).$$

It will assume that the microgrid is a balanced Three-Phase system, because of this assumption, $f_{0[\alpha(t)]} = 0$ and also if $\alpha(t) = \omega_0 t$ where ω_0 represents the synchronous rotating speed we can define a new base change to obtain the only two components

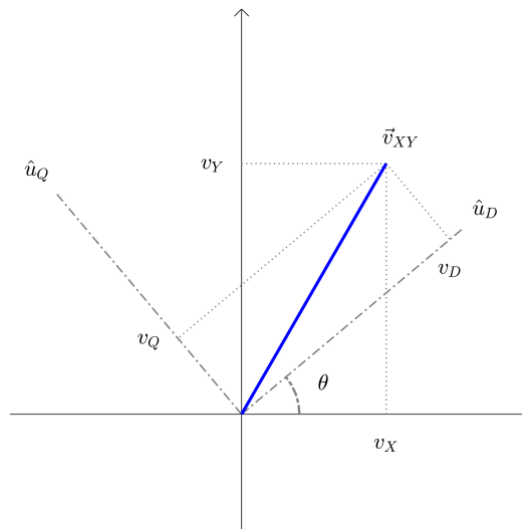


Figure 2.5 DQ0 Transformation components [3]

For the new base we need to define new vectors:

$$\hat{f}_{qd0[\alpha(t)]} = \begin{bmatrix} f_q[\alpha(t)] & f_d[\alpha(t)] \end{bmatrix}^T$$

Also:

$$\hat{f}_{qd0[\omega_0 t]} = \begin{bmatrix} f_q[\omega_0 t] & f_d[\omega_0 t] \end{bmatrix}^T$$

Finally, we define the matrix $K_2(\delta(t))$ such that:

$$\hat{f}_{qd0[\alpha(t)]} = K_2(\delta(t)) \hat{f}_{qd0[\omega_0 t]}$$

Where:

$$K_2(\delta(t)) = \begin{bmatrix} \cos(\delta(t)) & -\sin(\delta(t)) \\ \sin(\delta(t)) & \cos(\delta(t)) \end{bmatrix}$$

And finally:

$$\delta(t) = \alpha(t) - \omega_0 t$$

$$\frac{d\delta(t)}{dt} = \omega(t) - \omega_0$$

This way we are available to express the three-phase balanced components into only two components Quadrature and Direct

CHAPTER 3. ECONOMIC ANALYSIS

In this chapter, an economic analysis will be performed. It will be analyzed whether the use of the testbed to test and develop microgrids will reduce the development cost or not. As will be shown, HIL simulations not only are more cost-effective than testing with real components, also by using HIL simulations, a considerable reduction in the time needed for development is achieved

For this analysis, the data from [12] will be used in order to perform the analysis.

First of all, the microgrid component costs can be divided into:

- **DERs:** All the distributed energy resources. There are many DERs, but this study will focus especially on the models implemented in the thesis which are: Microturbine, solar PV, and energy storage units. Solar PV and energy storage units are considered to be implemented in this thesis because the models of the inverters in the thesis represent an inverter connected to a DERs which can be either solar PV or a storage unit.
- **Microgrid Controllers:** This section groups all the controllers. (Primary, secondary and tertiary). In this part not only is included the cost of the infrastructure, but also the cost of testing the control.
- **Additional Infrastructure:** This section groups all the other infrastructure apart from the electrical infrastructure: Information technology, Communication updates, metering. Etc.
- **Soft Costs:** Engineering, construction, and regulatory. This is the part where the testbed will have most of the impact because, with the creation of the testbed, the development costs will drastically reduce. The data from [12] will be used as the actual Soft Cost for microgrids, and the cost of developing the microgrid will be estimated in the following pages

On an introductory market analysis. The microgrid market can be divided into five main market segments. It is important to make this differentiation because the costs of microgrid development and operation vary between them. The principal market segments studied are:

- **Institutional:** These types of microgrids are designed to be used in critical places that need to maintain power supply in the case that the main grid goes down. Basically, places such as hospitals and universities. Also, the goal of this type of microgrid is to consume the less power from the grid as possible.
- **Commercial/industrial:** This market segment is similar to the institutional since this type of microgrids are also in places where the power supply cannot be interrupted. The difference is that these microgrids are used for manufacturing plants or other industrial plants. The clearest example would be the data storage facilities. Also, in some cases, the microgrid is available to supply all the power necessary for the plant operation.
- **Community:** These types of microgrids are used to supply power to a community. The microgrid is created to group all local DERs which individually are too small to provide regulation and control. Usually, they are connected to the grid, and their objective is just to consume less power from the grid. But also, as mentioned in previous chapters there are some community microgrids in places where the network is not available to get.
- **Utility:** Usually these types of microgrids are almost completely created by Solar PV. In fact, in the study, almost 96% of the DERs in this type of microgrids were solar PV. This type of microgrids are usually owned by electric distribution companies, and usually, they are solar farms
- **Military:** In this analysis, this type of microgrid will not be analyzed due to the lack of information about the cost of development.

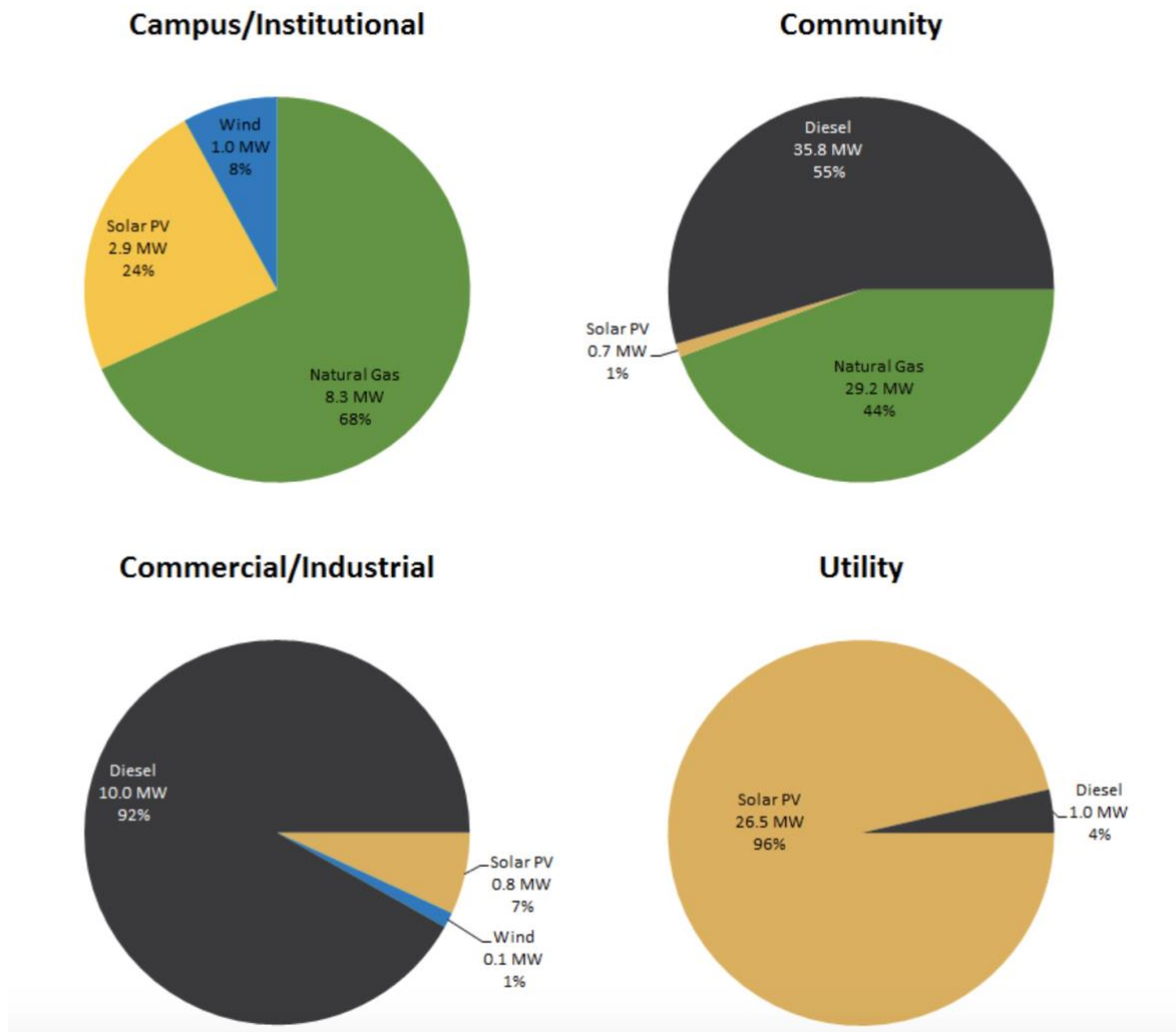
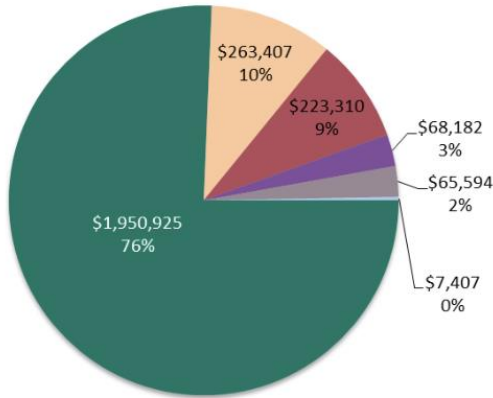


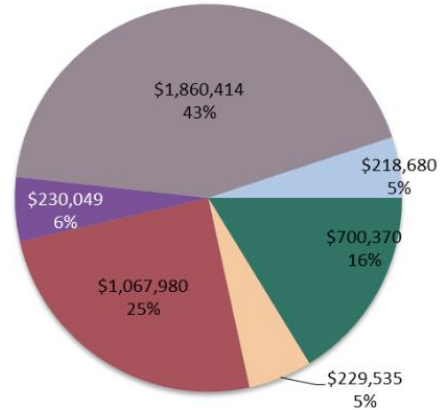
Figure 3.1 DERs composition by market segment [12]

This analysis could be divided into two steps, first of all, the reduction in the cost of development will be estimated in a general way. The second step would be analyzing if an engineering company will profit from the purchase of the Testbed presented in this Thesis. By changing the method of testing from the traditional with components to the testbed.

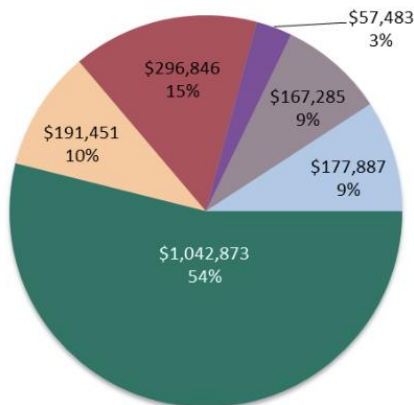
Campus/Institutional - Cost per MW by Component



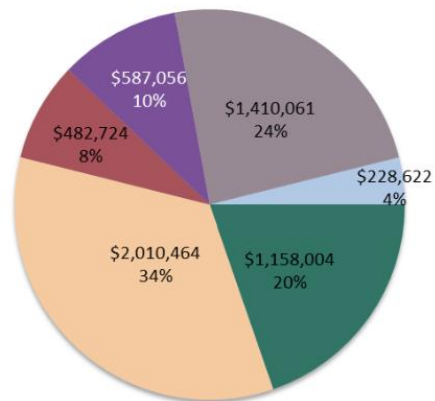
Commercial/Industrial - Cost per MW by Component



Community - Cost per MW by Component



Utility - Cost per MW by Component



■ Conventional Generation
 ■ Renewable Generation
 ■ Energy Storage
■ Controls
 ■ Soft Costs
 ■ Additional Infrastructure

Figure 3.2 Cost Distribution by component [12]

The soft costs are the costs that we are interested in for this analysis, but also the controls cost will be added up to the soft costs. The costs varies depending on the type of microgrid. An average value will be used in order to perform the analysis. The average development cost (obtained by adding up soft costs and controls) will be calculated below.

First of all, let's make the assumption that 40% of the cost of control is because of the required testing of the control. By adding: $\text{Soft Cost} + \text{Control Cost} * 0.4 = \text{Development Cost}$

$$\text{Average Development Cost/MW} = \frac{\text{Soft Cost} + \text{Control Cost} * 0.4}{4} = \frac{2,344,100}{4}$$

$$\text{Average Development Cost/MW} = \$ 583,525/\text{MW}$$

From this Average Development Cost, the Commissioning and regulatory costs need to be subtracted. An estimation of around 65,000\$/MW spent for this purpose. Based on the average salary per project it is fair to assume that another \$ 35,000/MW are used to pay for salaries and other fixed costs.

$$\text{Corrected Average Development Cost /MW} = \$ 483,525/\text{MW}$$

STEP 1: COST REDUCTION ESTIMATION

For this approach, the idea is to see how an individual company could reduce the cost development. First of all, the HIL simulations provide a much faster solution for microgrid testing. Actually, there are some HIL laboratories with some testbed implemented. They claim that for a task that would normally take 6 weeks, they can now do it in just a day. They claim that a week of simulations with real components is equivalent to just one hour of testing with HIL. Basically, using HIL simulations could have an impact on the working hours, making more efficient the use of these simulations since many more projects could be done in the same time. Based in all the assumptions presented above and some already implemented HIL testbeds, the cost reduction could be reduced about 50% by using the HIL testbed, but also as mentioned before a reduction of the total man hours could be reduced about 30%

$$\text{Cost Reduction Estimation/Mw} = \$ 483,525 / \text{MW} * 0.5 + \$35,000/\text{MW} * 0.3 = \$ 252,262/\text{MW}$$

STEP 2 INVESTMENT ANALYSIS

In this part, the cost reduction estimation calculated in step 1 will be used to analyze whether the investment required to create the testbed will produce a positive Net Present Value.

Investment Costs:

- Typhoon HIL Microgrid Testbed = \$ 100,000
- Model Implementation = \$ 5,000
- Additional Equipment = \$ 10,000
- Installation Costs = \$ 2,000

One important feature of Typhoon HIL's Microgrid Testbed is that it is scalable, which means that units can be added or removed at all time without modifications required.

On the other hand, we have the savings that the Testbed will produce. These savings were presented in step 1 and are the following:

- Estimated Cost Reduction = \$ 252,262/MW

Two assumptions will be made in order to simplify the calculations.

1. 1 project is done per year
2. The average power capacity per project is 1MW

Also, let's assume the discount rate to be 7% which is the average discount rate for energy projects. And for simplicity inflation effects will be ignored. The final assumption is that a Typhoon HIL device should be replaced for a new one in 5 years.

The final calculations and the cashflow diagram will be presented in the following page.

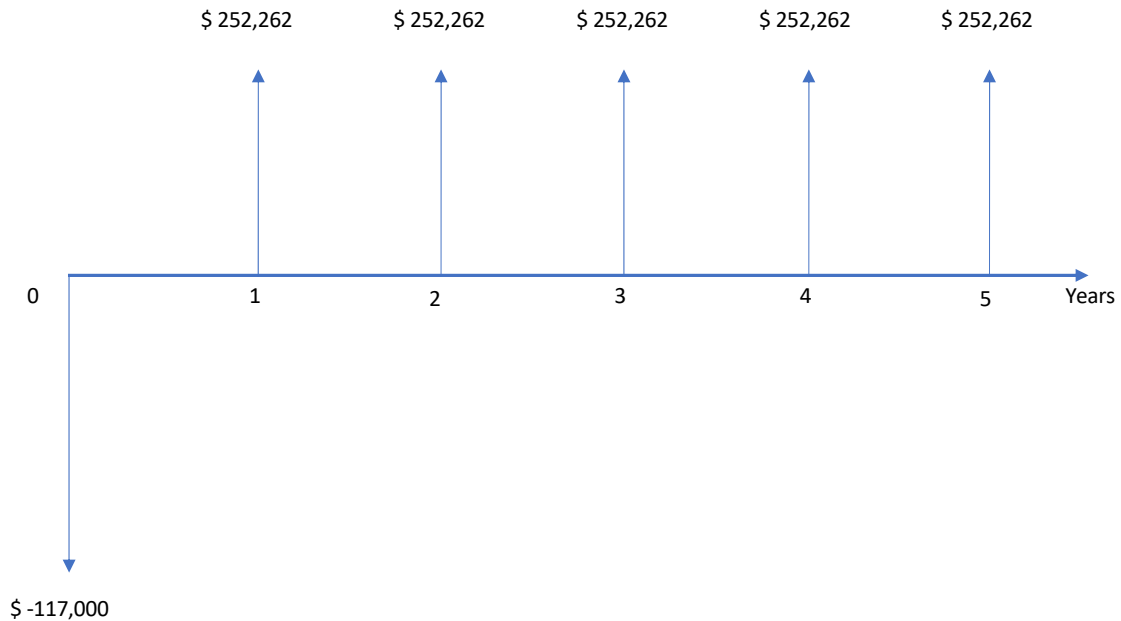


Figure 3.3 Cash Flow diagram

$$NPV = -117,000 + \frac{252,262}{1+0.07} + \frac{252,262}{(1+0.07)^2} + \frac{252,262}{(1+0.07)^3} + \frac{252,262}{(1+0.07)^4} + \frac{252,262}{(1+0.07)^5} = \$ 917,324$$

Also, by making the NPV=0 we obtain the internal rate of return.

$$0 = -117,000 + \frac{252,262}{1+x} + \frac{252,262}{(1+x)^2} + \frac{252,262}{(1+x)^3} + \frac{252,262}{(1+x)^4} + \frac{252,262}{(1+x)^5};$$

$$IRR = 2.149$$

The IRR shows that this investment will have a positive NPV for all discount rates smaller than 214.9 % which means that there is a lot of margin and that our assumption of the discount rate did not influence the solution. The NPV of the inversion is \$ 917,324 so as it was expected, the use of HIL simulations to test microgrids will reduce the development cost of microgrids. By the reduction of this cost, the microgrids should be more accessible and more microgrids should be created



UNIVERSIDAD PONTIFICIA COMILLAS
ESCUELA TÉCNICA SUPERIOR DE INGENIERÍA (ICAI)
GRADO EN INGENIERÍA EN TECNOLOGÍAS INDUSTRIALES

CHAPTER 4. MODEL IMPLEMENTATION

4.1 THE NETWORK MODEL

For the Network Model, all the lines will be represented by using the short transmission line model.

The network dynamics are described by:

$$\mathbf{l}^{(\mathcal{E})} \frac{d\mathbf{i}_{q[\omega_0 t]}^{(\mathcal{E})}(t)}{dt} = -\mathbf{r}^{(\mathcal{E})} \mathbf{i}_{q[\omega_0 t]}^{(\mathcal{E})}(t) - \omega_0 \mathbf{l}^{(\mathcal{E})} \mathbf{i}_{d[\omega_0 t]}^{(\mathcal{E})}(t) + \mathbf{M}^T \mathbf{v}_{q[\omega_0 t]}^{(\mathcal{V})}(t),$$

$$\mathbf{l}^{(\mathcal{E})} \frac{d\mathbf{i}_{d[\omega_0 t]}^{(\mathcal{E})}(t)}{dt} = -\mathbf{r}^{(\mathcal{E})} \mathbf{i}_{d[\omega_0 t]}^{(\mathcal{E})}(t) + \omega_0 \mathbf{l}^{(\mathcal{E})} \mathbf{i}_{q[\omega_0 t]}^{(\mathcal{E})}(t) + \mathbf{M}^T \mathbf{v}_{d[\omega_0 t]}^{(\mathcal{V})}(t).$$

Equations 4.1.1 Network dynamics [2]

Basically, for the network model, the power flow equations will be used in order to ignore the dynamics of the network. The model used will be presented below. Just a simple short transmission line model.

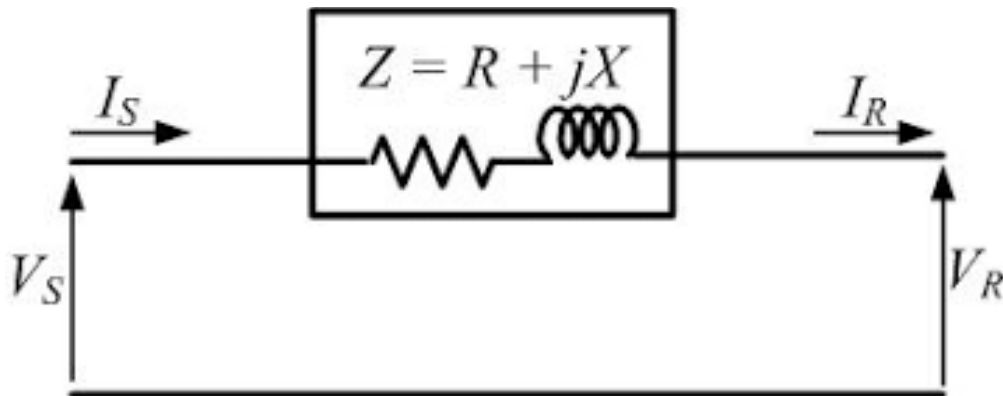


Figure 4.1.1 Short Transmission Line Model [8]

4.2 GRID-FEEDING INVERTER

4.2.1 INTRODUCTION

In this chapter, A Grid-Feeding inverter model will be implemented into Typhoon HIL. Two models will be implemented, a high-order model and a Reduced-order model. After the implementation, the fidelity of both models will be analyzed and compared.

The system to be implemented will be a simple one, in order to measure the performance of the grid-feeding inverter model. This system will consist of a set of batteries connected to an infinite network bus through an inverter.

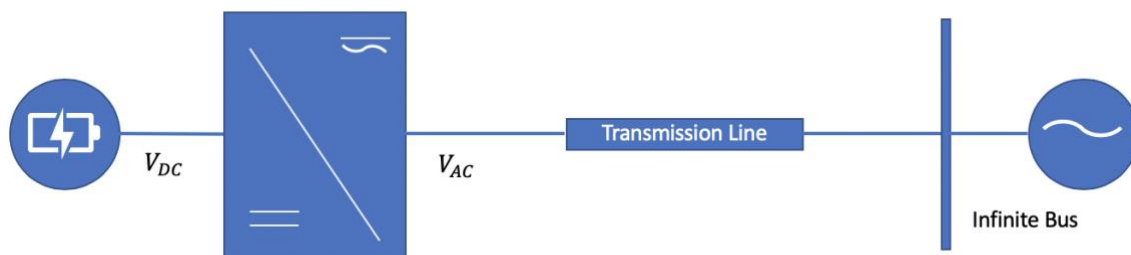


Figure 4.2.1.1 Inverter Scheme 1

In this system, the infinite network bus will have the voltage and the angle fixed. The grid-feeding inverter will have fixed the active and reactive power injected. It is important to mention that the equations stated afterward related to the grid-feeding inverter are written considering the inverter to be unconnected. In order to correctly implement this system, it is necessary to add the transmission line parameter to the LCL filter parameters.

The performance of the models will be tested by changing the reference and measuring the ability of the output to follow the reference.

As this is the first implementation, two figures will be presented to help illustrate the model.

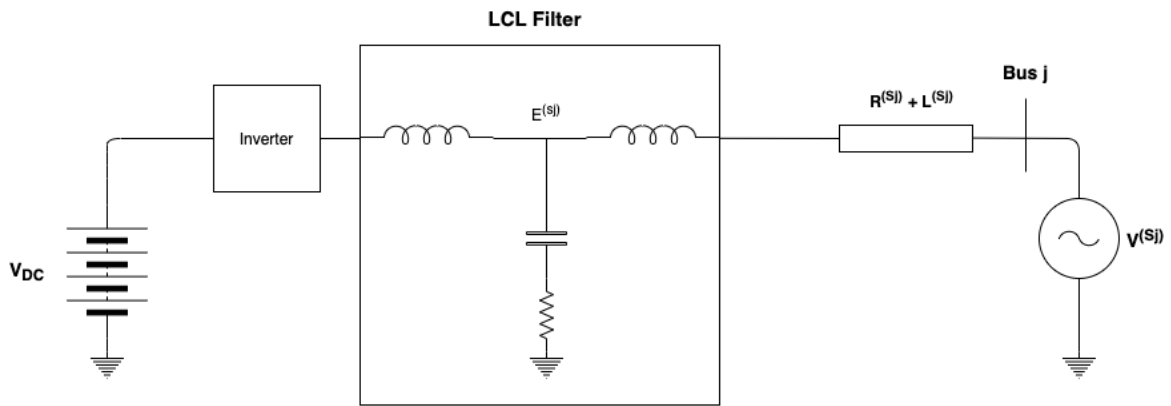


Figure 4.2.1.2 Inverter Scheme 2

Figure 4.2.1.2 tries to illustrate what the connections in this particular case are. It is important to notice that the system is a three-phase system.

Now figure 4.2.1.3 will illustrate in more detail the LCL filter.

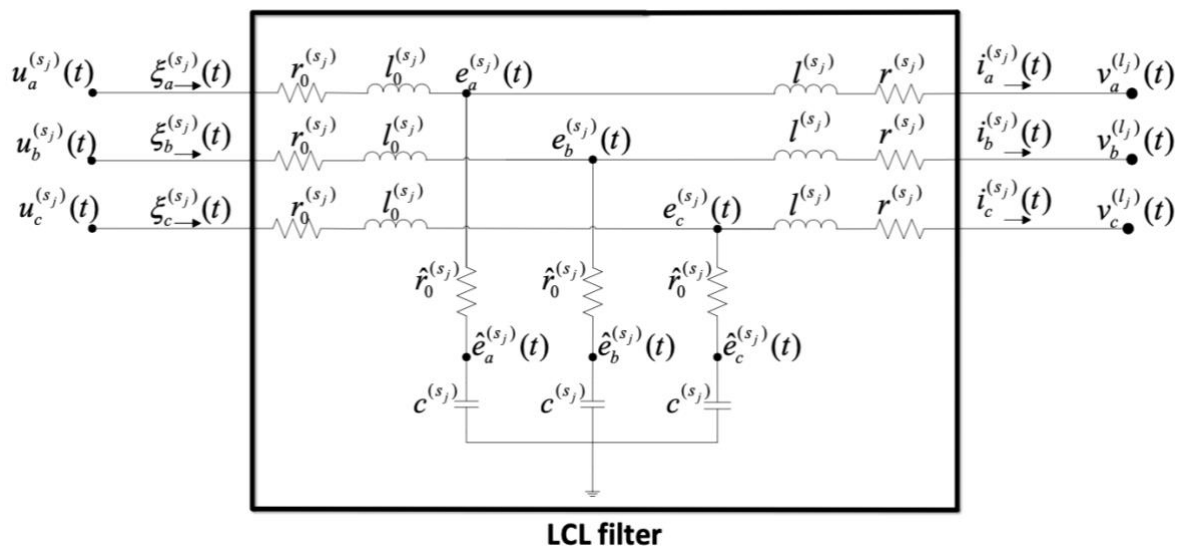


Figure 4.2.1.3 LCL Filter Representation [2]

4.2.2 TOPOLOGY AND CONTROLS

As mentioned before, the grid-feeding inverter has its real and reactive power controlled. They must follow a reference. Therefore, some controls need to achieve this objective. The topology and scheme of the Grid-Feeding inverter and the Grid-Forming are the same, the only difference is that the controls try to achieve different things in both cases (Track power reference in Grid-Feeding and Voltage reference in Grid-Forming)

The Grid-Feeding Inverter is composed of four components.

- **Three-Phase Inverter.** Converts DC power into AC power
- **LCL Filter.** Reduces the Outputs Ripple
- **Cascade Controller.** Used to track the active and reactive power references. It has 2 loops, an inner loop, and an outer loop. The inner loop has as feedback signal the filtered output power, and the outer loop has the filtered voltage as the feedback signal. By using the Parks qd0 transformation, the active and reactive power controls are decoupled
- **Phase-Locked loop.** Determines and tracks the angular position in which the Parks transformation can decouple both controls

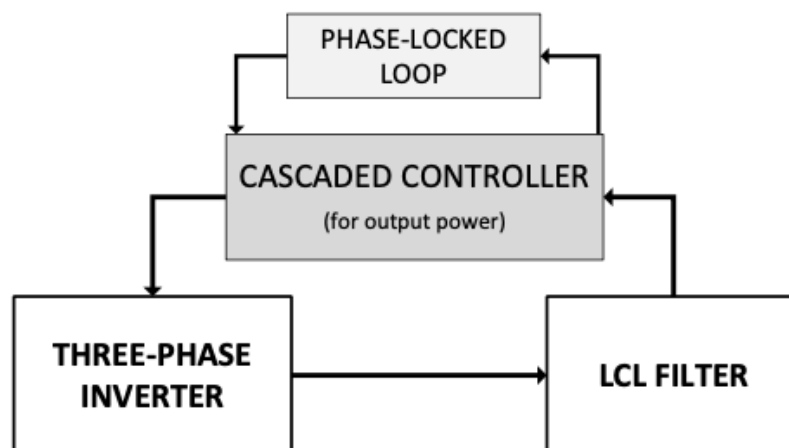


Figure 4.2.2.1 Grid-Feeding inverter control topology scheme [2]

The Phase-Lock-Loop has the following scheme:

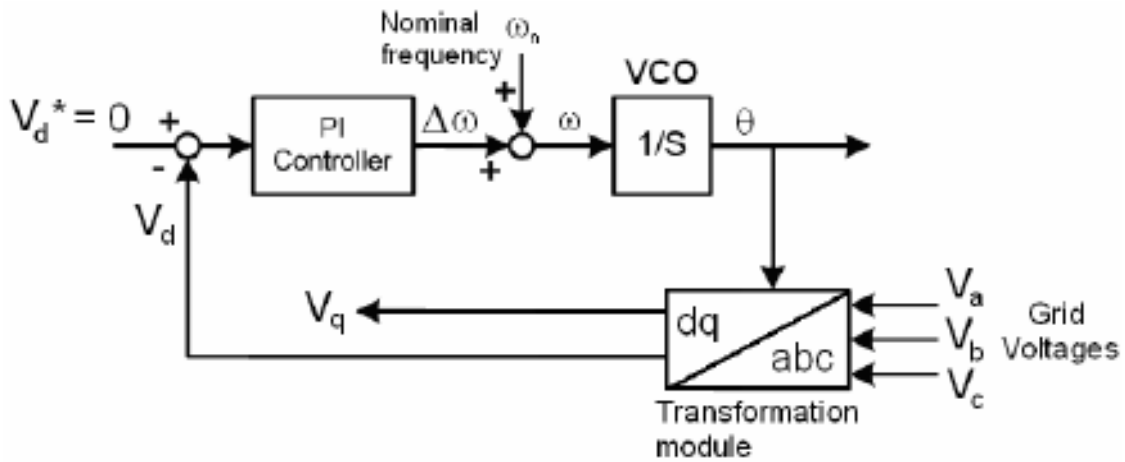


Figure 4.2.2.2 PLL control scheme [6]

The three-phase voltage enters the control, a dq transformation is done, and finally the way to make sure that the references are in synchronism is to make sure that the quadrature component of the grid voltage is 0.

The Cascade Control has the following scheme:

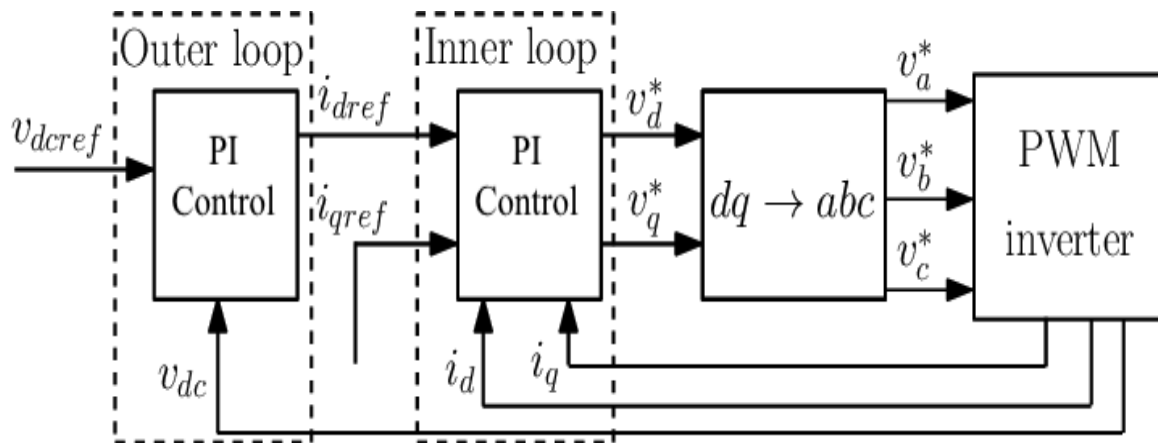


Figure 4.2.2.3 Cascade control scheme [7]

With the cascade controller, the inverter is available to follow the power reference. As mentioned before, there are two loops, The Outer loop, and the Inner loop.

The Outer loop measures the Vdc Voltage and sends I_{dref} as an input for the inner loop that measures the I

4.2.3 PARAMETER AND VARIABLES DEFINITION

<i>Table 4.2.3.1: Parameters</i>	
Parameter (p.u)	Physical equivalent
$\omega^{(Sj)}$	The measurement filter cut-off frequency, in radians per second
$P_r^{(Sj)}$	Real power reference
$Q_r^{(Sj)}$	Reactive power reference
$L_0^{(Sj)}$	LCL filter inductance
$L^{(Sj)}$	LCL filter inductance
$C^{(Sj)}$	LCL filter capacitance
$R_0^{(Sj)}$	Inverter and filter Resistance
$R^{(Sj)}$	Inverter and filter Resistance
$\hat{R}^{(Sj)}$	Inverter and filter Resistance
$R^{(em)}$	Transmission line Resistance
$L^{(em)}$	Transmission line Inductance
$K_{P\lambda}^{(Sj)}$	Proportional Gain of the current Controller
$K_{I\lambda}^{(Sj)}$	Integral Gain of the current Controller
$K_{P\gamma}^{(Sj)}$	Proportional Gain of the PLL
$K_{I\gamma}^{(Sj)}$	Integral Gain of the PLL

Table 4.2.3.2: Variables

Variable (p.u)	Physical equivalent
$V_{DC}^{(s_j)}$	DC voltage at the inverter input (Battery voltage)
$E^{(s_j)}$	Internal voltage of the inverter
$\hat{E}^{(s_j)}$	LCL filter capacitor voltage
$V^{(s_j)}$	Voltage at bus j
$\Xi^{(s_j)}$	Inverter output current
$I^{(s_j)}$	Filtered inverter output current
$\Gamma^{(s_j)}$	State variable for the current controller
$\Lambda^{(s_j)}$	State variable for the phase-locked loop
$P_f^{(s_j)}$	Filtered real power measured
$Q_f^{(s_j)}$	Filtered reactive power measured

4.2.4 REDUCED-ORDER MODEL

4.2.4.1 Introduction and Problems Faced

In this case, the reduced-order model inverter will be implemented. As the equations in this particular reduced-order model are just a modified version of the power flow equation, they will be presented below.

Many problems were faced when implementing this reduced-order model. First of all, the initial conditions needed to be calculated. A MATLAB code was created in order to solve for the initial conditions and parameters of this model (Code can be found in Appendix I). The second problem faced, was produced because of the form of the equations implemented. The reduced-order model equations do not have differential equations, this is important because when the implementation was done, Algebraic loops needed to be created. While in MATLAB there is a block that solves algebraic loops, in Typhoon HIL there is no such block. A delay block was used to input initial conditions. But even with this block, the model

seemed not to work. As the Rom does not have differential equations, the dynamics of the inverter are not completely represented by the model, in fact, without the delay block, the input would just be the output instantaneously because there are no dynamics in the model. After some time ‘fighting’ with the problem, it was discovered that typhoon hill can’t handle this kind of non-linear equations. Typhoon hill staff was contacted, and they confirmed the problem. Therefore, for the comparison, the Rom will be implemented into Simulink

Equations 4.2.4.1.1 and 4.2.4.1.2 describe the dynamics of the grid-feeding inverter connected to an electrical network through node j:

$$0 = -P_r^{(s_j)} + \hat{G}^{(s_j)} \left| \vec{E}^{(s_j)}(t) \right|^2 + G^{(s_j)} \left| \vec{E}^{(s_j)}(t) \right|^2 - \left| \vec{E}^{(s_j)}(t) \right| \left| \vec{V}^{(l_j)}(t) \right| \left(G^{(s_j)} \cos \left(\hat{\theta}^{(s_j)}(t) - \theta^{(l_j)}(t) \right) + B^{(s_j)} \sin \left(\hat{\theta}^{(s_j)}(t) - \theta^{(l_j)}(t) \right) \right),$$

$$0 = -Q_r^{(s_j)} - \hat{B}^{(s_j)} \left| \vec{E}^{(s_j)}(t) \right|^2 - B^{(s_j)} \left| \vec{E}^{(s_j)}(t) \right|^2 - \left| \vec{E}^{(s_j)}(t) \right| \left| \vec{V}^{(l_j)}(t) \right| \left(G^{(s_j)} \sin \left(\hat{\theta}^{(s_j)}(t) - \theta^{(l_j)}(t) \right) - B^{(s_j)} \cos \left(\hat{\theta}^{(s_j)}(t) - \theta^{(l_j)}(t) \right) \right),$$

Equations 4.2.4.1.1 and 4.2.4.1.2 Reduced Order Model Equations [2]

If equations 4.2.4.1.1 and 4.2.4.1.2 which are presented above are carefully observed. In this reduced-order model equations, there is a clear similarity with the power flow equations from node 1 which is the capacitor terminal in the LCL filter and node j. The first term is just the reference Power, the second term is the power consumed by the parallel branch formed by the capacitor and finally, the last term is just the power Exiting node i.

Equations 4.2.4.1.3 and 4.2.4.1.4 correspond to the measured real and reactive power measurement and can be described by:

$$\frac{1}{\omega_c^{(s_j)}} \frac{d\mathbf{P}_f^{(s_j)}(t)}{dt} = -\mathbf{P}_f^{(s_j)}(t) + \mathbf{P}_r^{(s_j)},$$

$$\frac{1}{\omega_c^{(s_j)}} \frac{d\mathbf{Q}_f^{(s_j)}(t)}{dt} = -\mathbf{Q}_f^{(s_j)}(t) + \mathbf{Q}_r^{(s_j)},$$

Equation 4.2.4.1.3 and 4.2.4.1.4 Active and Reactive Power Measurements [2]

As mentioned before, the transmission line parameters must be included in order to characterize the system properly. Now, the admittance parameter will be presented.

These parameters are only admittance matrix elements. If we consider the Ybus matrix known, the elements of the matrix could be used instead.

The following equations represent the admittance elements in terms of the given parameter stated on table 4.2.4.1

$$G^{(s_j)} = \frac{R^{(e_m)} + R^{(s_j)}}{\left(R^{(e_m)} + R^{(s_j)}\right)^2 + \left(L^{(e_m)} + L^{(s_j)}\right)^2}$$

$$B^{(s_j)} = \frac{-(L^{(e_m)} + L^{(s_j)})}{\left(R^{(e_m)} + R^{(s_j)}\right)^2 + \left(L^{(e_m)} + L^{(s_j)}\right)^2}$$

$$\hat{G}^{(s_j)} = \frac{R_0^{(s_j)}}{\left(R_0^{(s_j)}\right)^2 + \left(\frac{1}{C^{(s_j)}}\right)^2}$$

$$B^{(s_j)} = \frac{C^{(s_j)}}{\left(C^{(s_j)} * R_0^{(s_j)}\right)^2 + 1}$$

Equations 4.2.4.1.5 Parameter Calculation [2]

*Parameters used are presented in table 5.3.5.2

4.2.4.2 Results

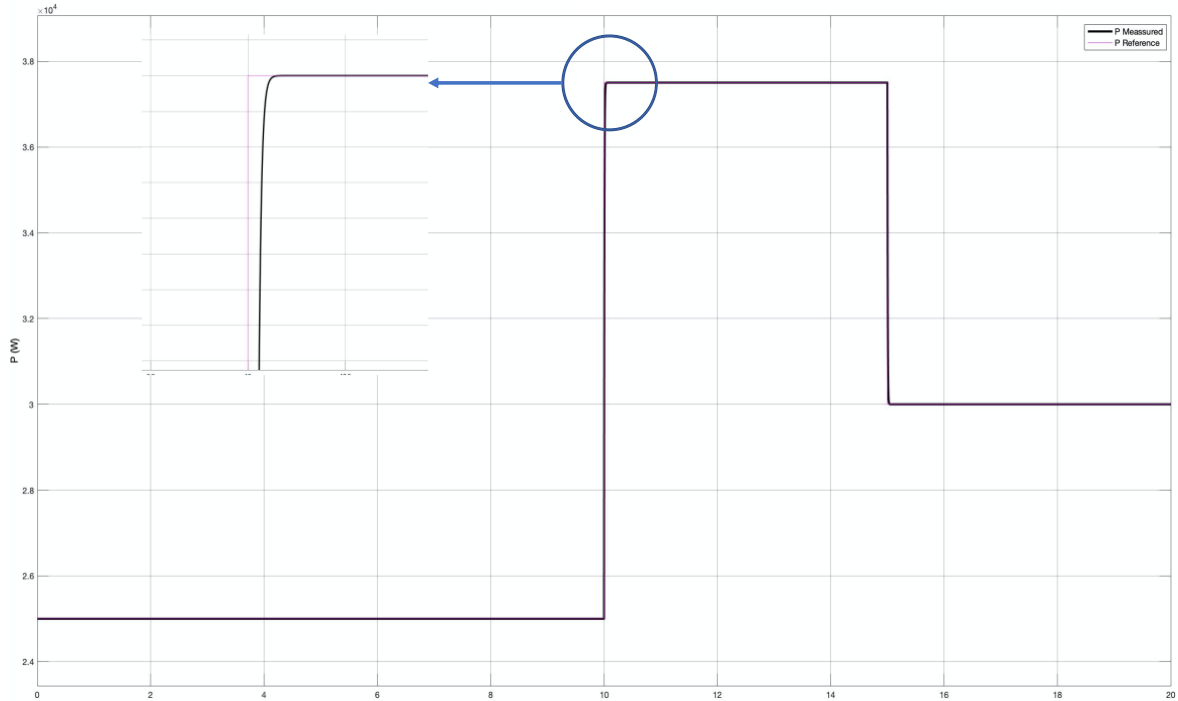


Figure 4.2.4.2.1 P Measured vs P Reference Plot

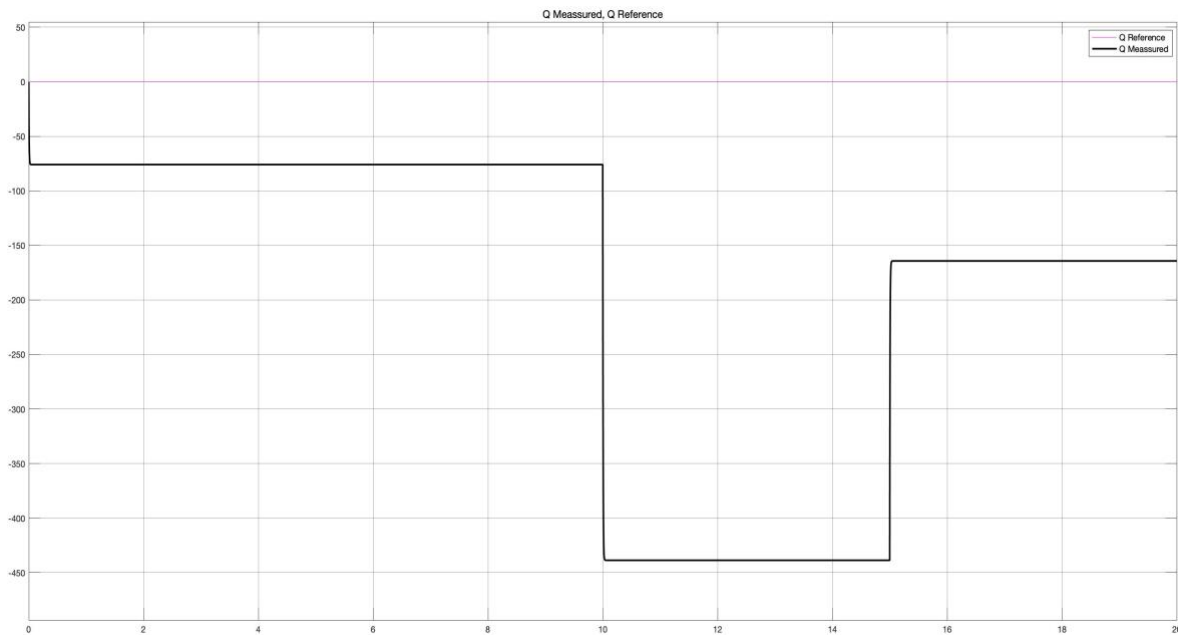


Figure 4.2.4.2.2 Q Measured vs Q Reference Plot

4.2.4.3 Conclusions

As it is expected, with these models, the whole dynamics of the physical components are not completely represented. The outputs seem to perfectly track the reference values, which makes sense because in this ROM2 the equations have been simplified from the original high-order model equations. If the results from the high-order model are compared with these results, there is a clear difference between both, the transients that can be seen in the high-order models can't be seen in the reduced-order models since the differential equations are not included in these reduced-order models.

The fact that the reduced-order model 2 does not have differential equations brought many problems. First of all, the first months were spent trying to find a solution or an alternative, but finally, it was discovered that Typhoon HIL is not available to work with the non-linearity of the algebraic loops and some other features such as the constant power load. Typhoon HIL was contacted and confirmed the problem, this was the reason why the models were implemented into Simulink.

The conclusions can be divided into two parts, The active power, and the reactive power.

The Active Power: The active power measurement follows perfectly the reference value. This should be expected, as the equations look really similar to the power flow equations from node j . Also, it can be spotted that there is a little difference between the reference slope and the measurement slope, this is caused because of the delays used to initialize the system.

The Reactive Power: The reactive power measurement has clear differences with the high-order model. While in the high-order model around 1.8 KVA are generated by the system, in this reduced order model, the reactive power is consumed. The maximum value that the reactive power takes is -450 VA which compared with the almost 40 KW being injected is a reasonable value.

Overall Performance: The model follows the reference of both active and reactive power. Also, the model is good enough when compared with the HOM since the response is similar

4.2.5 HIGH-ORDER MODEL

4.2.5.1 *Introduction and Problems Faced*

The model implemented will be based on the equations from [2] presented in Appendix I.

Before starting to implement the model, the initial conditions needed to be found. A MATLAB code was created in order to solve these initial conditions. The initial values of all the variables were calculated. And taken into Typhoon HIL

When implementing this model, some problems arise in relation to Typhoon HIL software. First of all, the model was implemented into Simulink. But when implementing the same model into Typhoon HIL the results weren't as expected, in fact the model did not even compile. A long time was spent debugging the model and changing some parameters.

The first problem faced was produced because of the simulation time-step, while on Simulink this time-step is automatic on Typhoon HIL the appropriate time-step needed to be found. Many values were tried until finally it was decided to use $T_s = 2^{-6}$ as the time step.

The second problem faced was Typhoon HIL's precision, Typhoon has single precision, in contrast to Simulink that has double precision. The numerical precision of the CPU was changed to double and the model now compiled. Finally, it was set to double precision. With this solved, the system was still unstable. So, the next step would be to try changing some parameters, the obvious parameters to change were the constants of both PI controls.

By choosing values for K_i and K_p in the Cascade controller, the output power tracked the power reference but somehow the frequency was not stable. This was caused because of the K_i of the PLL control being too big. It was making the system unstable. After testing many values for K_i , the optimal one was found.

Some pictures of the implemented model can be found in appendix I in addition to some codes used to calculate the initial conditions.

4.2.5.2 Parameters and Inputs

	<i>Table 4.2.5.2 : Parameters</i>	
	Parameter	Value
	$\omega^{(Sj)}$	377 rad/s
LCL Filter	$l_0^{(Sj)}$	$2.06374 * 10^{-3}$ H
	$l^{(Sj)}$	$30.6125 * 10^{-6}$ H
	$c^{(Sj)}$	$30.002852 * 10^{-6}$ F
	$r_0^{(Sj)}$	0.0407753 Ω
	$r^{(Sj)}$	0.1 Ω
	$\hat{r}_0^{(Sj)}$	0.427726 Ω
Network	$r^{(em)}$	$41.901 * 10^{-3}$ Ω
	$l^{(em)}$	$0.4 * 10^{-3}$ H
PLL	$K_{P\lambda}^{(Sj)}$	1
	$K_{I\lambda}^{(Sj)}$	0.32
Cascade Controller	$K_{P\gamma}^{(Sj)}$	$1.5 * 10^{-5}$
	$K_{I\gamma}^{(Sj)}$	0.1
Infinite Bus Voltage	<i>Voltage</i>	227 V
	<i>Angle</i>	0

The input power reference will be a time-varying signal in order to measure the capacity of the inverter to follow the power references.

$$Pr = \begin{cases} 25 \text{ kw} & \text{if}(t < 10) \\ 37,5 \text{ kw} & \text{if}(10 < t < 15) \\ 30 \text{ kw} & \text{if}(15 < t) \end{cases}$$

4.2.5.3 Results

The following results were obtained when implementing the model in Typhoon HIL:

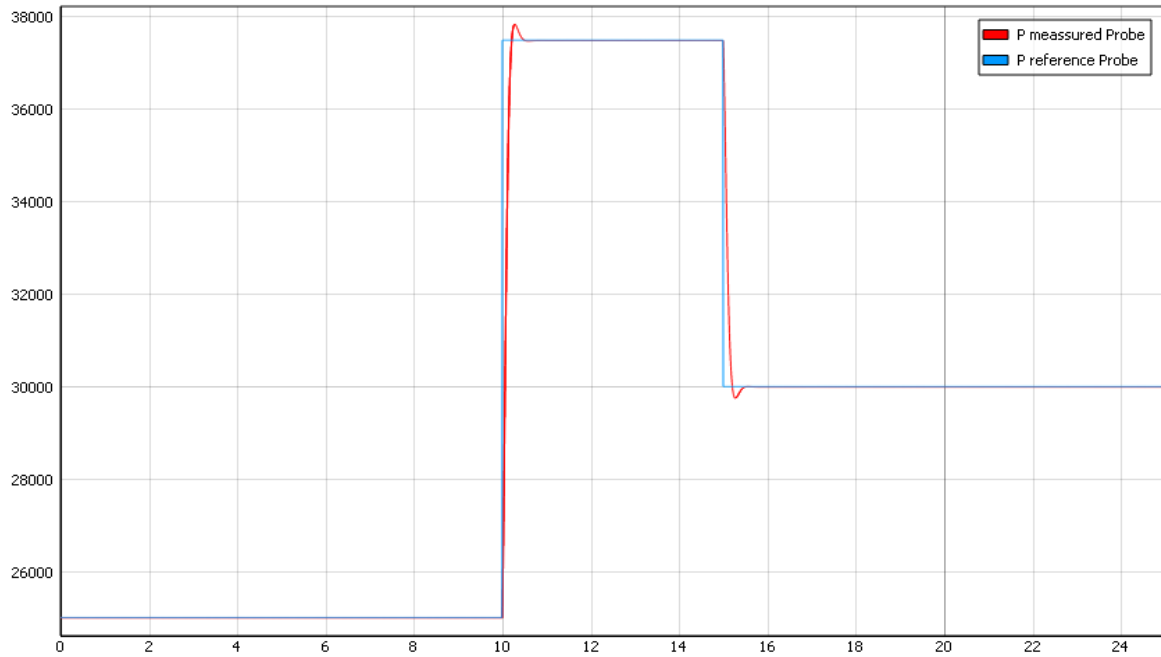


Figure 4.2.5.3.1 *P measured vs P reference plot*

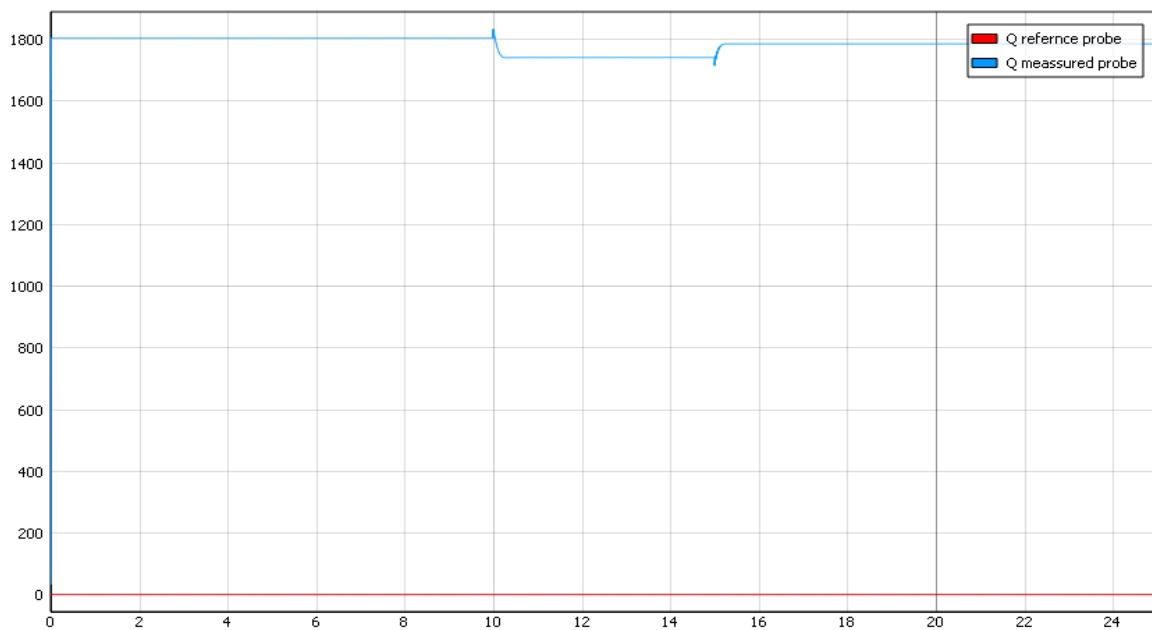


Figure 4.2.5.3.2 *Q measured vs Q reference plot*

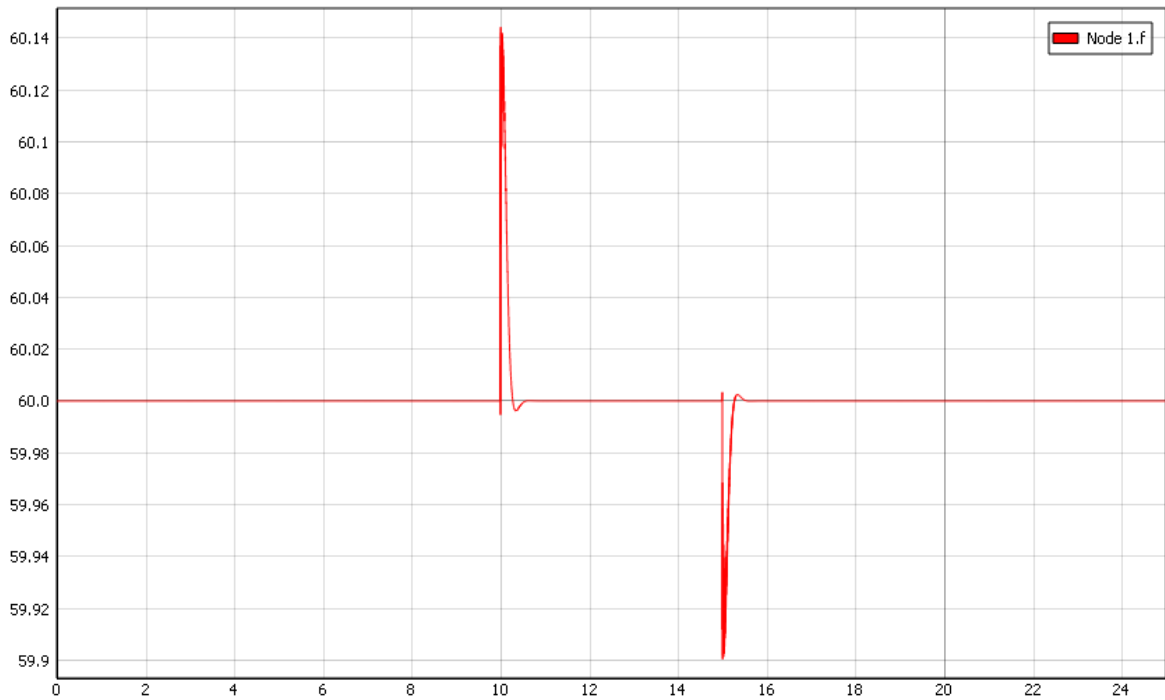


Figure 4.2.5.3.3 frequency plot

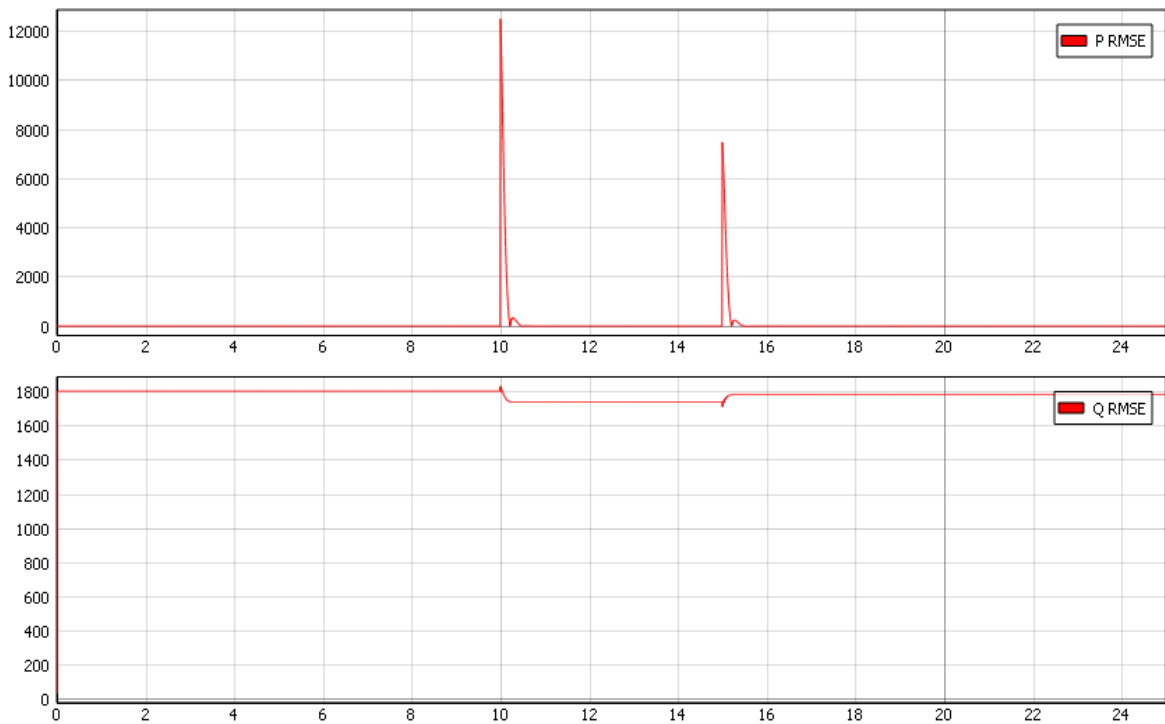


Figure 4.2.5.3.4 P RMSE – Q RMSE plot

4.2.5.4 Conclusions

As shown in the results section, the inverter follows the reference input perfectly especially with the active power, which is the most important. The conclusions will be divided into 3 parts, one for each of the most important results: Active Power, Reactive Power, and Frequency. The results of this high-order model represent all the transients and dynamics of the physical system. In contrast with the reduced-order model, some slight peaks in voltage, frequency, and power can be found in this high-order model results

Active Power: The active power output follows relatively well the input reference. As it can be seen, since there is a PI control, the error in the permanent regime is zero. Although the power has some peaks in the output, the time in which they occurred is small enough. It is important to keep in mind that the power is going from 25 kW to 37,5 kW which is a 150% increase in the reference.

Reactive Power: While the active power has no error in the permanent regime, the Reactive power does. This is because of the LCL filter, with it the output ripple reduces significantly but the capacitors are generating Reactive power, which is generating this constant RMSE error.

Frequency: The frequency stays within the limits (60.5-59.5 Hz) at all time, an increase of just 0.14Hz can be seen when changing the power references from 25 kW to 37,5 kW. The performance of the PLL controller is excellent.

Overall Performance: The model tracks the Active power references perfectly; The Ki was reduced to 0.001 in order to reduce the oscillations of the output. By reducing the oscillations, the price paid is to have a higher response time.

Also, the PLL is working perfectly, this can be seen in the small changes in the frequency, with such a big change in the power reference, the change in the frequency is just 0.14 Hz

4.3 GRID-FORMING INVERTER

4.3.1 INTRODUCTION

In this chapter, A Grid-Forming inverter model will be implemented into Typhoon HIL. Two models will be implemented, a high-order model, and a Reduced-order model. After the implementation, the fidelity of both models will be analyzed and compared.

The system to be implemented will be a simple one, in order to measure the performance of the grid-forming inverter model. This system will be a small microgrid formed by two grid-forming inverters connected to an RLC load.

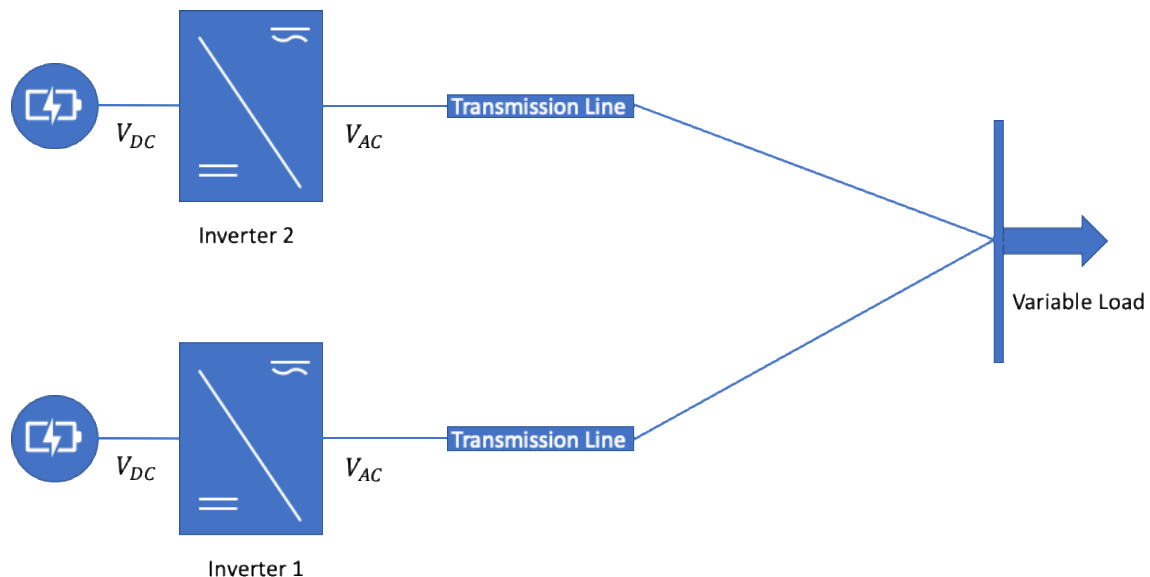


Figure 4.3.1.1 Model Scheme 1

In this system, the voltage needs to be fixed by both inverters, because this microgrid is working on islanded mode. Both inverters are converting to AC power the DC power coming from two battery storage units. For this model, the objectives are maintaining the voltages close to 1 p.u and frequency close to nominal (60Hz). Both inverters are seen from the load as voltage sources. As two inverters are being used in parallel, a droop control needs to be implemented

The performance of the models will be tested by changing the RLC load constantly and measuring how close to nominal values voltage and frequency are.

The following figure will help to illustrate the model.

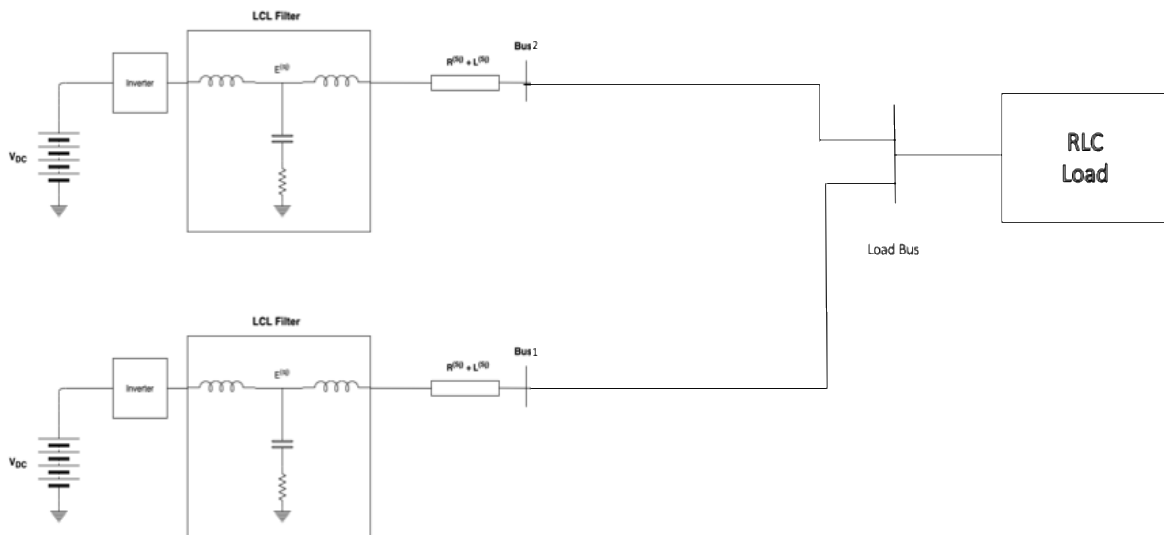


Figure 4.3.1.2 Inverter Scheme 2

Figure 4.3.1.2 tries to illustrate what the connections in this particular case are. It is important to notice that the system is a three-phase system.

The LCL filter is the same for the grid-forming inverter as for the grid-feeding inverter, so please refer to part 5.2.1 to review the LCL filter scheme. Another thing to take into consideration is that the two inverters have different ratings.

Also, as there are two inverters working in parallel a droop control has been included and will be presented with more details in the next part. For this implementation, three models will be implemented, first of all, both inverters. The model for the inverters will have incorporated into them all the components from the battery, to nodes 1 or 2 depending on which generator are we talking about. So basically, even the short transmission line will be inherent to the inverter model. Then the load model will be implemented separately and will have as inputs the current coming from both inverters and have as outputs the voltage. The last important consideration is that as both inverters are not the same, and have different bases, a base change in the currents needs to be done before inputting them to the load.

The Droop Control has the following Equations:

$$e_{rq[\alpha^{(j)}(t)]}^{(s_j)}(t) = E_B^{(s_j)} \left(E_0^{(s_j)} + \frac{1}{d_E^{(s_j)}} \left(Q_r^{(s_j)} - Q_f^{(s_j)}(t) \right) \right),$$

$$\omega^{(s_j)}(t) = \omega_0 + \frac{1}{d_\omega^{(s_j)}} \left(P_r^{(s_j)} - P_f^{(s_j)}(t) \right),$$

Equation 4.3.2.1. Droop control [2]

Where $P_f^{(s_j)}$ and $Q_f^{(s_j)}$ are the measured output active and reactive power respectively and $d_w^{(s_j)}$ and $d_E^{(s_j)}$ are the Frequency and the Voltage Droop coefficients respectively. This control is really intuitive since it is known the decoupled relationships Voltage-Reactive Power and Frequency-Active Power. Basically, if the Voltage is different from the reference, the reference input for the cascade controller will increase, in order to increase the Reactive power injection and therefore the Voltage and in the same way, if the output frequency is not equal to the reference, the reference for the cascade controller to track will increase in order to increase the Active power injection and therefore the frequency. (This works for an increase but also for reduction if the Output exceeds the reference.)

The following schemes obtained from [11] will help understand the model:

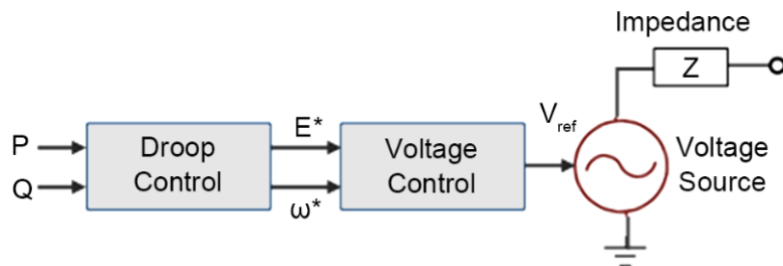


Figure 5.2.2.2 Simplified Inverter Control scheme [11]

The figure above shows a simplified model just to illustrate what the outputs and the inputs to each control stage are, also to give an overview.

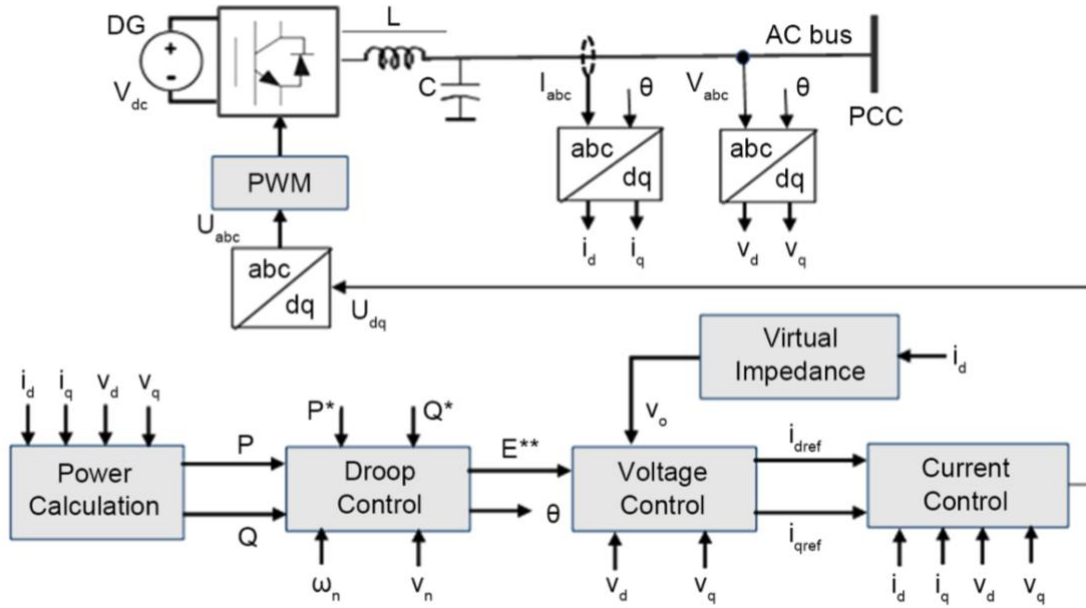


Figure 5.2.2.3 Inverter Control scheme [11]

This scheme shows in detail how each inverter is controlled and how is the transition through the control stages, starting with the measurement of the output current and voltage

The Load Equations: As mentioned before, the model for the load will be an RLC load model with varying values that will be presented in part 5.4.3. The model dynamics are represented in the following equations.

$$\frac{C^{(l_3)}}{\omega_0} \frac{dV_{q[\omega_0 t]}^{(l_3)}(t)}{dt} = -\frac{1}{R^{(l_3)}} V_{q[\omega_0 t]}^{(l_3)}(t) - C^{(l_3)} V_{d[\omega_0 t]}^{(l_3)}(t) - I_{lq[\omega_0 t]}^{(l_3)}(t) + I_{q[\omega_0 t]}^{(l_3)}(t),$$

$$\frac{C^{(l_3)}}{\omega_0} \frac{dV_{d[\omega_0 t]}^{(l_3)}(t)}{dt} = -\frac{1}{R^{(l_3)}} V_{d[\omega_0 t]}^{(l_3)}(t) + C^{(l_3)} V_{q[\omega_0 t]}^{(l_3)}(t) - I_{ld[\omega_0 t]}^{(l_3)}(t) + I_{d[\omega_0 t]}^{(l_3)}(t),$$

$$\frac{L^{(l_3)}}{\omega_0} \frac{dI_{lq[\omega_0 t]}^{(l_3)}(t)}{dt} = -L^{(l_3)} I_{ld[\omega_0 t]}^{(l_3)}(t) + V_{q[\omega_0 t]}^{(l_3)}(t),$$

$$\frac{L^{(l_3)}}{\omega_0} \frac{dI_{ld[\omega_0 t]}^{(l_3)}(t)}{dt} = L^{(l_3)} I_{lq[\omega_0 t]}^{(l_3)}(t) + V_{d[\omega_0 t]}^{(l_3)}(t),$$

Equation 5.2.2.2 Load Dynamic Equations [2]

4.3.3 PARAMETER AND VARIABLES DEFINITION

<i>Table 4.3.3.1 : Parameters</i>	
Parameter (p.u)	Physical equivalent
$\omega_c^{(Sj)}$	The measurement filter cut-off frequency, in radians per second
$P_r^{(Sj)}$	Real power reference
$Q_r^{(Sj)}$	Reactive power reference
$L_0^{(Sj)}$	LCL filter inductance
$L^{(Sj)}$	LCL filter inductance
$C^{(Sj)}$	LCL filter capacitance
$R_0^{(Sj)}$	Inverter and filter Resistance
$R^{(Sj)}$	Inverter and filter Resistance
$\hat{R}^{(Sj)}$	Inverter and filter Resistance
$R^{(em)}$	Transmission line Resistance
$L^{(em)}$	Transmission line Inductance
$K_{P\phi}^{(Sj)}$	Proportional Gain of the Voltage Controller
$K_{I\phi}^{(Sj)}$	Integral Gain of the Voltage Controller
$K_{P\gamma}^{(Sj)}$	Proportional Gain of Current Controller
$K_{I\gamma}^{(Sj)}$	Integral Gain of the Current Controller
$D_\omega^{(Sj)}$	Normalized Frequency Droop Coefficient
$D_E^{(Sj)}$	Normalized Voltage Droop Coefficient

Table 4.3.3.2: Variables

Variable (p.u)	Physical equivalent
$V_{DC}^{(s_j)}$	DC voltage at the inverter input (Battery voltage)
$E^{(s_j)}$	Internal voltage of the inverter
$\hat{E}^{(s_j)}$	LCL filter capacitor voltage
$V^{(s_j)}$	Voltage at bus j
$\Xi^{(s_j)}$	Inverter output current
$I^{(s_j)}$	Filtered inverter output current
$\Gamma^{(s_j)}$	State variable for the current controller
$\phi^{(s_j)}$	State variable for the phase-locked loop
$P_f^{(s_j)}$	Filtered real power measured
$Q_f^{(s_j)}$	Filtered reactive power measured

4.3.4 REDUCED-ORDER MODEL

4.3.4.1 Introduction and Problems Faced

In this case, the reduced-order model equations of the grid-forming inverters will be implemented into Typhoon HIL. All of the problems faced with the grid-feeding inverter appeared with this model as well. First of all, the initial conditions needed to be found, so a MATLAB code was created in order to obtain them. Then the model was implemented into Typhoon HIL by using delay blocks in order to initialize the model with the appropriate initial conditions. However, as with the grid-feeding inverter, Typhoon HIL could not handle the non-linearity of the algebraic loops. After contacting and informing Typhoon HIL, the models were finally implemented into Simulink.

The equations for the grid-forming inverter reduced-order model 2 will be presented below:

$$\begin{aligned}
 D_{\omega}^{(s_j)} \frac{d\hat{\theta}^{(s_j)}(t)}{dt} &= \mathbf{P}_r^{(s_j)} - \mathbf{P}_f^{(s_j)}(t), \\
 \frac{1}{\omega_c^{(s_j)}} \frac{d\mathbf{Q}_f^{(s_j)}(t)}{dt} &= -B^{(s_j)} \left| \vec{\mathbf{V}}^{(l_j)}(t) \right|^2 - \left| \vec{\mathbf{V}}^{(l_j)}(t) \right| \left| \vec{\mathbf{E}}^{(s_j)}(t) \right| \left(G^{(s_j)} \sin \left(\hat{\theta}^{(s_j)}(t) \right. \right. \\
 &\quad \left. \left. - \theta^{(l_j)}(t) \right) - B^{(s_j)} \cos \left(\hat{\theta}^{(s_j)}(t) - \theta^{(l_j)}(t) \right) \right) - \mathbf{Q}_f^{(s_j)}(t), \\
 \frac{1}{\omega_c^{(s_j)}} \frac{d\mathbf{P}_f^{(s_j)}(t)}{dt} &= G^{(s_j)} \left| \vec{\mathbf{E}}^{(s_j)}(t) \right|^2 - \left| \vec{\mathbf{V}}^{(l_j)}(t) \right| \left| \vec{\mathbf{E}}^{(s_j)}(t) \right| \left(G^{(s_j)} \cos \left(\hat{\theta}^{(s_j)}(t) \right. \right. \\
 &\quad \left. \left. - \theta^{(l_j)}(t) \right) + B^{(s_j)} \sin \left(\hat{\theta}^{(s_j)}(t) - \theta^{(l_j)}(t) \right) \right) - \mathbf{P}_f^{(s_j)}(t),
 \end{aligned}$$

with

$$\left| \vec{\mathbf{E}}^{(s_j)}(t) \right| = \frac{\left(K_{P\phi}^{(s_j)} \right)^2 \left(E_0^{(s_j)} + \frac{1}{D_E^{(s_j)}} \left(\mathbf{Q}_r^{(s_j)} - \mathbf{Q}_f^{(s_j)}(t) \right) \right)}{C^{(s_j)^2 \left(1 + K_{P\phi}^{(s_j)} \hat{R}_0^{(s_j)} \right)^2 + \left(K_{P\phi}^{(s_j)} \right)^2},$$

Equation 4.3.4.1.1 Grid-Feeding Inverter Reduced-Order Model 2 Equations [2]

Also, equations 4.3.4.1.2 Represent the parameters of the equations.

$$G(s_j) = \frac{R^{(e_m)} + R^{(s_j)}}{\left(R^{(e_m)} + R^{(s_j)}\right)^2 + \left(L^{(e_m)} + L^{(s_j)}\right)^2}$$

$$B(s_j) = \frac{-(L^{(e_m)} + L^{(s_j)})}{\left(R^{(e_m)} + R^{(s_j)}\right)^2 + \left(L^{(e_m)} + L^{(s_j)}\right)^2}$$

Equation 4.3.4.1.2 Grid-Forming Inverter Reduced Order Model Parameters [2]

The equations of the reduced-order model 2 in this case, have some differential equations so the work is easier since there are not so many algebraic loops.

5.3.4.2 Results

Now, the results obtained will be presented:

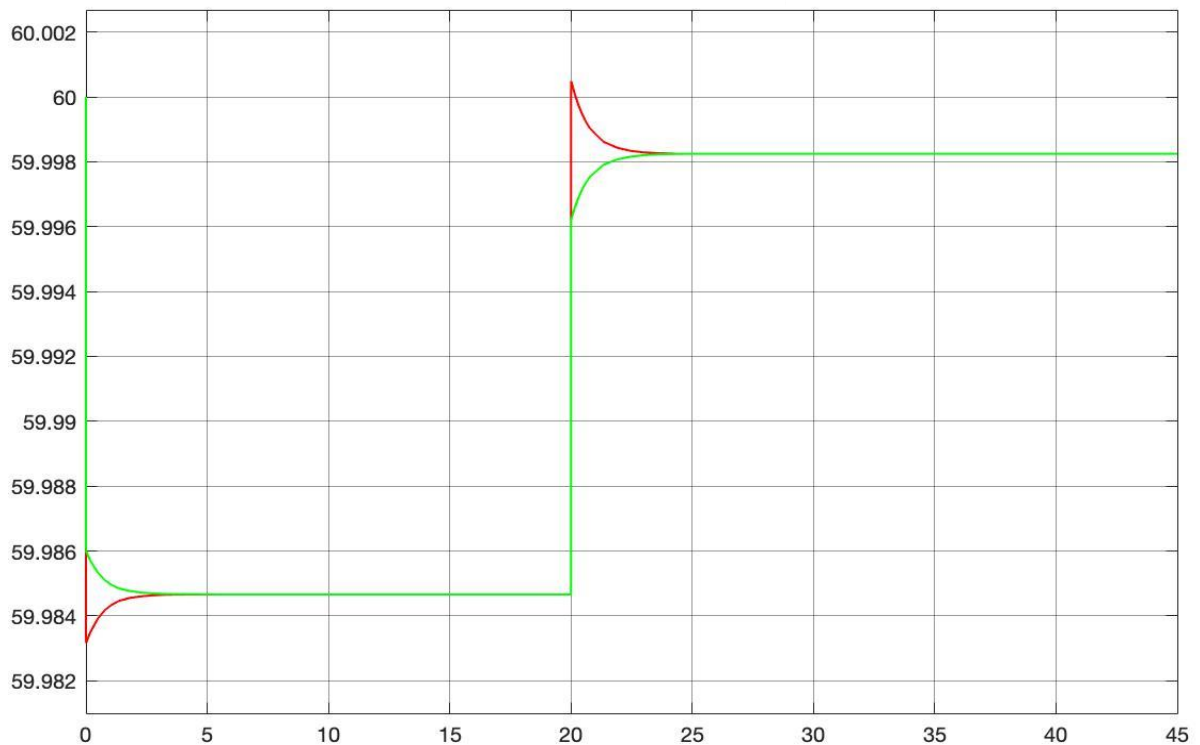


Figure 4.3.4.2.1 Inverters 1 and 2 Frequency (Hz)

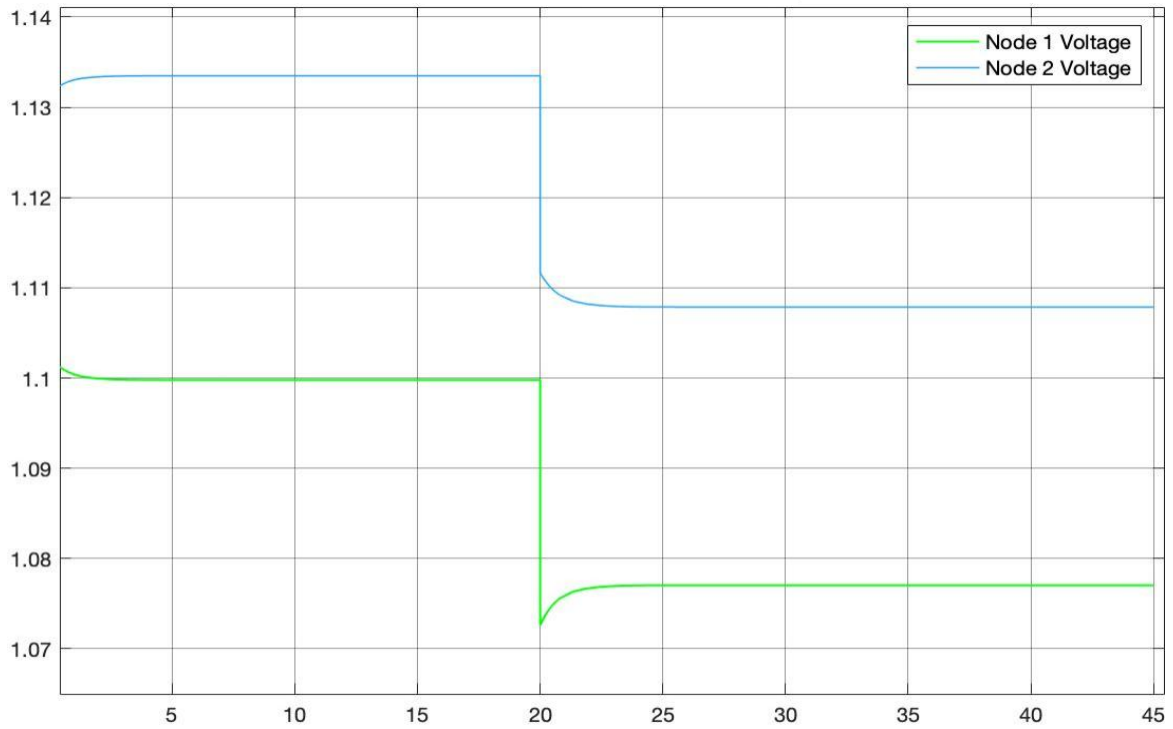


Figure 4.3.4.2.2 Voltage 1 and Voltage 2 (p.u)

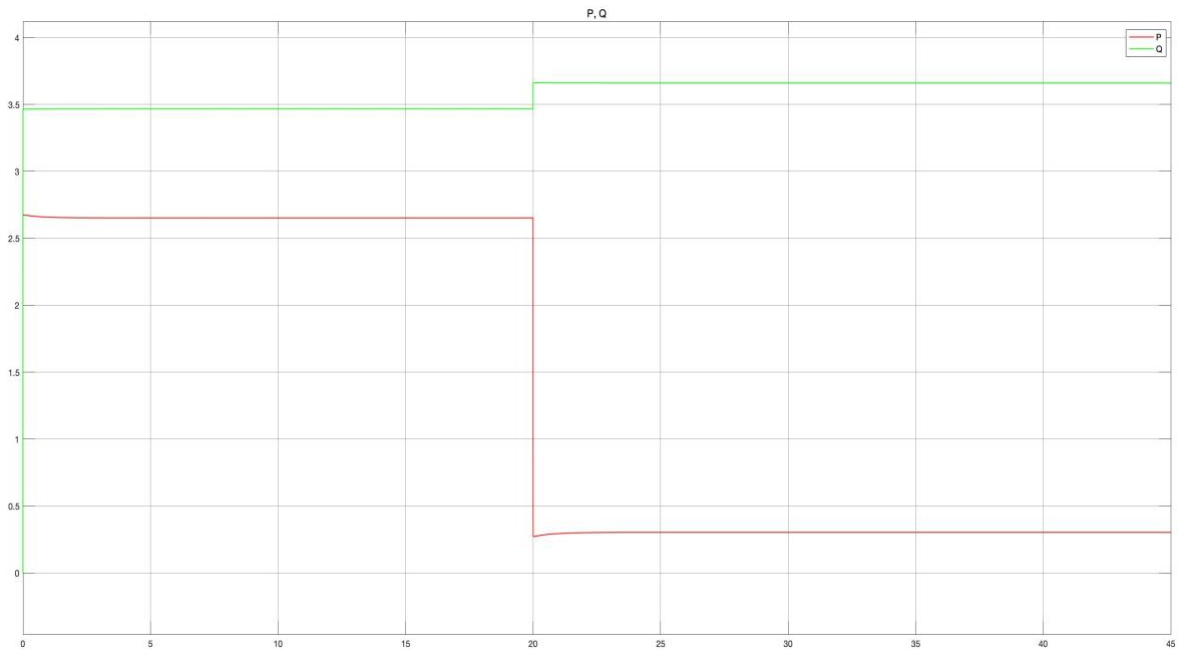


Figure 4.3.4.2.3 Total P and Q injected (p.u)

4.3.4.3 Conclusions

In this case, the results were similar to the high-order model. As it can be seen there are some transients that are not present in this reduced-order model. The reason why both models are similar is that in this ROM 2 there are differential equations that somehow represent the dynamics of the system. Also, it can be seen that the slopes in this reduced-order model are much steeper. The output, in this case, follows the reference more rapidly than on the other model.

The conclusions will be divided into 4 parts: Voltage, Frequency, Power injected, and finally overall performance

Voltage: It is remarkable that the voltages of both inverters are really high. The voltage of the load was not shown, but it stayed at 1 p.u at all times. Therefore, even though the voltage is high at the inverter, as the voltage at the load is 1 p.u it means that the inverters are increasing their voltage to provide a 1 p.u voltage at the load. It is important to mention that the voltage of the inverter is the voltage of the capacitor of the LCL filter which will differ with the ‘real’ output voltage of the inverter.

Frequency: In this case, in contrast with the HOM, oscillations cannot be observed. This is because they are part of the dynamics of the inverter, and in this model that part is not represented. The frequency of both inverters quickly converges back to the expected value. The performance of the frequency controller is excellent.

Power Injected: In the same way that oscillations cannot be observed in the frequency, also in the power injected the oscillations do not appear in this model. It is important to mention that even though the values in p.u seem high, it is because of the base chosen, both values calculated in each inverter’s base are less than 1 p.u, so the results are acceptable

Overall Performance: The performance of the model is excellent. It follows the reference faster than the high-order model. The dynamics of the model are not completely represented in this model because of the simplifications done. These simplifications explain why the oscillations do not appear in the outputs of the reduced-order models

4.3.5 HIGH-ORDER MODEL

4.3.5.1 *Introduction and Problems Faced*

In this chapter, the model of a grid-forming inverter will be implemented. More precisely, a microgrid composed of two grid-forming inverters and an RLC load. The equations from [2] that can be found on appendix I, were implemented into Typhoon HIL

During the implementation of these models, a few problems arise.

Before starting with the implementation of the model, the initial conditions for all the parameters and variables needed to be obtained. A MATLAB code was created in order to obtain these conditions and also another one that gave as outputs the parameters in the format that Typhoon HIL requires them.

Also, the same problems that Typhoon HIL had with the grid-feeding inverter, are occurring with this model. The models were first implemented into Simulink, but when implementing the same models into Typhoon HIL, the models were not working. After changing the numerical precision of the CPU to double (Typhoon HIL has Single as default) and looking for the appropriate time step (finally it was decided to use $T_s = 2^{-6}$ as the time step). The model compiled.

Now the model compiled but not converged to de desired value. Some changes were made in the droop coefficients of both inverters until the outputs converged to de desired reference values. In order for the inverters to generate power according to their bases, the Droop coefficients needed to be the same for both inverters. Finally, the values chosen were $D_\omega = 14.263$ and $D_E = 3.337$. In this case, the constants for both PI controllers weren't changed since the parameter optimized for the grid-feeding inverter worked also with this model.

Some pictures of the implemented model and the codes used to calculate the initial conditions can be found in appendix I.

4.3.5.2 Parameters and Inputs

	<i>Table 4.3.5.2 : Parameters</i>			
	Inverter 1		Inverter 2	
	Parameter	Value	Parameter	Value
	$\omega^{(s_j)}$	377 rad/s	$\omega_2^{(s_j)}$	377 rad/s
Rated Power	$S_1^{(s_j)}$	10 KVA	$S_2^{(s_j)}$	12 KVA
LCL Filter	$l_0^{(s_j)}$	$6 * 10^{-3} H$	$l_{02}^{(s_j)}$	$6 * 10^{-3} H$
	$l^{(s_j)}$	$3 * 10^{-4} H$	$l_2^{(s_j)}$	$3 * 10^{-4} H$
	$c^{(s_j)}$	$150 * 10^{-6} F$	$c_2^{(s_j)}$	$150 * 10^{-6} F$
	$r_0^{(s_j)}$	0.1 Ω	$r_{02}^{(s_j)}$	0.1 Ω
	$r^{(s_j)}$	$3 * 10^{-2} \Omega$	$r_2^{(s_j)}$	$3 * 10^{-2} \Omega$
	$\hat{r}_0^{(s_j)}$	$15 * 10^{-3} \Omega$	$\hat{r}_{02}^{(s_j)}$	$16 * 10^{-3} \Omega$
Network	$r^{(em)}$	0.35 Ω	$r_2^{(em)}$	0.4 Ω
	$l^{(em)}$	$1.5 * 10^{-3} H$	$l_2^{(em)}$	$2 * 10^{-3} H$
PLL	$K_{P\phi}^{(s_j)}$	$5 * 10^{-3}$	$K_{P\phi_2}^{(s_j)}$	$5 * 10^{-3}$
	$K_{I\phi}^{(s_j)}$	10	$K_{I\phi_2}^{(s_j)}$	10
Cascade Controller	$K_{P\gamma}^{(s_j)}$	$5 * 10^{-3}$	$K_{P\gamma_2}^{(s_j)}$	$5 * 10^{-3}$
	$K_{I\gamma}^{(s_j)}$	$10 * 10^{-3}$	$K_{I\gamma_2}^{(s_j)}$	$10 * 10^{-3}$
References	<i>Voltage</i>	227 V RMS	<i>Voltage</i>	227 V RMS
	<i>Frequency</i>	60 Hz	<i>Frequency</i>	60 Hz
Droop Controller	D_ω	14.263	D_{ω_2}	14.263
	D_E	3.337	D_{E_2}	3.337
Battery Voltage	V_{dc1}	900 V	V_{dc2}	900 V

The Load will be an RLC changing load, in order to measure the ability of both inverters to maintain voltage and frequency close to nominal values.

The load will be changing according to the following function:

$$R_{load} = \begin{cases} 0.373 p.u & if(t < 20) \\ 6.469 p.u & if(t \geq 20) \end{cases}$$

$$L_{load} = \begin{cases} 0.268 p.u & if(t < 20) \\ 0.244 p.u & if(t \geq 20) \end{cases}$$

$$C_{load} = \begin{cases} 0.373 p.u & if(t < 20) \\ 0.408 p.u & if(t \geq 20) \end{cases}$$

Equation 4.3.5.2 Load distribution

The base used in this simulation is $S_{base} = 10 KVA$.

Also, the dynamic equations for the load were presented before in 4.3.1

4.3.5.3 Results

The following results were obtained when implementing the models into Typhoon HIL.

More results will be presented in Appendix I, to make this Thesis as concise as possible. Please refer to this appendix to see the complete equations implemented, or more detailed results. Also, some pictures of the model implemented in case the reader wants to get an insight of how the implementation looks like.

The results provided have incorporated an optimized selection of parameters, such as voltage and frequency droop coefficients and also the cut-off frequency.

In the following pages the most relevant results will be shown: The load voltage, Inverters frequency, Inverters voltage, and finally P and Q consumed by the load. In this case, the results are shown in per unit representation.

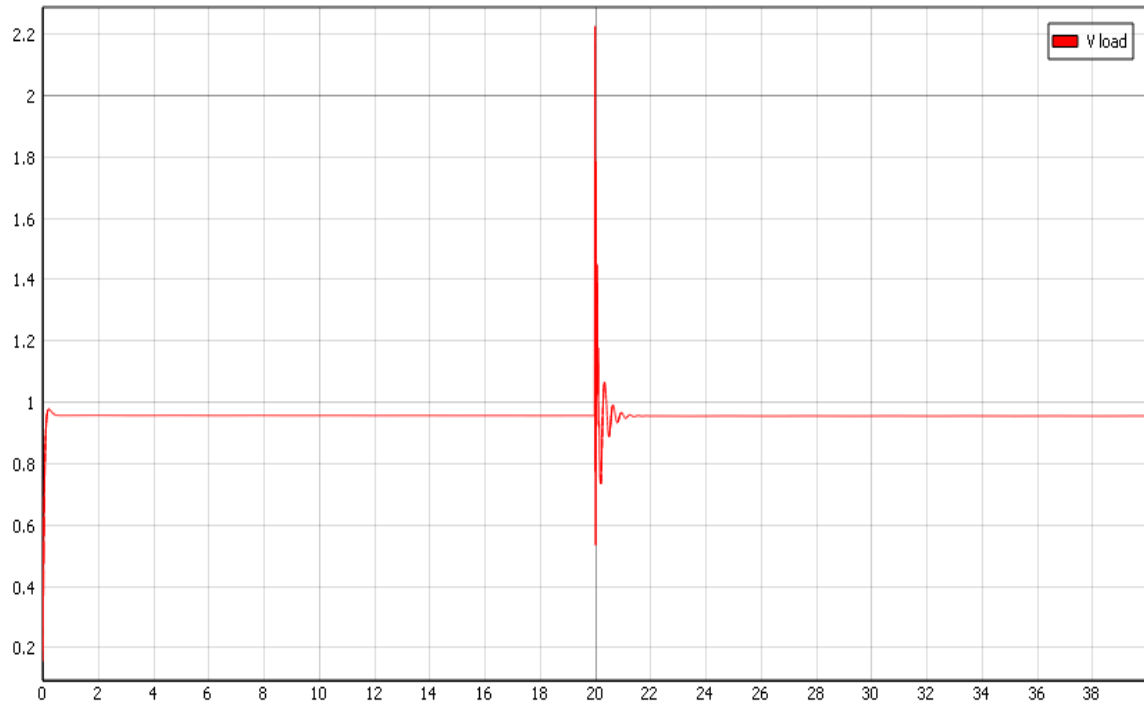


Figure 4.3.5.3.1 Load Voltage



Figure 4.3.5.3.2 Inverter's Voltage

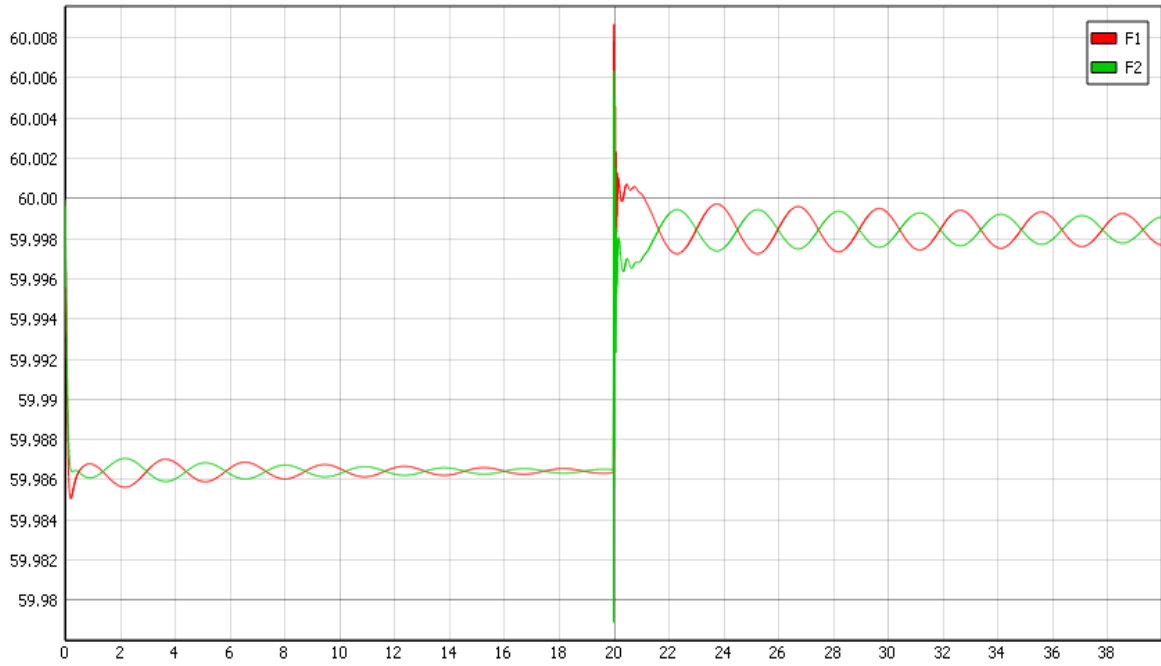


Figure 4.3.5.3.3 Inverter's Frequency



Figure 4.3.5.3.4 Total P and Q

4.3.5.4 Conclusions

The results for the grid-forming inverter are excellent. And both voltage and frequency stay between the allowable limits. The result analysis will be divided into three main blocks. First of all, the voltage, then the frequency and finally the Power consumed by the load. It is also important to realize that both inverters have different bases.

Voltage: Inverter's voltage seems slightly high (values up to 1.09 p.u). But looking at the load's voltage, it is obvious that this is because the inverters are increasing their voltage in order to increase the load's voltage and maintain its value close to 1 p.u. The most important voltage to analyze is the load's voltage, and it is constantly between the limits ($0.95 \leq V_l \leq 1.05$). Also, the voltage on the inverters stays always in the range ($0.90 \leq V_i \leq 1.1$). It is important to mention that the voltage that is being controlled is the load's voltage. To conclude, the voltage control performance is extraordinary.

Frequency: In this case, there is no need to measure the load's frequency and it will be considered to be the same as the inverter's frequency. Both inverter's frequency is as expected, with values in the range ($59.98 \text{ Hz} \leq f \leq 60.006 \text{ Hz}$), at all times including transients. The frequency first oscillates around the desired frequency and finally converges to this value.

Power Consumed: Looking at the total power plots, it is clear that both Active and Reactive power are stable. Power is not included in any control's objectives, but it is necessary to make sure that the values are constants since the load is only changing at $t = 20\text{s}$. Power generation is not the same on both inverters, because they have different bases, but the power generation is distributed according to Droop control equations. The power generated by each inverter can be found in appendix I.

Overall Performance: As discussed in the previous paragraphs, this model is working perfectly on its job of providing constant voltage and with an appropriate frequency to the load. Both inverters can provide this constant voltage even with changing loads.

4.4 MICROTURBINE V-F

4.4.1 INTRODUCTION

In this section, a model of a microturbine will be presented. A microturbine can also be seen as a Diesel engine connected to a synchronous machine. The model of a Diesel engine and a synchronous machine will be implemented into Typhoon HIL. The microturbine V-f model is working islanded, connected to a load. As shown in figure 4.4.1.1

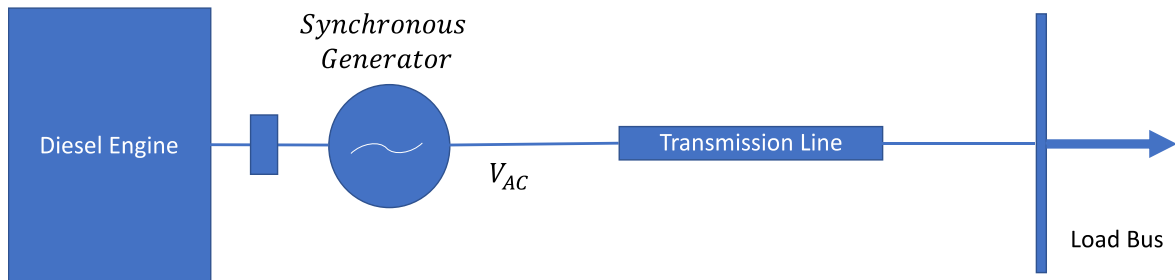


Figure 4.4.1 Microturbine V-F model scheme

This model is similar to the grid-forming inverter model since the microturbine is providing power to the load by fixing the voltage and frequency. The load sees the generator as a voltage source that provides power at constant voltage and frequency. The other mode of operation of the microturbine (Which is not implemented in this thesis) would be the P-Q mode, where the voltage and frequency would be fixed by the network or other generator and the generator will be just providing the desired P and Q to the load.

The performance of the microturbine will be tested by changing the load's value and measuring the ability of the model to maintain the voltage and frequency constant. The model implementation could be divided into the implementation of the following individual components that all together form the microturbine: Damper windings, stator windings and short transmission line, excitation system, governor control, and diesel engine

4.4.2 TOPOLOGY AND CONTROLS

In this part, the topology of the microturbine will be described. As mentioned before, the microturbine models could be divided into some elements that all together form the microturbine model. This section will be divided into parts, one for each part of the model. To keep this thesis short, the equations will be presented in appendix II.

4.4.2.1 Damper Windings

Damper windings that can also be called squirrel cage windings are a set of short-circuited windings around the rotor. They have two principal objectives in the synchronous machine.

1. When a change in the load or a change in excitation occurs. The rotor will move to its new position; however, it could stay oscillating around that point, with the danger of losing synchronism. In these cases where the speed of the rotor is temporarily different from the electrical speed, a current is induced in the damper windings. This current produces a force that brings back the rotor to nominal speed.
2. These windings also produce the necessary torque to start the machine, for the same principle mentioned before. The machine will start the same way as an induction machine. Until finally, the induction current in the damper windings will be zero when the machine has reached synchronism

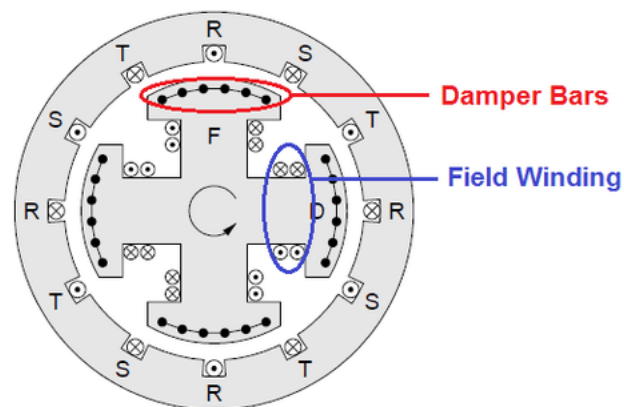


Figure 4.4.2.1 Damper Windings Scheme [14]

4.4.2.2 Stator Windings and Short Transmission line

This model is just a three-phase winding connected to the transmission line, the three-phase alternating voltage generates a rotating magnetic field that rotates at the electrical speed. This model is formed by the synchronous reactance and the resistance of the stator winding, connected to the short transmission line parameters. The synchronous reactance groups together all the magnetic effects in the stator.

4.4.2.3 Excitation System

For the excitation system, IEE DC1 Exciter was chosen and implemented. As a brief introduction to the excitation system, it could be said that the excitation system is in charge of controlling the voltage. In this islanded mode, its job is crucial since the voltage needs to be constantly regulated. The exciter can modify the voltage in the following way: the rotor has a DC winding which produces an electric field rotating at the rotor's speed. The magnitude of this electric field depends on the DC current going through the rotor DC windings. The excitation system changes this current to maintain the voltage close to 1 p.u.

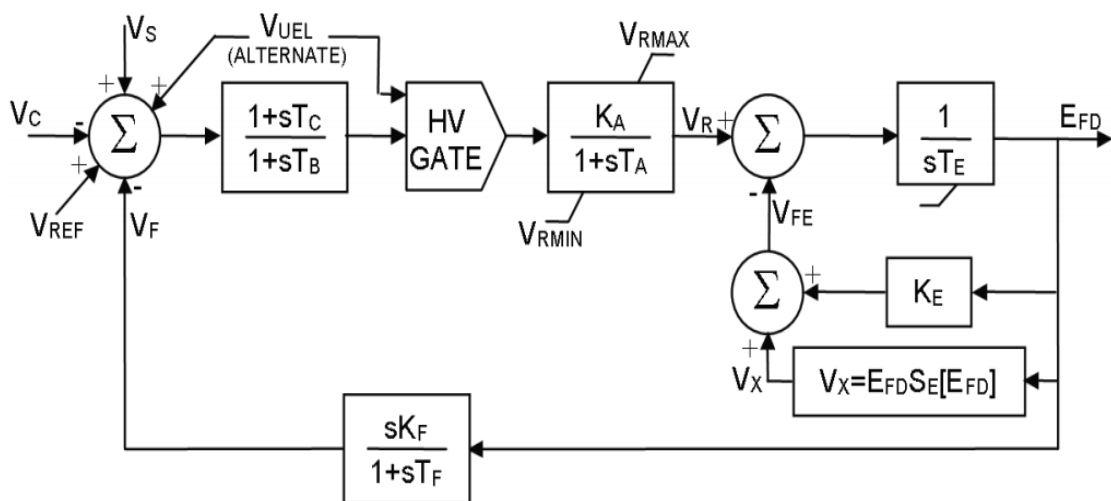


Figure 4.4.2.3 IEE DC1 Exciter Scheme [15]

4.4.2.4 Governor

The governor chosen and implemented was the DEGOV1 model. The governor is in charge of maintaining the frequency close to 60 Hz. The governor controls the diesel engine by changing the amount of fuel going into the motor. The governor has as an input the frequency and adjusts the diesel engine speed to meet the frequency requirements. Also, when the microturbine is not working on islanded mode, by following the frequency reference also the active power required is generated.

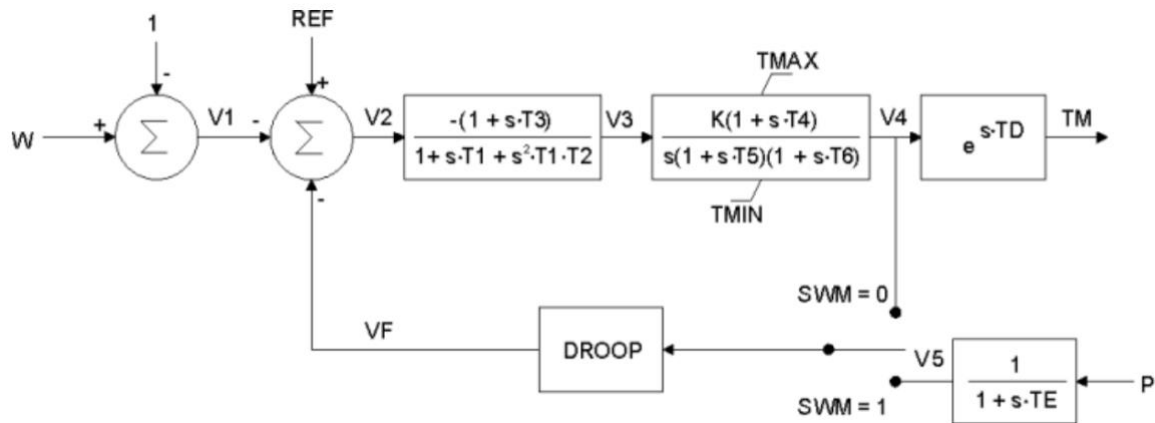


Figure 4.4.2.4. DEGOV1 Scheme [16]

4.4.2.5 Diesel Engine

A diesel engine model was implemented, the diesel engine is connected to the synchronous machine in order to generate electric power. The speed of the diesel engine is regulated by the governor model.

All the models presented above are appropriately connected with each other and form the microturbine V-f model. The functioning is the following: The Diesel engine is regulated by the governor and tries to maintain frequency at 60 Hz, the diesel engine then is connected to the rotor of the synchronous machine. The voltage of the machine is regulated by the Excited, which regulates the DC current of the rotor to maintain voltages close to 1 p.u. This way, both the voltage and the frequency are regulated in this model.

4.4.3 PARAMETER AND VARIABLES DEFINITION

Parameter (p.u)	Physical equivalent
$X_k^{(Sj)}$	Machine leakage reactance
$X^{(Sj)}$	Machine stator reactance
$X'^{(Sj)}$	Machine transient reactance
$X''^{(Sj)}$	Machine sub-transient reactance
$X_{k2}^{(Sj)}$	Leakage reactance
$X_{k1}^{(Sj)}$	Leakage reactance
$X_{kf}^{(Sj)}$	Leakage reactance
$X_m^{(Sj)}$	Mutual reactance
$R_2^{(Sj)}$	Winding resistance
$R_1^{(Sj)}$	Winding resistance
$R^{(Sj)}$	Per-Phase line resistance
$X^{(Sj)}$	Per-Phase line inductance
ω_0	Nominal frequency (rad/s)
$V_r^{(Sj)}$	Reference voltage magnitude
$V_{Kp}^{(Sj)}$	Proportional control gain
$V_{Ki}^{(Sj)}$	Integral control gain
$\tau_u^{(Sj)}$	Amplifier time constant
$K_u^{(Sj)}$	Amplifier Gain
$X_f^{(Sj)}$	Field winding reactance
$R_f^{(Sj)}$	Field winding resistance

Parameter (p.u)	Physical equivalent
$L_f^{(s_j)}$	Unsaturated field inductance
$K_g^{(s_j)}$	Slope of the unsaturated part of the saturation curve
$\bar{R}_f^{(s_j)}$	Exciter circuit resistance
$\tau_1^{(s_j)}, \tau_2^{(s_j)}, \tau_3^{(s_j)} \dots$	Time constants of the control system
$\kappa^{(s_j)}$	Controller gain of the actuator
$P_f^{(s_j)}$	Power change setting
$M^{(s_j)}$	Inertia of the machine
$\bar{D}_0^{(s_j)}$	Friction and windage dumping
$R_D^{(s_j)}$	Droop coefficient

$$\bar{D}_0^{(s_j)} = \frac{1}{R_D^{(s_j)} * \omega_0}$$

Table 4.4.3.2: Variables

Variable (p.u)	Physical equivalent
$\phi^{(s_j)}$	Flux linkage of the damper windings
$E_r^{(s_j)}$	Flux linkage of the damper windings
$I^{(s_j)}$	Stator output current
$\omega^{(s_j)}$	Machine angular speed (rad/s)
$V^{(s_j)}$	Output voltage
$\delta^{(s_j)}$	Power angle of the microturbine (rad)
$V^{(l_j)}$	Load's Voltage
$\delta^{(l_j)}$	Voltage phase (rad)
$E_f^{(s_j)}$	Output voltage of the excitation system

Variable (p.u)	Physical equivalent
$\bar{U}_f^{(s_j)}$	Feedback of the voltage regulator
$U_f^{(s_j)}$	Input of the Exciter control
$T_m^{(s_j)}$	Mechanical torque output
$\omega_r^{(s_j)}$	Reference frequency
$P_u^{(s_j)}$	Valve position of the diesel engine

$$R_{load} = \begin{cases} 20 \ \Omega & \text{if } (t < 10) \\ 24 \ \Omega & \text{if } (t \geq 10) \end{cases}$$

4.4.4 REDUCED-ORDER MODEL

4.4.4.1 Introduction and problems faced

In this part, the reduced-order model equations of the microturbine will be implemented. The first step is to calculate the initial conditions for the model. In this case, the MATLAB code which will be used for the high-order model equations will be used. As with the other reduced-order models, this model was first implemented into Typhoon HIL. The same problems with the non-linearity of the algebraic loops appeared, this was, in fact, the most ‘problematic’ model, since it has algebraic loops which Typhoon HIL can’t handle and also it is connected to a constant power load which as will be mentioned in the high-order model it can’t neither be computed by Typhoon HIL. After discovering all these problems, Typhoon HIL was contacted and confirmed the problems. The model then will be implemented into Simulink.

For this reduced-order model, the equations of the high-order model were modified and simplified. The equations of the damper winding, stator winding, and short transmission line are retained from the high-order model equations. However, the excitation system equations and the governor and prime mover have been reduced and will be presented in the following page. The fact that some equations have not been modified suggests that this model will

contain most of the high-order model dynamics and transients. Below, equations 4.4.4.1.1 and 4.4.4.1.2 will represent the exciter and governor respectively.

$$\begin{aligned} \tau_{d'}^{(s_j)} \frac{dE_{q'}^{(s_j)}(t)}{dt} = & - \left(X_d^{(s_j)} - X_{d'}^{(s_j)} \right) \left(I_d^{(s_j)}(t) - \frac{X_{d'}^{(s_j)} - X_{d''}^{(s_j)}}{\left(X_{d'}^{(s_j)} - X_k^{(s_j)} \right)^2} \left(\Phi_{d_1}^{(s_j)}(t) \right. \right. \\ & \left. \left. + \left(X_{d'}^{(s_j)} - X_k^{(s_j)} \right) I_d^{(s_j)}(t) - E_{q'}^{(s_j)}(t) \right) \right) + V_{K_i}^{(s_j)} x_f^{(s_j)}(t) \\ & + \frac{V_{K_p}^{(s_j)} K_u^{(s_j)}}{K_f^{(s_j)}} \left(\mathbf{V}_r^{(s_j)} - V^{(s_j)}(t) \right) - E_{q'}^{(s_j)}(t), \end{aligned}$$

$$\frac{dx_f^{(s_j)}(t)}{dt} = \frac{K_u^{(s_j)}}{K_f^{(s_j)}} \left(\mathbf{V}_r^{(s_j)} - V^{(s_j)}(t) \right),$$

Figure 4.4.4.1.1 Reduced-Order Model 2 Excitation System Equations [2]

$$\begin{aligned} M^{(s_j)} \frac{d\omega^{(s_j)}(t)}{dt} &= T_m^{(s_j)}(t) - \Phi_d^{(s_j)}(t) I_q^{(s_j)}(t) + \Phi_q^{(s_j)}(t) I_d^{(s_j)}(t) - \tilde{D}_0^{(s_j)} \omega^{(s_j)}(t), \\ \tau_m^{(s_j)} \frac{dT_m^{(s_j)}(t)}{dt} &= -T_m^{(s_j)}(t) + P_u^{(s_j)}(t), \\ \frac{dP_u^{(s_j)}(t)}{dt} &= \frac{\kappa^{(s_j)}}{\bar{D}_0^{(s_j)} \omega_0} \left(P_c^{(s_j)}(t) - P_u^{(s_j)}(t) \right) - \kappa^{(s_j)} \left(\frac{\omega^{(s_j)}(t)}{\omega_0} - \omega_r^{(s_j)}(t) \right). \end{aligned}$$

Figure 4.4.4.1.2 Reduced-Order Model 2 Governor and Primer Mover Equations [2]

4.4.4.2 Results

In this section, the results obtained from implementing the model into Typhoon HIL will be presented. The results should be similar to the ones obtained with the high-order model since as mentioned before, most of the equations have not been modified. Only the equations for the prime mover + governor and the equations for the excitations system have been modified. The results that will be presented on the following page are: Frequency, Voltages, and Power. *Parameters can be found in table 4.4.5.2*

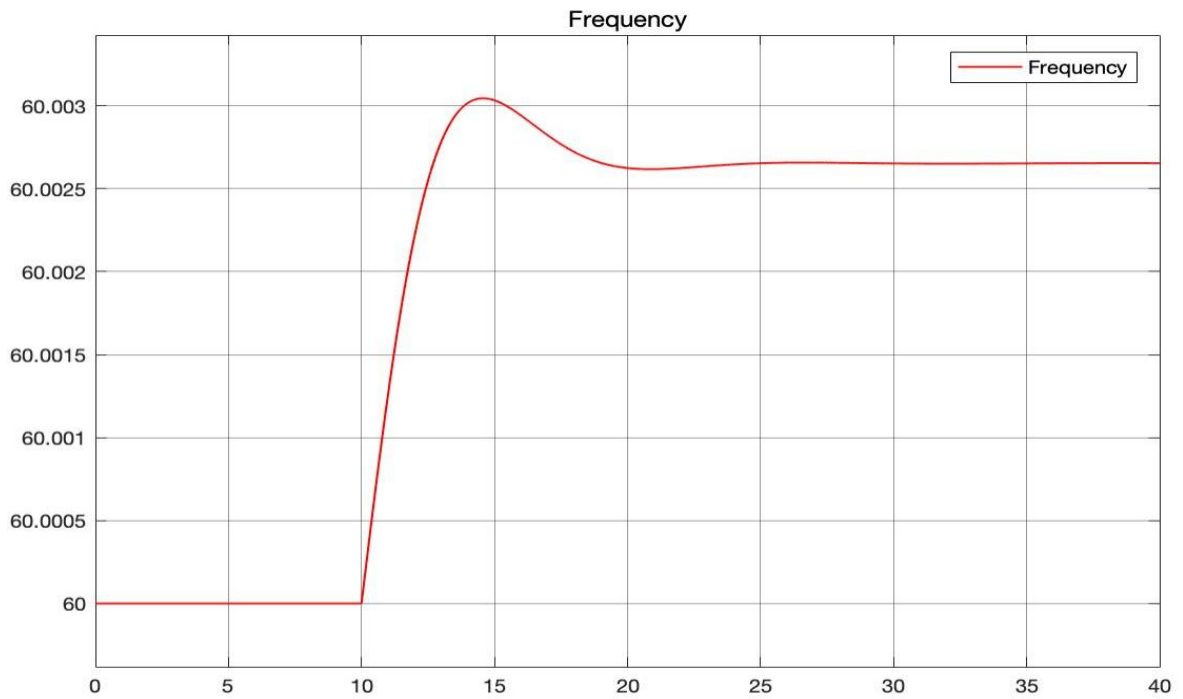


Figure 4.4.4.2.1 Frequency plot

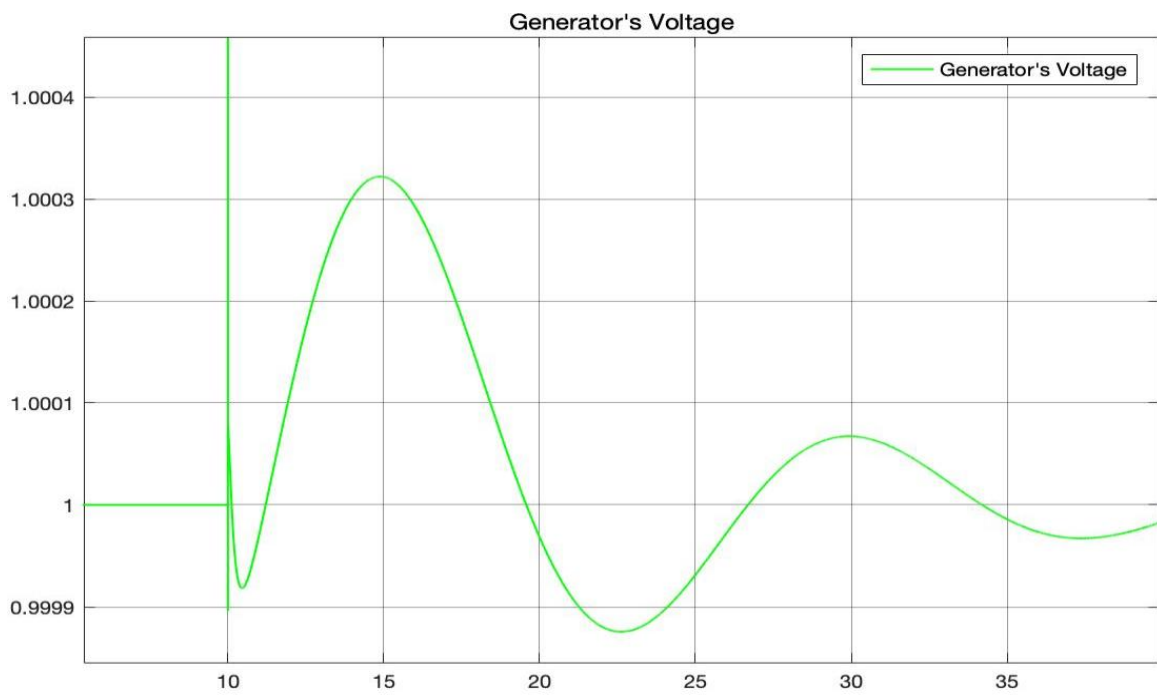


Figure 4.4.4.2.2 Generator's Voltage Plot

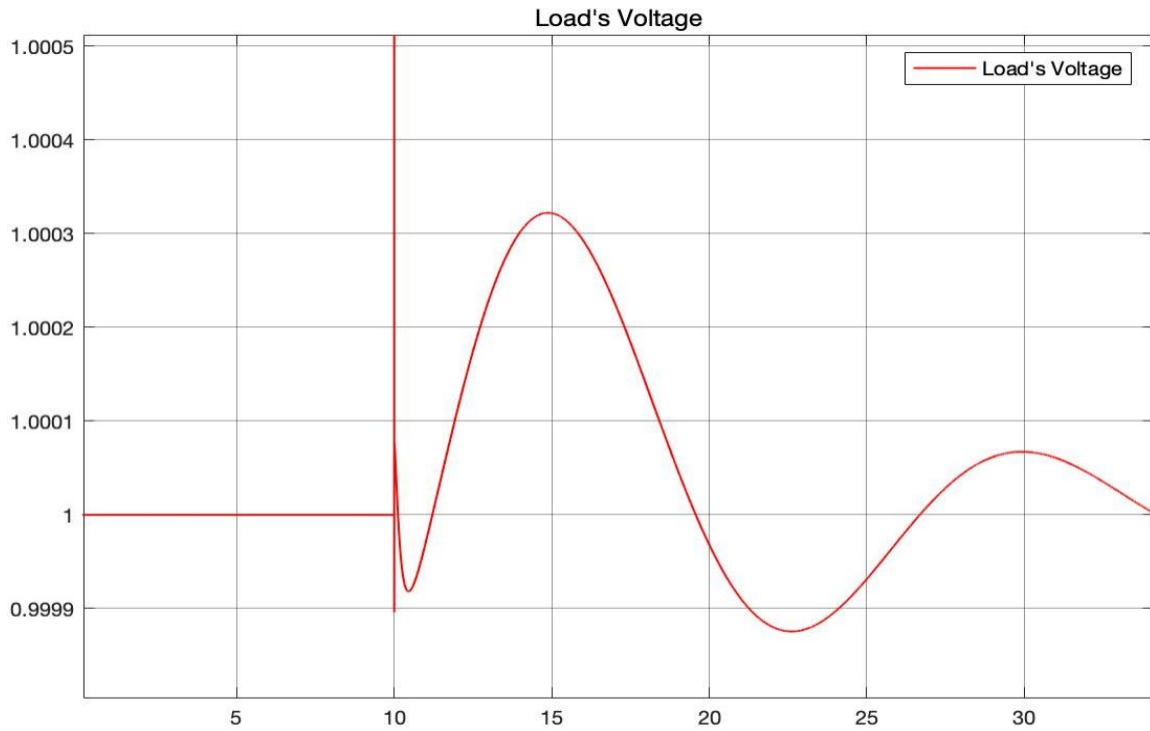


Figure 4.4.4.2.3 Load's Voltage Plot

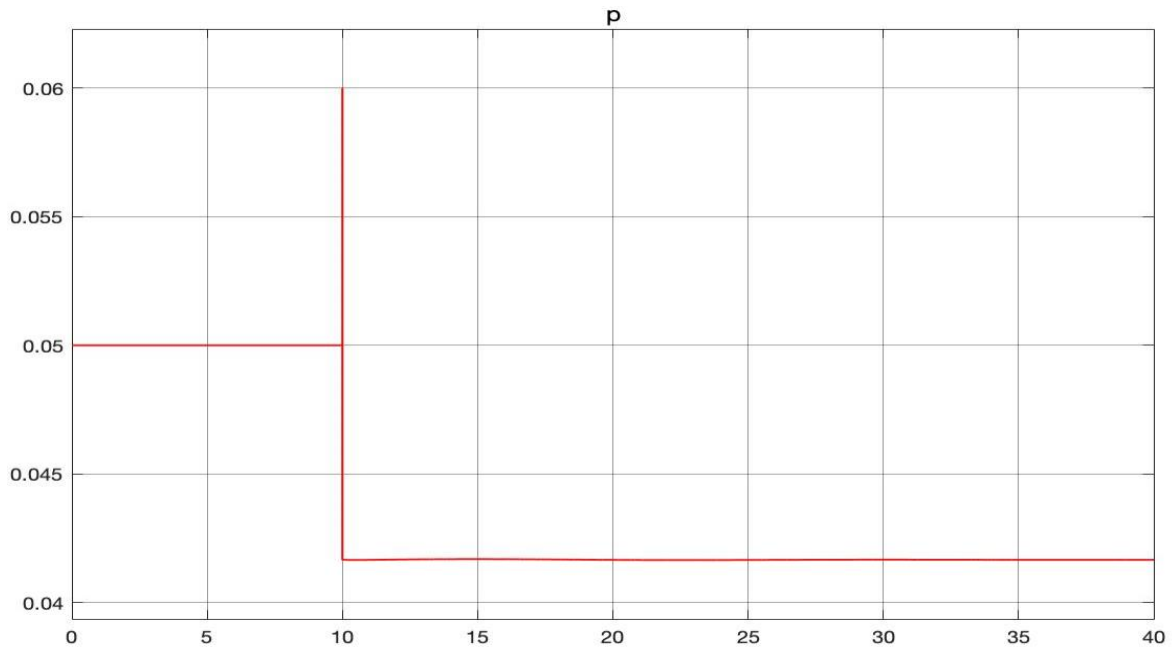


Figure 4.4.4.2.4 Power Consumed by The Load

4.4.4.3 Conclusions

The conclusions for this reduced-order model will be divided into sections as usual. These sections will help to point out the most important features per result. These subsections are the following: Frequency, Voltage, Power, and Overall performance.

Frequency: The frequency response looks exactly the same as the high-order model response that can be found in figure 4.4.5.3.1 This is because the reductions made in this model did not affect the performance of the governor. In this reduced-order model, the dynamics and transients are completely the same as the high-order model. Also, as it will be mentioned in the high-order model conclusions, the frequency does not return to 60 Hz after the perturbation. This is because the secondary control is not included in this model because it is being developed by the other members of the team. The goal of this testbed in fact, is to test the performance of these controls.

Voltage: For the voltage, the output does not look similar to the high-order model results. In fact, it is interesting because the reduced-order models have some oscillations that the high-order model does not. This suggests that the simplifications done have affected the performance of the voltage. However, the voltage converges back quickly to the expected value, so the results are acceptable.

Power: The power consumed by the load looks really similar to the power consumed by the high-order model system's load, the only difference is that on this reduced-order model it appears an instantaneous peak when the power changes, however, the time at which it occurs is small enough to say that the power output of this reduced-order model is the same that the high-order model

Overall Performance: The overall performance of this model is excellent. This reduced-order model is the one that can imitate best the high-order model output. In fact, the frequency response is exactly the same. Also, although the voltage is not exactly the same, the performance of the exciter is excellent. To conclude, this reduced-order model could be used perfectly to substitute the high-order model.

4.4.5 HIGH-ORDER MODEL

4.4.5.1 *Introduction and Problems Faced*

The model implemented will be based on the equations from [2] presented in Appendix II.

Before starting to implement the model, the initial conditions needed to be found. A MATLAB code was created in order to solve these initial conditions. The initial values of all the variables were calculated and taken into Typhoon HIL.

When implementing this model, the same problems arise in relation to Typhoon HIL software. First of all, the model was implemented into Simulink. But when implementing this same model into Typhoon HIL the model did not compile. Something particularly interesting happened when implementing this model. After some debugging, the model compiles and it was stable. The problem was that when any variable slightly changed, the voltage instantaneously dropped to 0 causing the system to become unstable. After individually examining all the individual models implemented, it became obvious that there was a software problem since every small change was making the system unstable, also because before the perturbation, that occurred at $T=10$ the output was as expected, this means that the models must be working.

After this issue, the next step would be changing the time-step of the simulation to check if the stability problem was caused by the time-step. After some time, the problem was discovered. The problem that was causing this instability was that Typhoon HIL has a problem when working with constant power loads. The non-linearity makes it impossible for Typhoon HIL to handle it, in fact, to make sure that this was the problem, other types of loads were tried. Finally, it was found that the error was indeed the non-linearity of the load. Also, the pre-loaded model that Typhoon HIL provides for the constant power load, is a linear model that considers the current to be constant and just changes the voltage. Typhoon HIL's Development team were contacted to inform them of this problem. Finally, the model worked with a constant impedance load. The final step was to play with the parameters of the model to make the model work optimally. After some changes in the Governor's Droop coefficient. and the exciter's PI the optimal parameters were found

4.4.5.2 Parameters and Inputs

Parameter (p.u)	Physical equivalent
S_{base}	835 GVA
V_{base}	15.011 KV
$X^{(S_j)}$	1.7997 p.u
$X_{k2}^{(S_j)}$	0.0939 p.u
$X_{k1}^{(S_j)}$	0.0812 p.u
$X_{kf}^{(S_j)}$	0.0812 p.u
$X_m^{(S_j)}$	1.0907 p.u
$R_2^{(S_j)}$	0.0084 p. u
$R_1^{(S_j)}$	0.0018 p. u
$R^{(S_j)}$	0 p.u
$X^{(S_j)}$	0 p.u
ω_0	377 (rad/s)
$V_r^{(S_j)}$	1 p.u
$V_{Kp}^{(S_j)}$	1.5
$V_{Ki}^{(S_j)}$	1
$\bar{R}_f^{(S_j)}$	0 p.u
$\kappa^{(S_j)}$	10
$M^{(S_j)}$	188.4956 p.u
$\bar{D}_0^{(S_j)}$	$9.7358 * 10^{-5}$ p.u
$R_D^{(S_j)}$	0.05 p.u

4.4.5.3 Results

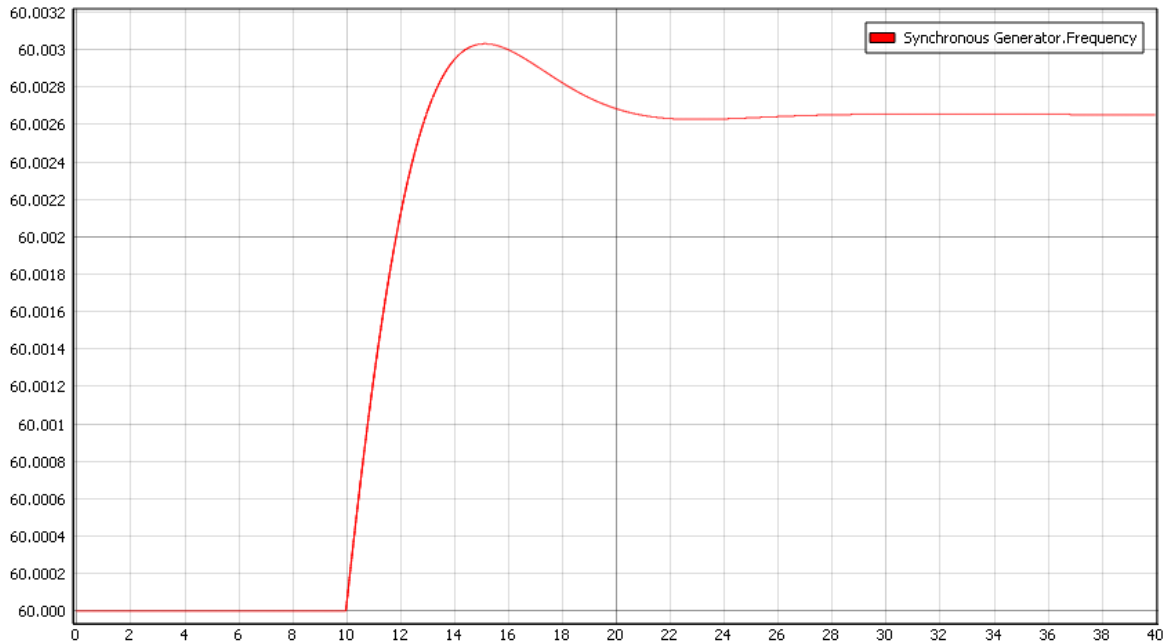


Figure 4.4.5.3.1 Synchronous generator's Frequency

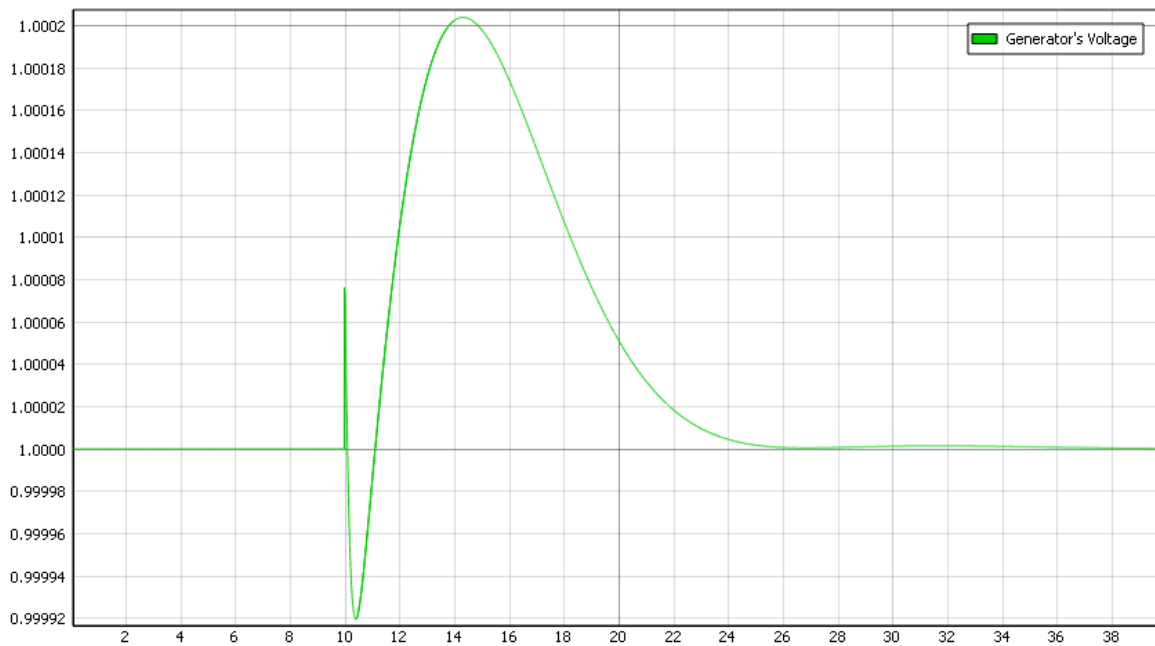


Figure 4.4.5.3.2 Synchronous generator's Voltage

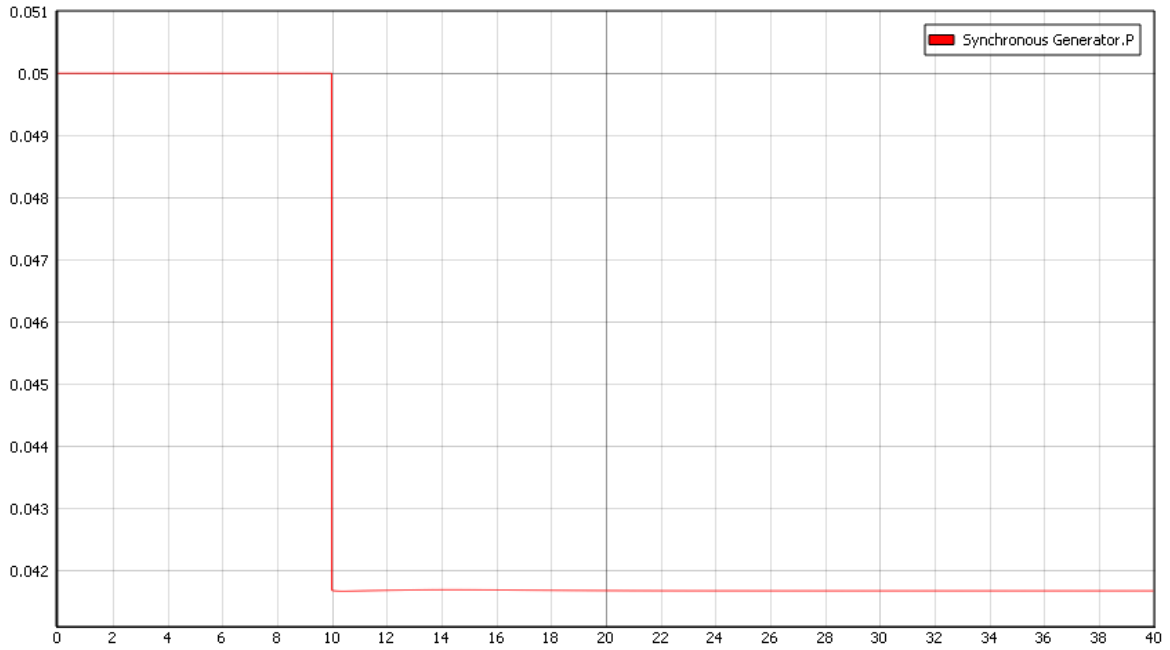


Figure 4.4.5.3.3 Synchronous generator's Active Power

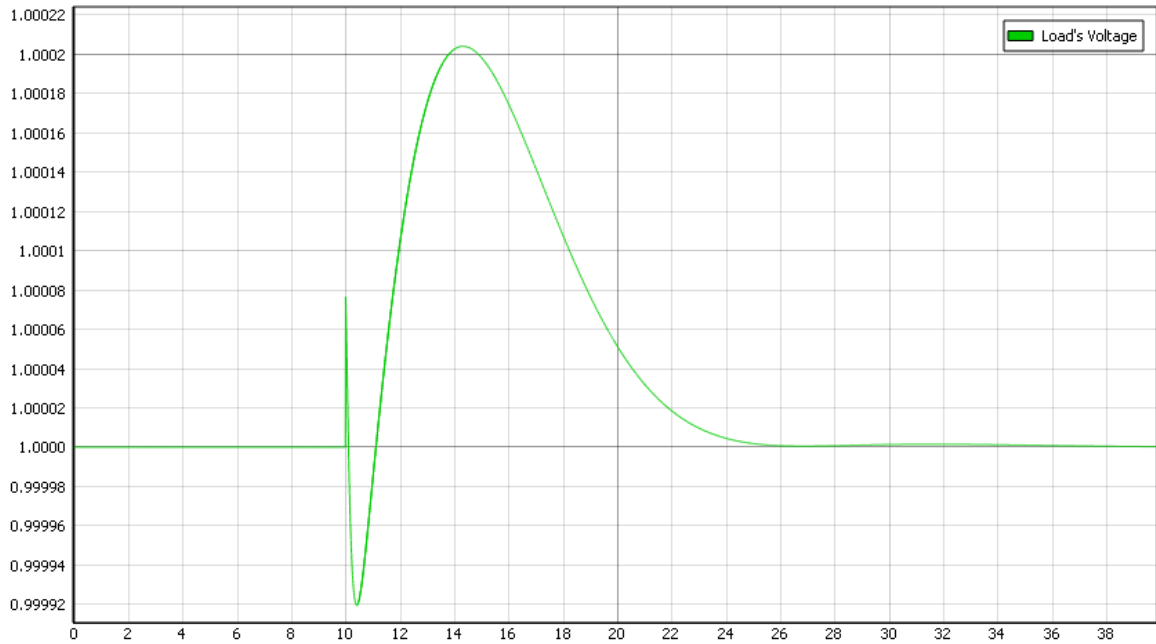


Figure 4.4.5.3.4 Load's Voltage

4.4.5.4 Conclusions

First of all, it is important to mention that some parameters have “Strange values” but this is because of the Bases chosen. These bases were chosen because they were the ones used in [2].

The most important parameters, results, and equations were presented above, however, there is some extra information like the equations implemented that can be found in appendix II.

This conclusion could be divided into 3 main aspects of the Microturbine model: Voltage, Frequency, and Power Generated. Also, the overall performance will be examined.

Voltage: The changes in the voltage are small and relatively quickly return to 1 p.u. The maximum deviation from this value is just 0.0002 p.u. Since the line parameters were ignored, the voltage of the load and the Generator is the same. At first, the time until the voltage converged back to 1 p.u was too large (about 2 minutes.), but after some changes in the parameters, it only takes about 20 seconds, which is reasonably good for the model.

Frequency: The first important consideration is that the secondary control is not included in this model since it is part of the distributed control architecture being developed. This is the reason why the frequency does not return to 60 Hz after the perturbation. The governor quickly acts and corrects the frequency deviation. Due to the quick response of the generator’s Governor, the frequency only increased to 60.003 Hz. The Droop coefficient used was 0.05. The overall performance of the governor and the diesel engine is excellent

Power: The power was kept constant until $T=10$ where the power decreases from 0.05 p.u to about 0.041 p.u, which looks like a small change but remember the base used for this model. The power changes immediately.

Overall Performance: The overall performance of the model was excellent, with changes in the load, the frequency, and the voltage quickly returned to their expected values, and what is more important, the values of both frequency and voltage stayed at all times within the allowable limits, thus ensuring that no equipment will be harmed because of high voltages or non-nominal frequency.



UNIVERSIDAD PONTIFICIA COMILLAS
ESCUELA TÉCNICA SUPERIOR DE INGENIERÍA (ICAI)
GRADO EN INGENIERÍA EN TECNOLOGÍAS INDUSTRIALES

CHAPTER 5. CONCLUDING REMARKS & FURTHER STEPS

In chapter 5 the final conclusions will be presented but also the further steps in the project. In this thesis 3 high-order models were implemented; these three models constitute almost all the Banshee distribution network components.

5.1 CONCLUDING REMARKS

In this part, the final conclusions will be presented. In this thesis, three DERs were implemented into Typhoon HIL: Grid-feeding inverter, Grid-Forming inverter, and Microturbine. Two models were implemented of each element, a high-order model which represents the complete dynamical response of each element, and a reduced-order model where the model has been simplified.

First of all, the problems faced with Typhoon HIL should be mentioned, since they were the most complicated part of this project. These problems that Typhoon has, slowed down the project substantially. There appeared problems with all of the model implementations. The models were previously implemented into MATLAB, however, when implementing these same models into Typhoon HIL, they were not working. In most cases, the model was not even compiling, this meaning that the system was not stable. Something interesting happened when implementing the high-order model equations of the microturbine. The model was stable with the initial conditions, but a small perturbation in any input would make the system unstable. In addition, there are some blocks and features available in MATLAB but not in Typhoon HIL. First of all, Simulink can incorporate MATLAB scripts to make calculations or even compute the initial conditions of the system. In Typhoon HIL, the initial conditions of the models were calculated in MATLAB and then transformed into the format that Typhoon HIL requires. Also, for the reduced-order models, MATLAB works with algebraic loops, but Typhoon does not. To deal with all these problems, the parameters

of the models were changed in order to make the system work. First of all, the filter parameters were chosen, after this, the constants and parameters of all the controls were modified to obtain the optimal solution. Typhoon HIL's developers were contacted on many occasions to inform them of some problems with the software. The final problem faced with Typhoon HIL is that the default CPU precision is set to single precision, while in MATLAB the default precision is set to double.

When comparing the high-order models with the reduced-order models, the difference can be easily spotted. The response and output of the high-order models show perfectly the dynamics of the models, the changes in variables are not produced instantaneously and the system has some inertia. The reduced-order models represent “Most” of the model dynamics, however, it is clear by seeing the output that some order reductions were performed. In these models, the output had constant slope responses in most cases and in other more reduced-order models, the output made instantaneous changes with ∞ slope.

As a final conclusion, it must be mentioned that even though Typhoon HIL has all the problems mentioned before, and has room for improvements, actually Typhoon HIL is the industry leader in hardware-in-the-loop simulations. Typhoon HIL is growing exponentially and will continue growing with the years since the hardware-in-the-loop simulations are the best way to test microgrids. Hopefully, the models implemented in this thesis will help the development of testbeds for microgrid development and therefore it will contribute to the microgrid construction. With this increase of microgrids, the technology and costs will get more competitive due to the economies of scale and the experience. With this cost reduction, microgrids could be used to take electricity to places where the grid is not available to get and especially to undeveloped countries. Also, the creation of community microgrids in developed countries helps reduce energy costs since the community microgrids are created to group DERs such as PV panels which produce cheaper energy. Both things mentioned before help directly to goal 7 of the SDGs that asks for affordable access to energy for anyone. In addition, the creation of new microgrids will reduce the amount of CO₂ produced since most of DERs are renewable energy.

5.2 FURTHER STEPS

In this thesis, the models of three elements were presented: Grid-feeding inverter, Grid-forming inverter, and Microturbine. Basically, these three elements are the only DERs that exist in the Banshee distribution network presented in [9]. The next step of the project would be implementing the Banshee distribution network. Load models need to be created.

After connecting together all the models in this thesis and forming the Banshee network and when the distributed control architecture is completely developed, this control will be tested and improved using the testbed. This control architecture will be a cheaper and more reliable alternative to conventional centralized control.

After all these steps are completed, the last step would be the development and implementation of new models. The three models implemented in this thesis were the ones required for the Banshee network, however, the goal is to create an adaptable microgrid testbed, to achieve this, more models should be implemented to make the testbed adaptable to new topologies and models. The final goal would be implementing a testbed as complete as possible that includes all the components that commonly are present in microgrids

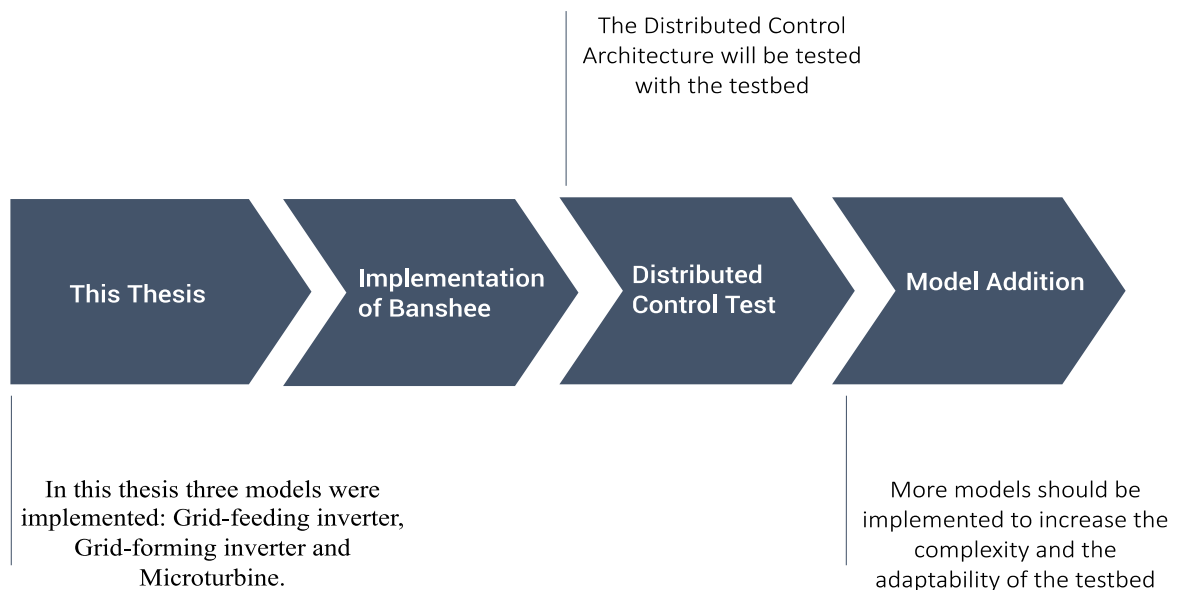


Figure 5.1 Further Steps



UNIVERSIDAD PONTIFICIA COMILLAS
ESCUELA TÉCNICA SUPERIOR DE INGENIERÍA (ICAI)
GRADO EN INGENIERÍA EN TECNOLOGÍAS INDUSTRIALES

APPENDIX I. INVERTER MODELS

This appendix contains more information and details on the implementation of the two inverter models. This appendix will be divided into two parts.

- 1. Grid-Feeding Inverter**
- 2. Grid-Forming Inverter**

Also, inside these two parts there will be some subparts.

1.1 Equations

In this subpart, the equations that were implemented will be presented. Some of the equations were already presented in the thesis, so in this subpart, only the equations that were too long to be included in the thesis will be presented: Grid-forming inverter HO model equations, grid-feeding inverter HO model equations. Also, it is important to remark that these equations were taken from Ajala Olaoluwapo's Dissertation thesis [2].

1.2 Codes

In this subpart, the codes used to obtain the initial conditions will be presented. Since most codes are long and if all of them were presented this appendix would be too long, only the code for the grid-feeding inverter reduced-order model will be presented. Other codes are similar to this one and have the same structure.

1.3 Model Schemes

This part should give an overview of how the equations look like when implemented into Typhoon HIL's Schematic Editor. The size of the pictures is too large to fit in the thesis properly, however the pictures were placed just to give an idea of the topology.

1.4 Results

The results presented in this appendix are the ones that could not be presented in the thesis, but that may be interesting for the reader.

1. GRID-FEEDING INVERTER

1.1 EQUATIONS

$$\begin{aligned} \frac{1}{\omega_c^{(s_j)}} \frac{d\mathbf{P}_f^{(s_j)}(t)}{dt} &= -\mathbf{P}_f^{(s_j)}(t) + E_{q[\omega_0 t]}^{(s_j)}(t) I_{q[\omega_0 t]}^{(s_j)}(t) + E_{d[\omega_0 t]}^{(s_j)}(t) I_{d[\omega_0 t]}^{(s_j)}(t), \\ \frac{1}{\omega_c^{(s_j)}} \frac{d\mathbf{Q}_f^{(s_j)}(t)}{dt} &= -\mathbf{Q}_f^{(s_j)}(t) + E_{q[\omega_0 t]}^{(s_j)}(t) I_{d[\omega_0 t]}^{(s_j)}(t) - E_{d[\omega_0 t]}^{(s_j)}(t) I_{q[\omega_0 t]}^{(s_j)}(t), \\ \frac{1}{\omega_0} \frac{d\delta^{(s_j)}(t)}{dt} &= -K_{P\lambda}^{(s_j)} E_{d[\alpha^{(j)}(t)]}^{(s_j)}(t) + K_{I\lambda}^{(s_j)} \Lambda_{[\alpha^{(j)}(t)]}^{(s_j)}(t) - 1, \\ \frac{L^{(s_j)}}{\omega_0} \frac{dI_{q[\omega_0 t]}^{(s_j)}(t)}{dt} &= -R^{(s_j)} I_{q[\omega_0 t]}^{(s_j)}(t) - L^{(s_j)} I_{d[\omega_0 t]}^{(s_j)}(t) + E_{q[\omega_0 t]}^{(s_j)}(t) - V_{q[\omega_0 t]}^{(l_j)}(t), \\ \frac{L^{(s_j)}}{\omega_0} \frac{dI_{d[\omega_0 t]}^{(s_j)}(t)}{dt} &= L^{(s_j)} I_{q[\omega_0 t]}^{(s_j)}(t) - R^{(s_j)} I_{d[\omega_0 t]}^{(s_j)}(t) + E_{d[\omega_0 t]}^{(s_j)}(t) - V_{d[\omega_0 t]}^{(l_j)}(t), \\ \frac{C^{(s_j)}}{\omega_0} \frac{d\hat{E}_{q[\omega_0 t]}^{(s_j)}(t)}{dt} &= -I_{q[\omega_0 t]}^{(s_j)}(t) - C^{(s_j)} \hat{E}_{d[\omega_0 t]}^{(s_j)}(t) + \Xi_{q[\alpha^{(j)}(t)]}^{(s_j)}(t) \cos(\delta^{(s_j)}(t)) \\ &\quad + \Xi_{d[\alpha^{(j)}(t)]}^{(s_j)}(t) \sin(\delta^{(s_j)}(t)), \\ \frac{C^{(s_j)}}{\omega_0} \frac{d\hat{E}_{d[\omega_0 t]}^{(s_j)}(t)}{dt} &= -I_{d[\omega_0 t]}^{(s_j)}(t) + C^{(s_j)} \hat{E}_{q[\omega_0 t]}^{(s_j)}(t) - \Xi_{q[\alpha^{(j)}(t)]}^{(s_j)}(t) \sin(\delta^{(s_j)}(t)) \\ &\quad + \Xi_{d[\alpha^{(j)}(t)]}^{(s_j)}(t) \cos(\delta^{(s_j)}(t)), \\ \frac{L_0^{(s_j)}}{\omega_0} \frac{d\Xi_{q[\alpha^{(j)}(t)]}^{(s_j)}(t)}{dt} &= \frac{V_{DC}^{(s_j)}(t) K_{I\gamma}^{(s_j)}}{2} \Gamma_{q[\alpha^{(j)}(t)]}^{(s_j)}(t) \\ &\quad - \left(R_0^{(s_j)} + \frac{V_{DC}^{(s_j)}(t) K_{P\gamma}^{(s_j)}}{2} \right) \Xi_{q[\alpha^{(j)}(t)]}^{(s_j)}(t) \\ &\quad + \frac{V_{DC}^{(s_j)}(t) K_{P\gamma}^{(s_j)} P_r^{(s_j)} E_{q[\alpha^{(j)}(t)]}^{(s_j)}(t) - Q_r^{(s_j)} E_{d[\alpha^{(j)}(t)]}^{(s_j)}(t)}{2 E_{q[\alpha^{(j)}(t)]}^{(s_j)}(t)^2 + E_{d[\alpha^{(j)}(t)]}^{(s_j)}(t)^2}, \\ \frac{L_0^{(s_j)}}{\omega_0} \frac{d\Xi_{d[\alpha^{(j)}(t)]}^{(s_j)}(t)}{dt} &= \frac{V_{DC}^{(s_j)}(t) K_{I\gamma}^{(s_j)}}{2} \Gamma_{d[\alpha^{(j)}(t)]}^{(s_j)}(t) \\ &\quad - \left(R_0^{(s_j)} + \frac{V_{DC}^{(s_j)}(t) K_{P\gamma}^{(s_j)}}{2} \right) \Xi_{d[\alpha^{(j)}(t)]}^{(s_j)}(t) \\ &\quad + \frac{V_{DC}^{(s_j)}(t) K_{P\gamma}^{(s_j)} P_r^{(s_j)} E_{d[\alpha^{(j)}(t)]}^{(s_j)}(t) + Q_r^{(s_j)} E_{q[\alpha^{(j)}(t)]}^{(s_j)}(t)}{2 E_{q[\alpha^{(j)}(t)]}^{(s_j)}(t)^2 + E_{d[\alpha^{(j)}(t)]}^{(s_j)}(t)^2}, \end{aligned}$$

$$\begin{aligned} \frac{1}{\omega_0} \frac{d\Gamma_{q[\alpha^{(j)}(t)]}^{(s_j)}}{dt}(t) &= \frac{P_r^{(s_j)} E_{q[\alpha^{(j)}(t)]}^{(s_j)}(t) - Q_r^{(s_j)} E_{d[\alpha^{(j)}(t)]}^{(s_j)}(t)}{E_{q[\alpha^{(j)}(t)]}^{(s_j)}(t)^2 + E_{d[\alpha^{(j)}(t)]}^{(s_j)}(t)^2} - \Xi_{q[\alpha^{(j)}(t)]}^{(s_j)}(t), \\ \frac{1}{\omega_0} \frac{d\Gamma_{d[\alpha^{(j)}(t)]}^{(s_j)}}{dt}(t) &= \frac{P_r^{(s_j)} E_{d[\alpha^{(j)}(t)]}^{(s_j)}(t) + Q_r^{(s_j)} E_{q[\alpha^{(j)}(t)]}^{(s_j)}(t)}{E_{q[\alpha^{(j)}(t)]}^{(s_j)}(t)^2 + E_{d[\alpha^{(j)}(t)]}^{(s_j)}(t)^2} - \Xi_{d[\alpha^{(j)}(t)]}^{(s_j)}(t), \\ \frac{1}{\omega_0} \frac{d\Lambda_{[\alpha^{(j)}(t)]}^{(s_j)}}{dt}(t) &= -E_{d[\alpha^{(j)}(t)]}^{(s_j)}(t), \\ E_{q[\alpha^{(j)}(t)]}^{(s_j)}(t) &= \left(-I_{q[\alpha^{(j)}(t)]}^{(s_j)}(t) + \Xi_{q[\alpha^{(j)}(t)]}^{(s_j)}(t) \right) \hat{R}_0^{(s_j)} \\ &\quad + \hat{E}_{q[\alpha^{(j)}(t)]}^{(s_j)}(t), \\ E_{d[\alpha^{(j)}(t)]}^{(s_j)}(t) &= \left(-I_{d[\alpha^{(j)}(t)]}^{(s_j)}(t) + \Xi_{d[\alpha^{(j)}(t)]}^{(s_j)}(t) \right) \hat{R}_0^{(s_j)} \\ &\quad + \hat{E}_{d[\alpha^{(j)}(t)]}^{(s_j)}(t), \\ \hat{\mathbf{E}}_{qd0[\alpha^{(j)}(t)]}(t) &= \mathbf{K}_2(\delta^{(s_j)}(t)) \hat{\mathbf{E}}_{qd0[\omega_0 t]}(t), \end{aligned}$$

Equation 1.1 Grid-Forming Inverter high-order model equations [2]

The equations presented above (from [2]) were implemented into Typhoon HIL to simulate the dynamics of a grid-feeding inverter. The parameters and variables definition can be found in the thesis.

1.2 CODES

As mentioned in the thesis, before implementing the models, the initial conditions needed to be calculated. In order to keep this appendix short, only the code for the grid-forming inverter will be presented, but the codes for other models have a similar structure.

The code that will be presented in the next page, is the code used to obtain the initial conditions of the grid-forming inverter reduced-order model. Since this is just a simple model and the inverter dynamics are not present in the model, the code just solves the newton Raphson algorithm between two nodes (i and j). The equations shown are the equations of node j since the inverter has its voltage and angle fixed, so there are not unknown variables.

```

clear all;
clc
%Bases definition
Sbase=10e3;%Watt
Vbase=227;%Volts

%Bases Calculations
Zbase=(Vbase^2)/Sbase;
Ibase=Sbase/Vbase;

%Epsilon
epsilon=1e-12;

%Variable Definition
syms V_1;
syms T_1;
syms V_2;
syms T_2;

%Parameter definition
Qr=(0)/Sbase; %reactive power reference in p.u
Pr=(20e3)/Sbase; %active power reference in p.u
Po=(10e3)/Sbase;
Qo=(0)/Sbase;
V2=227/Vbase;
T2=0;

ro_bar=15e-3;%Ohms
lo=3e-3;
cs=20e-6;%F
rs=1e-3;%Ohms
ls=2e-6;%H
re=8e-3;%Ohms
le=3e-6;%H
ro=0.1;%Ohms

%All Impedances are calculated in per unit
Ro_bar=ro_bar/Zbase;
Rs=rs/Zbase;
Re=re/Zbase;
Ls=(2*pi*60*ls)/Zbase;
Le=(2*pi*60*le)/Zbase;
Cs=Zbase/(1/(2*pi*60*cs));

%Parameter Calculations
G_bar=Ro_bar/((Ro_bar)^2+(1/Cs)^2);

B_bar=Cs/((Ro_bar*Cs)^2+1);

B=-((Le+Ls)/((Rs+Re)^2+(Le+Ls)^2);

G=(Rs+Re)/((Rs+Re)^2+(Le+Ls)^2);

%Mismatch Equations
P1(V_1,V_2,T_1,T_2)=-Pr+(G_bar+G)*((V_1)^2)-V_1*V_2*(G*cos(T_1-T_2)+B*sin(T_1-T_2));
Q1(V_1,V_2,T_1,T_2)=-Qr-(B_bar+B)*((V_1)^2)-V_1*V_2*(G*sin(T_1-T_2)-B*cos(T_1-T_2));

%PV nodes equations

```

```

P2(V_1,V_2,T_1,T_2)=-((V_2)^2*G-V_1*V_2*(G*cos(T_2-T_1)+B*sin(T_2-T_1)));
Q2(V_1,V_2,T_1,T_2)=-((V_2)^2*B-V_1*V_2*(G*sin(T_2-T_1)-B*cos(T_2-T_1)));

V=[P1,Q1];

%Jacobian
P=jacobian([P1,Q1],[T_1,V_1]);

% initialization
% initial condition
% [Theta,Voltage]
T=(transpose([0,1]));
    i=0;
    x=1;

%NEWTON RAPHSON ITERATIONS
while abs(max(x)) >= epsilon
    Q=T;

    J=double(P(T(2),V2,T(1),T2));
    i=i+1;

    %Makes sure the Jacobian is invertible
    if abs(det(J))<=1e-10
        disp("The Jacobian is not invertible")
        break
    end

    %Calculate The update
    C=(T)-(double(inv(J))*transpose(double([P1(T(2),V2,T(1),T2),Q1(T(2),V2,T(1),T2)])));
    T=C;
    x=Q-T;

    %If the Mismatch grows too much ends the program
    if max(x)>1e9
        disp("The Mismatch is to High, Program terminating");
        break
    end
end
P_injected=double((P2(T(2),V2,T(1),T2)*Sbase)/1000);
Q_injected=double((Q2(T(2),V2,T(1),T2)*Sbase)/1000);
Degrees=(T(1)*180)/pi;
Volts=T(2)*Vbase;

t=max(x);

disp("          RESULTS          ");
disp("The number of iterations was "+t);
disp("The mistmach was " + t);
disp("The Voltage 1 is "+ T(2)+" p.u and "+Volts+" Volts");
disp("The angle in node 1 is " + T(1)+" p.u and " +Degrees+ " Degree" );
disp("The Active Power injected to the grid is " +P_injected+"KW");
disp("The Reactive Power injected to the grid is " +Q_injected+"KVAR");

RESULTS
The number of iterations was 4
The mistmach was 0
The Voltage 1 is 1.0035 p.u and 227.7934 Volts
The angle in node 1 is 0.00066096 p.u and 0.03787 Degree
The Active Power injected to the grid is 19.9306KW
The Reactive Power injected to the grid is 0.3767KVAR

```

1.3 MODEL SCHEMES

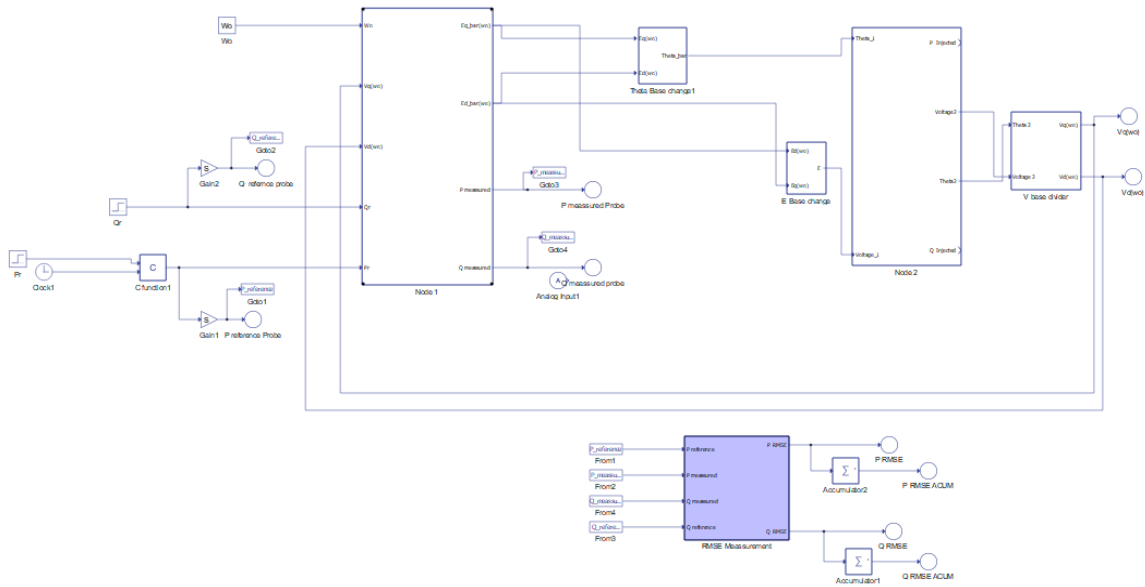


Figure 3.3.1 grid-feeding inverter HO model

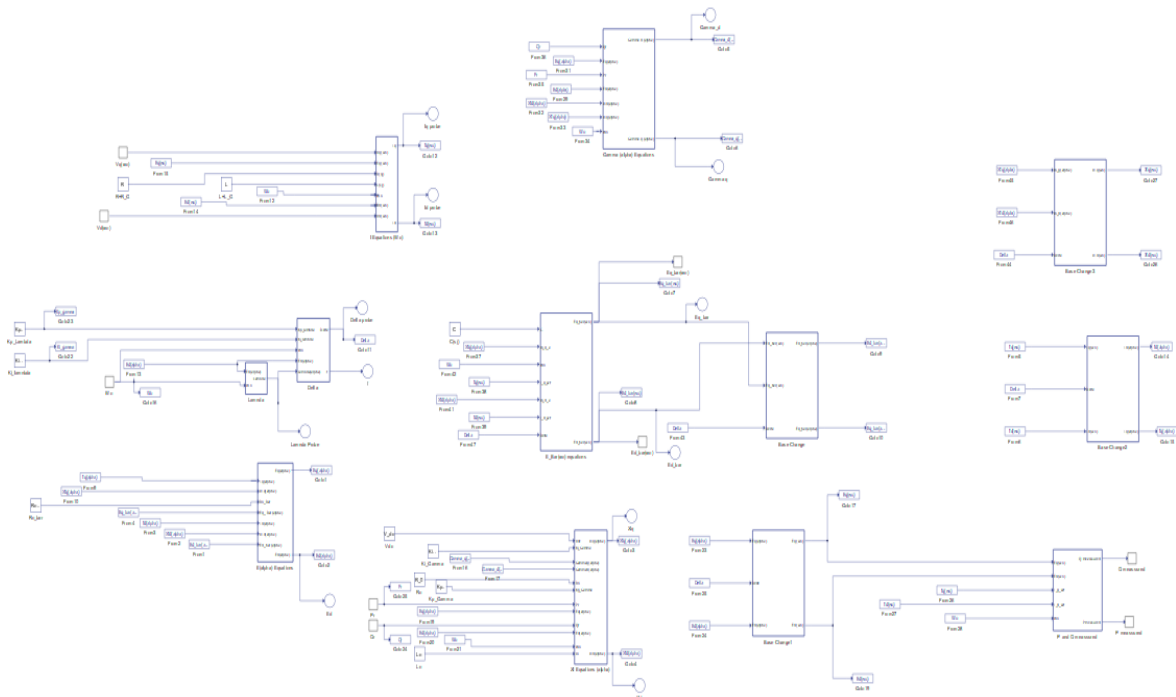


Figure 1.3.2 Node 1

1.4 RESULTS

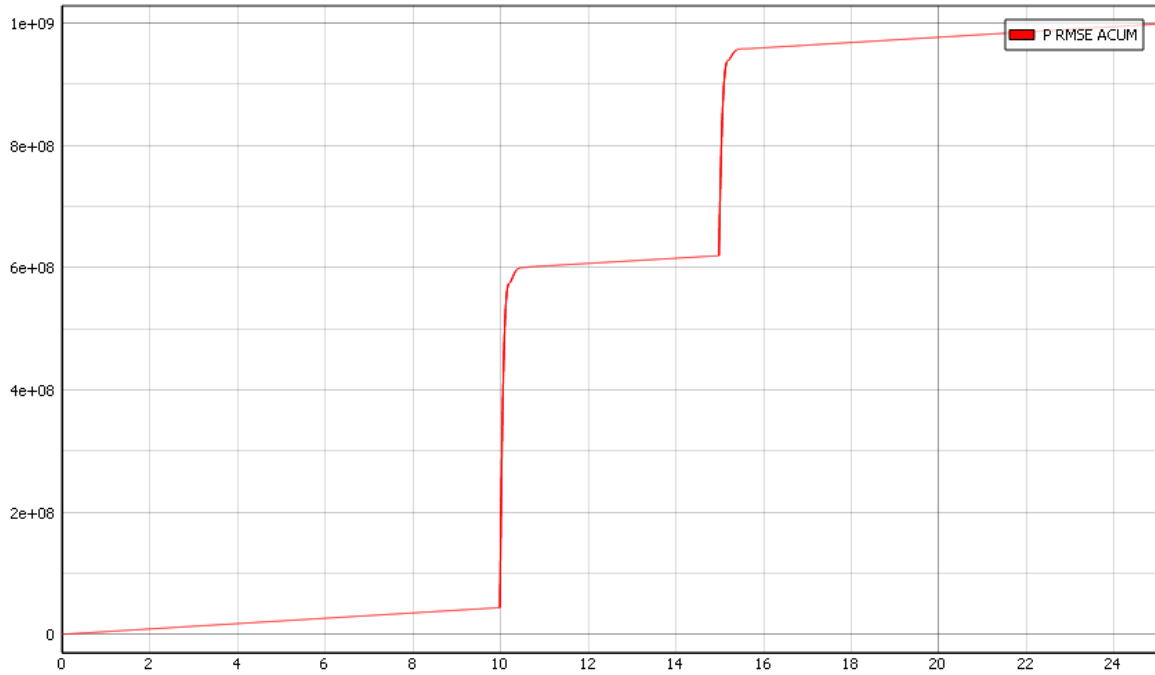


Figure 1.4.1 Accumulated Active Power RMSE

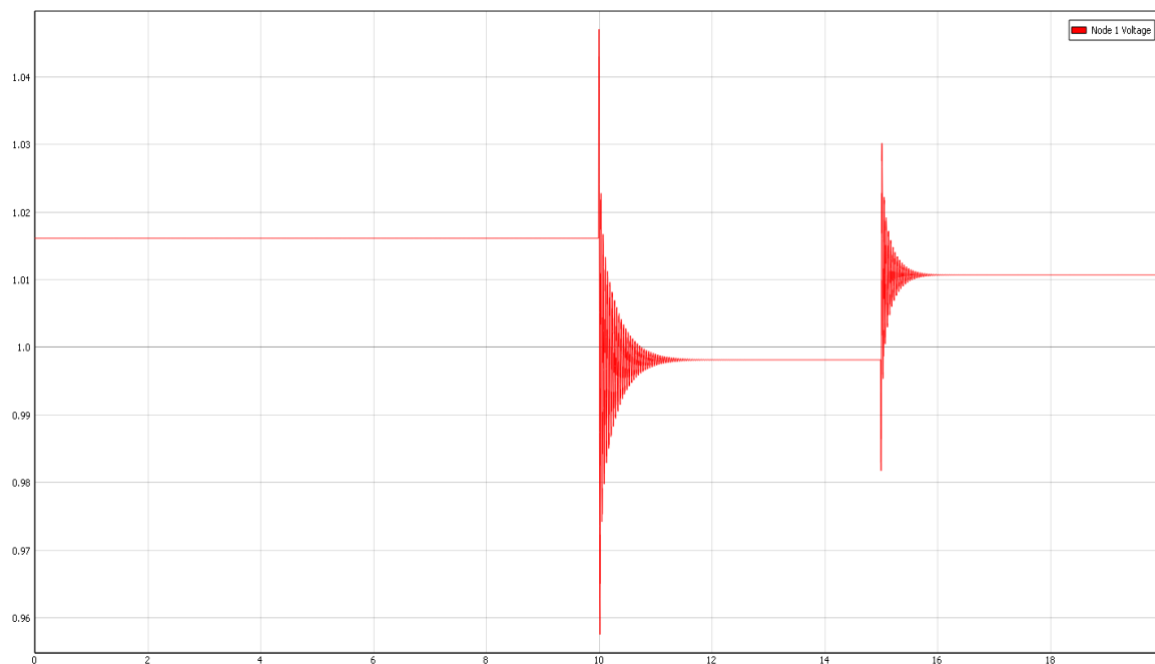


Figure 1.4.2 Node 1 Voltage Plot

2. GRID-FORMING INVERTER

2.1 EQUATIONS

$$\begin{aligned}
D_{\omega}^{(s_j)} \frac{d\delta^{(s_j)}(t)}{dt} &= P_r^{(s_j)} - P_f^{(s_j)}(t), \\
\frac{1}{\omega_c^{(s_j)}} \frac{dQ_f^{(s_j)}(t)}{dt} &= -Q_f^{(s_j)}(t) + E_{q[\omega_0 t]}^{(s_j)}(t) I_{d[\omega_0 t]}^{(s_j)}(t) - E_{d[\omega_0 t]}^{(s_j)}(t) I_{q[\omega_0 t]}^{(s_j)}(t), \\
\frac{1}{\omega_c^{(s_j)}} \frac{dP_f^{(s_j)}(t)}{dt} &= -P_f^{(s_j)}(t) + E_{q[\omega_0 t]}^{(s_j)}(t) I_{q[\omega_0 t]}^{(s_j)}(t) + E_{d[\omega_0 t]}^{(s_j)}(t) I_{d[\omega_0 t]}^{(s_j)}(t), \\
\frac{L^{(s_j)}}{\omega_0} \frac{dI_{q[\omega_0 t]}^{(s_j)}(t)}{dt} &= -R^{(s_j)} I_{q[\omega_0 t]}^{(s_j)}(t) - L^{(s_j)} I_{d[\omega_0 t]}^{(s_j)}(t) + E_{q[\omega_0 t]}^{(s_j)}(t) - V_{q[\omega_0 t]}^{(l_j)}(t), \\
\frac{L^{(s_j)}}{\omega_0} \frac{dI_{d[\omega_0 t]}^{(s_j)}(t)}{dt} &= L^{(s_j)} I_{q[\omega_0 t]}^{(s_j)}(t) - R^{(s_j)} I_{d[\omega_0 t]}^{(s_j)}(t) + E_{d[\omega_0 t]}^{(s_j)}(t) - V_{d[\omega_0 t]}^{(l_j)}(t), \\
\frac{1}{\omega_0} \frac{d\Phi_{q[\alpha^{(j)}(t)]}^{(s_j)}(t)}{dt} &= -\hat{E}_{q[\omega_0 t]}^{(s_j)}(t) \cos(\delta^{(s_j)}(t)) + \hat{E}_{d[\omega_0 t]}^{(s_j)}(t) \sin(\delta^{(s_j)}(t)) \\
&\quad + \hat{R}_0^{(s_j)} I_{q[\omega_0 t]}^{(s_j)}(t) \cos(\delta^{(s_j)}(t)) - \hat{R}_0^{(s_j)} I_{d[\omega_0 t]}^{(s_j)}(t) \sin(\delta^{(s_j)}(t)) \\
&\quad - \frac{1}{D_E^{(s_j)}} Q_f^{(s_j)}(t) + E_0^{(s_j)} + \frac{1}{D_E^{(s_j)}} Q_r^{(s_j)} - \hat{R}_0^{(s_j)} \Xi_{q[\alpha^{(j)}(t)]}^{(s_j)}(t), \\
\frac{1}{\omega_0} \frac{d\Phi_{d[\alpha^{(j)}(t)]}^{(s_j)}(t)}{dt} &= -\hat{E}_{q[\omega_0 t]}^{(s_j)}(t) \sin(\delta^{(s_j)}(t)) - \hat{E}_{d[\omega_0 t]}^{(s_j)}(t) \cos(\delta^{(s_j)}(t)) \\
&\quad + \hat{R}_0^{(s_j)} I_{q[\omega_0 t]}^{(s_j)}(t) \sin(\delta^{(s_j)}(t)) + \hat{R}_0^{(s_j)} I_{d[\omega_0 t]}^{(s_j)}(t) \cos(\delta^{(s_j)}(t)) \\
&\quad - \hat{R}_0^{(s_j)} \Xi_{d[\alpha^{(j)}(t)]}^{(s_j)}(t), \\
\frac{C^{(s_j)}}{\omega_0} \frac{d\hat{E}_{q[\omega_0 t]}^{(s_j)}(t)}{dt} &= -I_{q[\omega_0 t]}^{(s_j)}(t) - C^{(s_j)} \hat{E}_{d[\omega_0 t]}^{(s_j)}(t) + \Xi_{q[\alpha^{(j)}(t)]}^{(s_j)}(t) \cos(\delta^{(s_j)}(t)) \\
&\quad + \Xi_{d[\alpha^{(j)}(t)]}^{(s_j)}(t) \sin(\delta^{(s_j)}(t)), \\
\frac{C^{(s_j)}}{\omega_0} \frac{d\hat{E}_{d[\omega_0 t]}^{(s_j)}(t)}{dt} &= -I_{d[\omega_0 t]}^{(s_j)}(t) + C^{(s_j)} \hat{E}_{q[\omega_0 t]}^{(s_j)}(t) - \Xi_{q[\alpha^{(j)}(t)]}^{(s_j)}(t) \sin(\delta^{(s_j)}(t)) \\
&\quad + \Xi_{d[\alpha^{(j)}(t)]}^{(s_j)}(t) \cos(\delta^{(s_j)}(t)), \\
\frac{L_0^{(s_j)}}{\omega_0} \frac{d\Xi_{q[\alpha^{(j)}(t)]}^{(s_j)}(t)}{dt} &= K_{P\gamma}^{(s_j)} \left(1 + \frac{V_{DC}^{(s_j)}(t) K_{P\phi}^{(s_j)} \hat{R}_0^{(s_j)}}{2} \right) I_{q[\omega_0 t]}^{(s_j)}(t) \cos(\delta^{(s_j)}(t)) \\
&\quad - K_{P\gamma}^{(s_j)} \left(1 + \frac{V_{DC}^{(s_j)}(t) K_{P\phi}^{(s_j)} \hat{R}_0^{(s_j)}}{2} \right) I_{d[\omega_0 t]}^{(s_j)}(t) \sin(\delta^{(s_j)}(t)) \\
&\quad - \left(R_0^{(s_j)} + \frac{V_{DC}^{(s_j)}(t) K_{P\gamma}^{(s_j)}}{2} \left(1 + K_{P\phi}^{(s_j)} \hat{R}_0^{(s_j)} \right) \right) \Xi_{q[\alpha^{(j)}(t)]}^{(s_j)}(t)
\end{aligned}$$

$$\begin{aligned}
& - \frac{V_{DC}^{(s_j)}(t) K_{P\gamma}^{(s_j)} K_{P\phi}^{(s_j)}}{2} \hat{E}_{q[\omega_0 t]}^{(s_j)}(t) \cos(\delta^{(s_j)}(t)) \\
& + \frac{V_{DC}^{(s_j)}(t) K_{P\gamma}^{(s_j)} K_{P\phi}^{(s_j)}}{2} \hat{E}_{d[\omega_0 t]}^{(s_j)}(t) \sin(\delta^{(s_j)}(t)) \\
& + \frac{V_{DC}^{(s_j)}(t) K_{P\gamma}^{(s_j)} K_{I\phi}^{(s_j)}}{2} \Phi_{q[\alpha^{(j)}(t)]}^{(s_j)}(t) + \frac{V_{DC}^{(s_j)}(t) K_{P\gamma}^{(s_j)} K_{P\phi}^{(s_j)}}{2D_E^{(s_j)}} \mathbf{Q}_r^{(s_j)} \\
& - \frac{V_{DC}^{(s_j)}(t) K_{P\gamma}^{(s_j)} K_{P\phi}^{(s_j)}}{2D_E^{(s_j)}} \mathbf{Q}_f^{(s_j)}(t) + \frac{V_{DC}^{(s_j)}(t) K_{P\gamma}^{(s_j)} K_{P\phi}^{(s_j)}}{2} E_0^{(s_j)} \\
& + \frac{K_{P\gamma}^{(s_j)} C^{(s_j)}}{D_\omega^{(s_j)} \omega_0} \left(\mathbf{P}_r^{(s_j)} - \mathbf{P}_f^{(s_j)}(t) \right) \hat{E}_{q[\omega_0 t]}^{(s_j)}(t) \sin(\delta^{(s_j)}(t)) \\
& + K_{P\gamma}^{(s_j)} C^{(s_j)} \hat{E}_{d[\omega_0 t]}^{(s_j)}(t) \cos(\delta^{(s_j)}(t)) + \frac{V_{DC}^{(s_j)}(t) K_{I\gamma}^{(s_j)}}{2} \Gamma_{q[\alpha^{(j)}(t)]}^{(s_j)} \\
& + \frac{K_{P\gamma}^{(s_j)} C^{(s_j)}}{D_\omega^{(s_j)} \omega_0} \left(\mathbf{P}_r^{(s_j)} - \mathbf{P}_f^{(s_j)}(t) \right) \hat{E}_{d[\omega_0 t]}^{(s_j)}(t) \cos(\delta^{(s_j)}(t)) \\
& + K_{P\gamma}^{(s_j)} C^{(s_j)} \hat{E}_{q[\omega_0 t]}^{(s_j)}(t) \sin(\delta^{(s_j)}(t)), \\
\frac{L_0^{(s_j)}}{\omega_0} \frac{d\xi_{d[\alpha^{(j)}(t)]}^{(s_j)}}{dt}(t) & = K_{P\gamma}^{(s_j)} \left(1 + \frac{V_{DC}^{(s_j)}(t) K_{P\phi}^{(s_j)} \hat{R}_0^{(s_j)}}{2} \right) I_{q[\omega_0 t]}^{(s_j)}(t) \sin(\delta^{(s_j)}(t)) \\
& + K_{P\gamma}^{(s_j)} \left(1 + \frac{V_{DC}^{(s_j)}(t) K_{P\phi}^{(s_j)} \hat{R}_0^{(s_j)}}{2} \right) I_{d[\omega_0 t]}^{(s_j)}(t) \cos(\delta^{(s_j)}(t)) \\
& - \left(\hat{R}_0^{(s_j)} + \frac{V_{DC}^{(s_j)}(t) K_{P\gamma}^{(s_j)}}{2} \left(1 + K_{P\phi}^{(s_j)} \hat{R}_0^{(s_j)} \right) \right) \Xi_{d[\alpha^{(j)}(t)]}^{(s_j)}(t) \\
& - \frac{V_{DC}^{(s_j)}(t) K_{P\gamma}^{(s_j)} K_{P\phi}^{(s_j)}}{2} \hat{E}_{q[\omega_0 t]}^{(s_j)}(t) \sin(\delta^{(s_j)}(t)) \\
& - \frac{V_{DC}^{(s_j)}(t) K_{P\gamma}^{(s_j)} K_{P\phi}^{(s_j)}}{2} \hat{E}_{d[\omega_0 t]}^{(s_j)}(t) \cos(\delta^{(s_j)}(t)) \\
& - \frac{K_{P\gamma}^{(s_j)} C^{(s_j)}}{D_\omega^{(s_j)} \omega_0} \left(\mathbf{P}_r^{(s_j)} - \mathbf{P}_f^{(s_j)}(t) \right) \hat{E}_{q[\omega_0 t]}^{(s_j)}(t) \cos(\delta^{(s_j)}(t)) \\
& + \frac{K_{P\gamma}^{(s_j)} C^{(s_j)}}{D_\omega^{(s_j)} \omega_0} \left(\mathbf{P}_r^{(s_j)} - \mathbf{P}_f^{(s_j)}(t) \right) \hat{E}_{d[\omega_0 t]}^{(s_j)}(t) \sin(\delta^{(s_j)}(t)) \\
& - K_{P\gamma}^{(s_j)} C^{(s_j)} \hat{E}_{q[\omega_0 t]}^{(s_j)}(t) \cos(\delta^{(s_j)}(t)) + \frac{V_{DC}^{(s_j)}(t) K_{I\gamma}^{(s_j)}}{2} \Gamma_{d[\alpha^{(j)}(t)]}^{(s_j)} \\
& + K_{P\gamma}^{(s_j)} C^{(s_j)} \hat{E}_{d[\omega_0 t]}^{(s_j)}(t) \sin(\delta^{(s_j)}(t)) \\
& + \frac{V_{DC}^{(s_j)}(t) K_{P\gamma}^{(s_j)} K_{I\phi}^{(s_j)}}{2} \Phi_{d[\alpha^{(j)}(t)]}^{(s_j)}(t),
\end{aligned}$$

$$\begin{aligned}
\frac{1}{\omega_0} \frac{d\Gamma_{q[\alpha^{(j)}(t)]}^{(s_j)}(t)}{dt} &= \left(\frac{2}{V_{DC}^{(s_j)}(t)} + K_{P\phi}^{(s_j)} \hat{R}_0^{(s_j)} \right) I_{q[\omega_0 t]}^{(s_j)}(t) \cos(\delta^{(s_j)}(t)) \\
&- \left(\frac{2}{V_{DC}^{(s_j)}(t)} + K_{P\phi}^{(s_j)} \hat{R}_0^{(s_j)} \right) I_{d[\omega_0 t]}^{(s_j)}(t) \sin(\delta^{(s_j)}(t)) \\
&- K_{P\phi}^{(s_j)} (\hat{E}_{q[\omega_0 t]}^{(s_j)}(t) \cos(\delta^{(s_j)}(t)) - \hat{E}_{d[\omega_0 t]}^{(s_j)}(t) \sin(\delta^{(s_j)}(t))) \\
&- \left(1 + K_{P\phi}^{(s_j)} \hat{R}_0^{(s_j)} \right) \Xi_{q[\alpha^{(j)}(t)]}^{(s_j)}(t) + K_{I\phi}^{(s_j)} \Phi_{q[\alpha^{(j)}(t)]}^{(s_j)}(t) \\
&+ \frac{2C^{(s_j)}}{V_{DC}^{(s_j)}(t)} (\hat{E}_{q[\omega_0 t]}^{(s_j)}(t) \sin(\delta^{(s_j)}(t)) + \hat{E}_{d[\omega_0 t]}^{(s_j)}(t) \cos(\delta^{(s_j)}(t))) \\
&+ \frac{2C^{(s_j)}}{V_{DC}^{(s_j)}(t) D_\omega^{(s_j)} \omega_0} (\mathbf{P}_r^{(s_j)} - \mathbf{P}_f^{(s_j)}(t)) \hat{E}_{q[\omega_0 t]}^{(s_j)}(t) \sin(\delta^{(s_j)}(t)) \\
&+ \frac{2C^{(s_j)}}{V_{DC}^{(s_j)}(t) D_\omega^{(s_j)} \omega_0} (\mathbf{P}_r^{(s_j)} - \mathbf{P}_f^{(s_j)}(t)) \hat{E}_{d[\omega_0 t]}^{(s_j)}(t) \cos(\delta^{(s_j)}(t)) \\
&+ K_{P\phi}^{(s_j)} E_0^{(s_j)} + \frac{K_{P\phi}^{(s_j)}}{D_E^{(s_j)}} (\mathbf{Q}_r^{(s_j)} - \mathbf{Q}_f^{(s_j)}(t)), \\
\frac{1}{\omega_0} \frac{d\Gamma_{d[\alpha^{(j)}(t)]}^{(s_j)}(t)}{dt} &= \left(\frac{2}{V_{DC}^{(s_j)}(t)} + K_{P\phi}^{(s_j)} \hat{R}_0^{(s_j)} \right) I_{q[\omega_0 t]}^{(s_j)}(t) \sin(\delta^{(s_j)}(t)) \\
&+ \left(\frac{2}{V_{DC}^{(s_j)}(t)} + K_{P\phi}^{(s_j)} \hat{R}_0^{(s_j)} \right) I_{d[\omega_0 t]}^{(s_j)}(t) \cos(\delta^{(s_j)}(t)) \\
&- K_{P\phi}^{(s_j)} (\hat{E}_{q[\omega_0 t]}^{(s_j)}(t) \sin(\delta^{(s_j)}(t)) + \hat{E}_{d[\omega_0 t]}^{(s_j)}(t) \cos(\delta^{(s_j)}(t))) \\
&- \left(1 + K_{P\phi}^{(s_j)} \hat{R}_0^{(s_j)} \right) \Xi_{d[\alpha^{(j)}(t)]}^{(s_j)}(t) + K_{I\phi}^{(s_j)} \Phi_{d[\alpha^{(j)}(t)]}^{(s_j)}(t) \\
&- \frac{2C^{(s_j)}}{V_{DC}^{(s_j)}(t)} (\hat{E}_{q[\omega_0 t]}^{(s_j)}(t) \cos(\delta^{(s_j)}(t)) - \hat{E}_{d[\omega_0 t]}^{(s_j)}(t) \sin(\delta^{(s_j)}(t))) \\
&- \frac{2C^{(s_j)}}{V_{DC}^{(s_j)}(t) D_\omega^{(s_j)} \omega_0} (\mathbf{P}_r^{(s_j)} - \mathbf{P}_f^{(s_j)}(t)) \hat{E}_{q[\omega_0 t]}^{(s_j)}(t) \cos(\delta^{(s_j)}(t)) \\
&+ \frac{2C^{(s_j)}}{V_{DC}^{(s_j)}(t) D_\omega^{(s_j)} \omega_0} (\mathbf{P}_r^{(s_j)} - \mathbf{P}_f^{(s_j)}(t)) \hat{E}_{d[\omega_0 t]}^{(s_j)}(t) \sin(\delta^{(s_j)}(t)), \\
E_{q[\omega_0 t]}^{(s_j)}(t) &= -\hat{R}_0^{(s_j)} I_{q[\omega_0 t]}^{(s_j)}(t) + \hat{R}_0^{(s_j)} \Xi_{q[\alpha^{(j)}(t)]}^{(s_j)}(t) \cos(\delta^{(s_j)}(t)) \\
&+ \hat{R}_0^{(s_j)} \Xi_{d[\alpha^{(j)}(t)]}^{(s_j)}(t) \sin(\delta^{(s_j)}(t)) + \hat{E}_{q[\omega_0 t]}^{(s_j)}(t), \\
E_{d[\omega_0 t]}^{(s_j)}(t) &= -\hat{R}_0^{(s_j)} I_{d[\omega_0 t]}^{(s_j)}(t) - \hat{R}_0^{(s_j)} \Xi_{q[\alpha^{(j)}(t)]}^{(s_j)}(t) \sin(\delta^{(s_j)}(t)) \\
&+ \hat{R}_0^{(s_j)} \Xi_{d[\alpha^{(j)}(t)]}^{(s_j)}(t) \cos(\delta^{(s_j)}(t)) + \hat{E}_{d[\omega_0 t]}^{(s_j)}(t).
\end{aligned}$$

Equations 2.1 Grid-Forming Inverter high-order model Inverter equations.[2]

2.2 CODES

As mentioned before the codes for the rest of the models will not be presented in order to keep this appendix short. But please refer to part 1.2 to see how the code structure is.

These codes were used to calculate the initial conditions of the models, also there are some codes that change the format of the results and outputs the results in the format that Typhoon HIL requires.

2.3 MODEL SCHEMES

The purpose of this section is to give an overview of what the implementation looks like in the Typhoon HIL's Schematic Editor. Also, to give an idea of how the models look like.

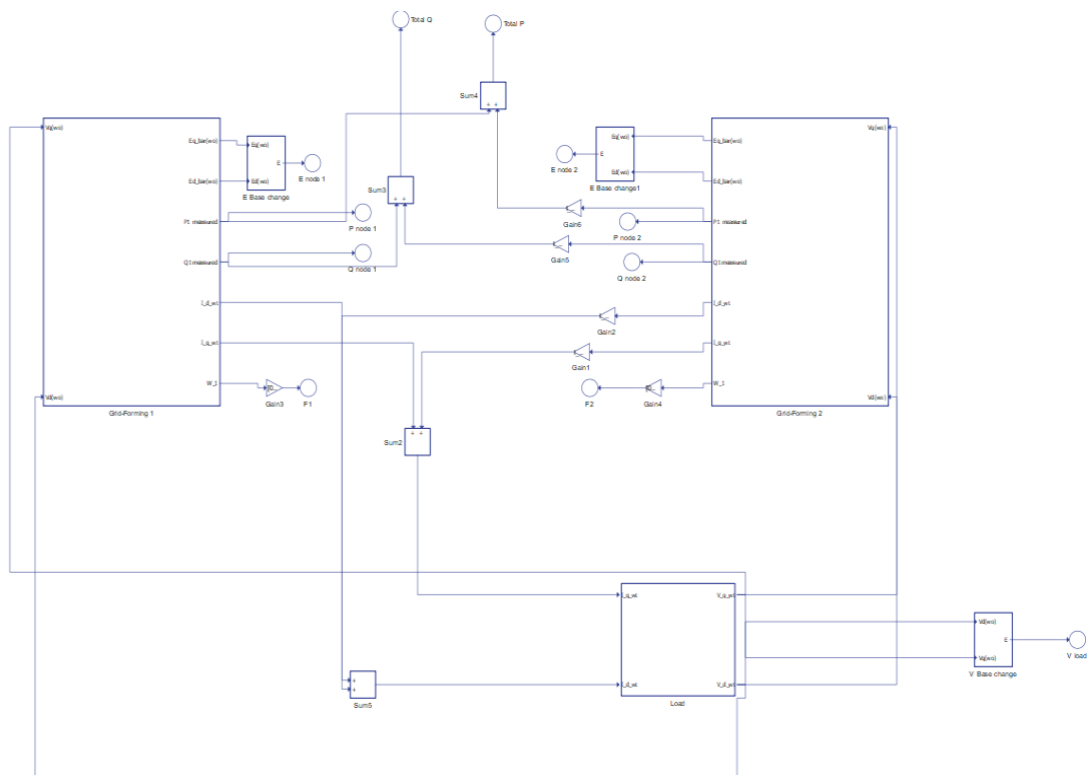


Figure 2.3.1 Microgrid Scheme

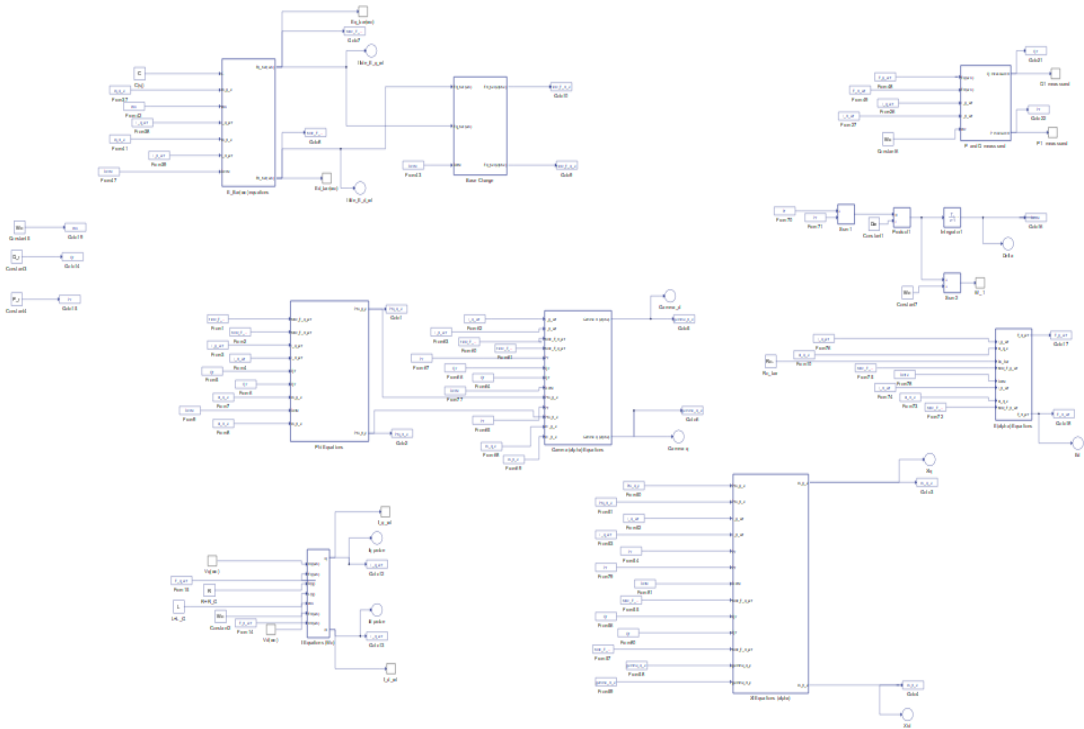


Figure 2.3.2. Inverter 1 Scheme.

2.4 RESULTS

On this part some extra results will be presented. In the thesis the only results that were shown were: The load's Voltage, the voltage of both inverters, the frequency of both inverters and finally the total P and Q consumed by the load.

On this appendix some extra results will be presented:

- Inverter 1's Voltage (p.u)
- Inverter 2's Voltage (p.u)
- Active power generated by each inverter (p.u)
- Reactive power generated by each inverter (p.u)

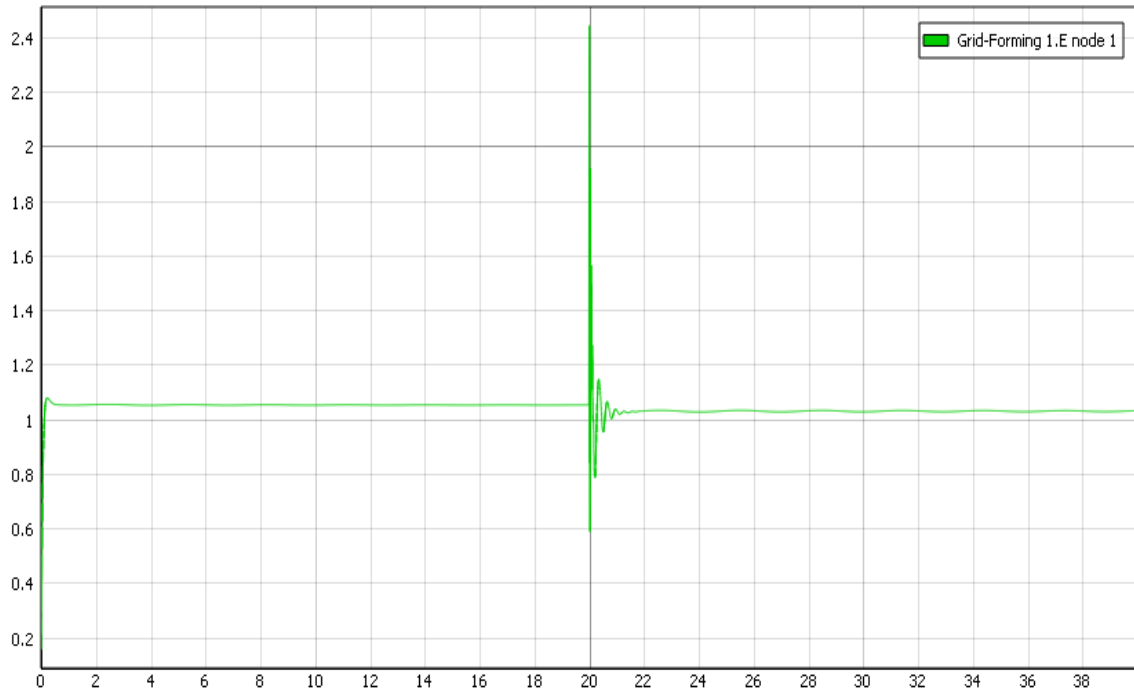


Figure 2.4.1 Inverter 1 Voltage

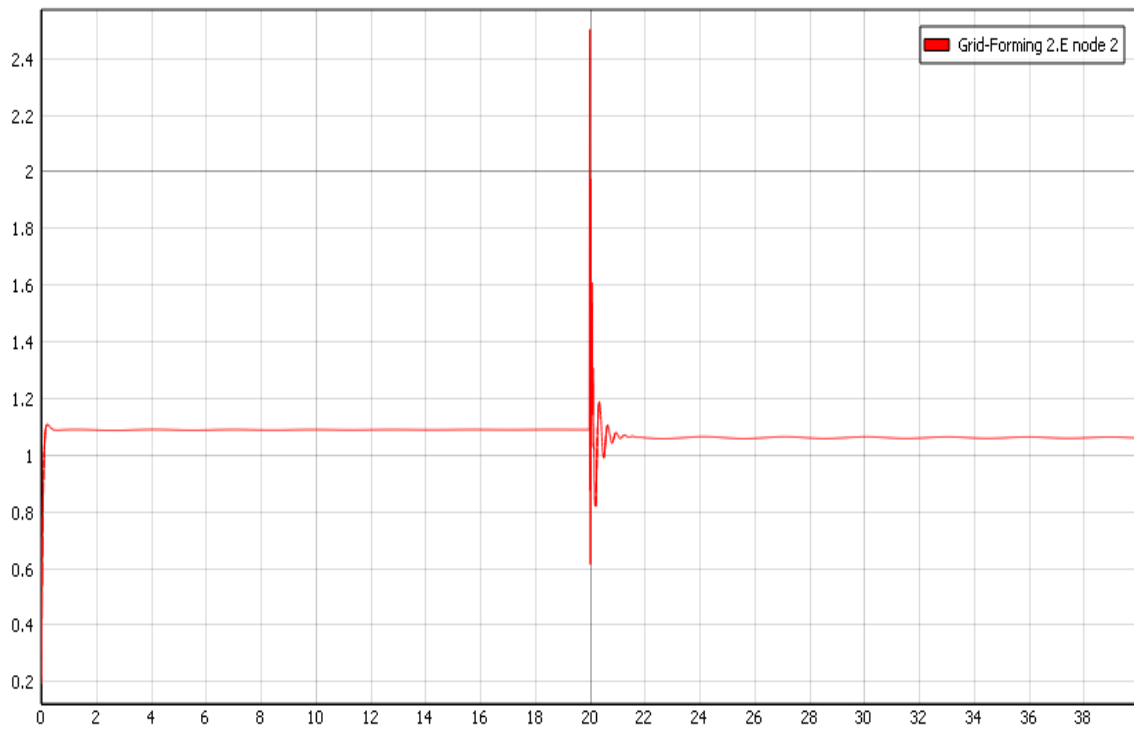


Figure 2.4.2 Inverter 2 Voltage

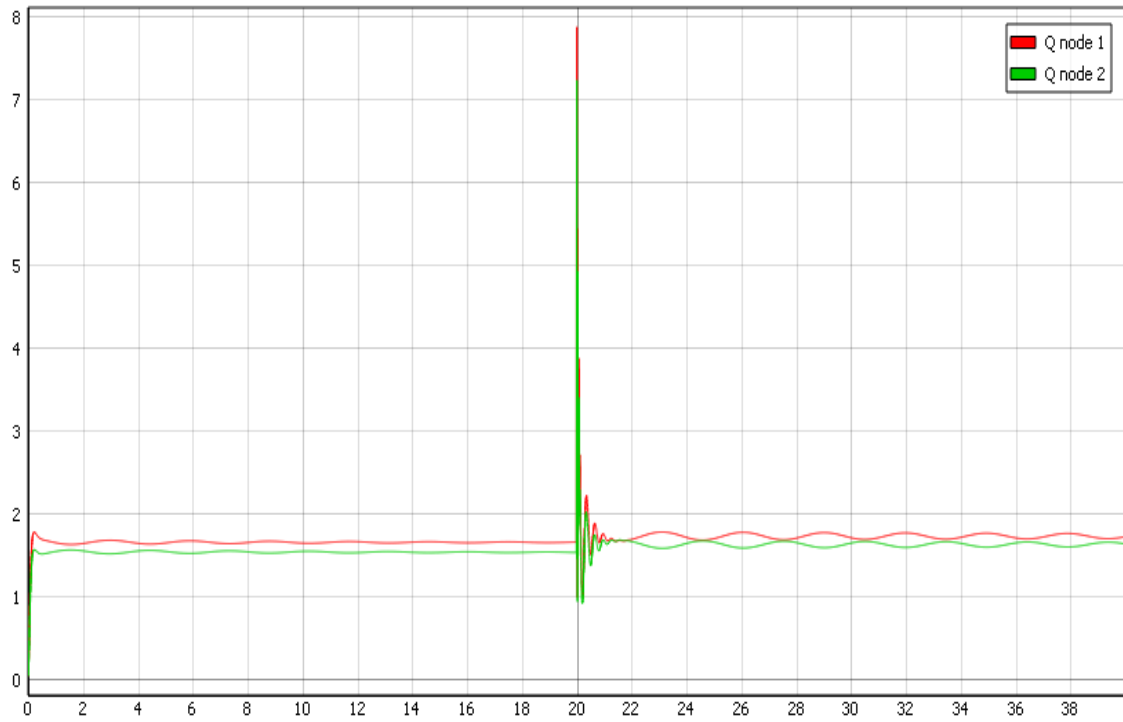


Figure 2.4.3 Active power generated by each inverter

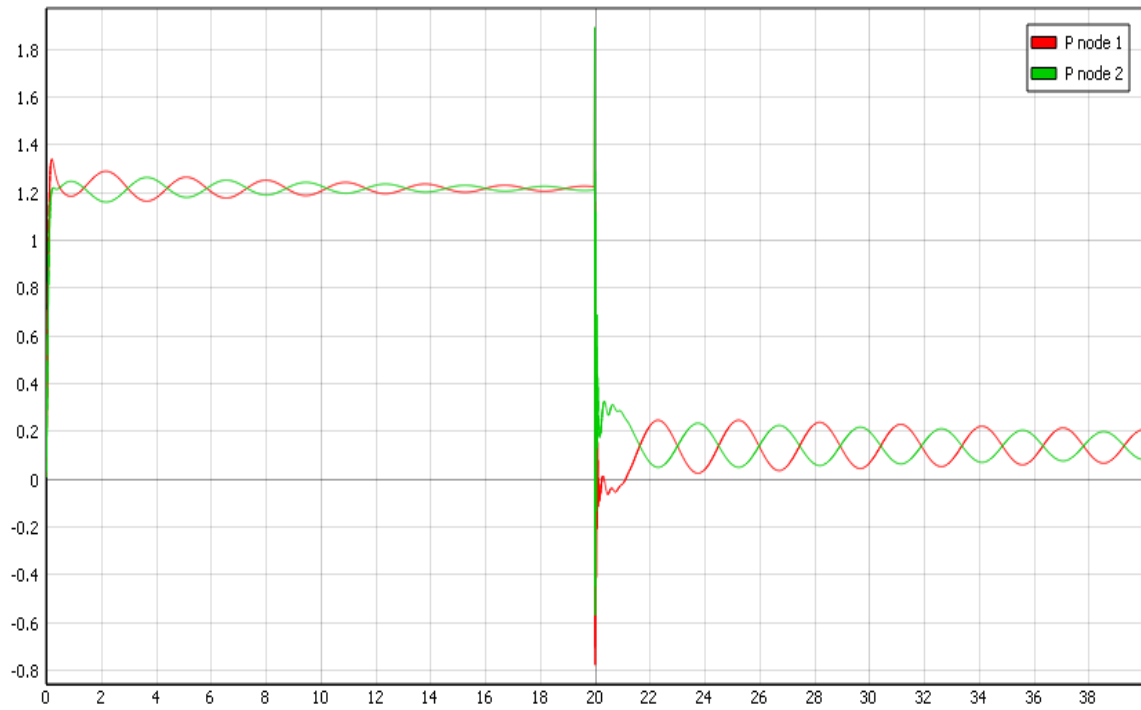


Figure 2.4.4 Reactive power generated by each inverter

APPENDIX II. MICROTURBINE MODEL

This appendix contains more information and details on the implementation of the microturbine model

This appendix will be divided into some parts subparts.

1.1 Equations

In this subpart, the equations that were implemented will be presented. Some of the equations were already presented in the thesis, so in this subpart, only the equations that were too long to be included in the thesis will be presented: Microturbine HO model equations. Also, it is important to remark that these equations were taken from Ajala Olaoluwapo's Dissertation thesis [2].

1.2 Model Schemes

This part should give an overview of how the equations look like when implemented into Typhoon HIL's Schematic Editor. The size of the pictures is too large to fit in the thesis properly, however, the pictures were placed just to give an idea of the topology.

In this appendix, neither the code nor the extra results will be shown. First of all, the code will not be shown since the code in appendix I for the grid feeding-inverter has the same format as this one, so to keep this appendix short please refer to appendix I for the code. Also, no results need to be shown in this appendix, since all the relevant results were shown in the thesis.

1.1 EQUATIONS

In this part, the equations from [2] will be presented. These equations will be presented by the different elements involved in the model. The model's equation will be the following: Damper winding Model, Stator and short transmission line, Excitation System, and finally the governor model. All of these individual models form the microturbine.

1.1.1 DAMPER WINDING MODEL

$$\begin{aligned}\tau_{q''}^{(s_j)} \frac{d\Phi_{q_2}^{(s_j)}(t)}{dt} &= -\Phi_{q_2}^{(s_j)}(t) - \left(X_{q'}^{(s_j)} - X_k^{(s_j)}\right) I_q^{(s_j)}(t) - E_{d'}^{(s_j)}(t), \\ \tau_{d''}^{(s_j)} \frac{d\Phi_{d_1}^{(s_j)}(t)}{dt} &= -\Phi_{d_1}^{(s_j)}(t) - \left(X_{d'}^{(s_j)} - X_k^{(s_j)}\right) I_d^{(s_j)}(t) + E_{q'}^{(s_j)}(t), \\ \tau_{q'}^{(s_j)} \frac{dE_{d'}^{(s_j)}(t)}{dt} &= \left(X_q^{(s_j)} - X_{q'}^{(s_j)}\right) \left(I_q^{(s_j)}(t) - \frac{X_{q'}^{(s_j)} - X_{q''}^{(s_j)}}{\left(X_{q'}^{(s_j)} - X_k^{(s_j)}\right)^2} \left(\Phi_{q_2}^{(s_j)}(t) \right. \right. \\ &\quad \left. \left. + \left(X_{q'}^{(s_j)} - X_k^{(s_j)}\right) I_q^{(s_j)}(t) - E_{d'}^{(s_j)}(t) \right) \right) - E_{d'}^{(s_j)}(t),\end{aligned}$$

Equations 1.1.1 Damper Winding model Equations [2]

1.1.2 STATOR WINDINGS AND SHORT TRANSMISSION LINE

$$\begin{aligned}V_q^{(l_j)}(t) &:= V^{(l_j)}(t) \cos \left(\delta^{(s_j)}(t) - \delta^{(l_j)}(t) \right), \\ V_d^{(l_j)}(t) &:= V^{(l_j)}(t) \sin \left(\delta^{(s_j)}(t) - \delta^{(l_j)}(t) \right).\end{aligned}$$

$$\begin{aligned}\frac{d\delta^{(s_j)}(t)}{dt} &= \omega^{(s_j)}(t) - \omega_0, \\ \frac{1}{\omega_0} \frac{d\Phi_q^{(s_j)}(t)}{dt} &= -\frac{\omega^{(s_j)}(t)}{\omega_0} \Phi_d^{(s_j)}(t) + V_q^{(l_j)}(t) + \left(R_s^{(s_j)} + R^{(s_j)}\right) I_q^{(s_j)}(t), \\ \frac{1}{\omega_0} \frac{d\Phi_d^{(s_j)}(t)}{dt} &= \frac{\omega^{(s_j)}(t)}{\omega_0} \Phi_q^{(s_j)}(t) + V_d^{(l_j)}(t) + \left(R_s^{(s_j)} + R^{(s_j)}\right) I_d^{(s_j)}(t), \\ -\frac{X^{(s_j)}}{\omega_0} \frac{dI_q^{(s_j)}(t)}{dt} &= R^{(s_j)} I_q^{(s_j)}(t) + \frac{X^{(s_j)}}{\omega_0} \omega^{(s_j)}(t) I_d^{(s_j)}(t) - V_q^{(s_j)}(t) + V_q^{(l_j)}(t),\end{aligned}$$

$$\begin{aligned}
-\frac{X^{(s_j)}}{\omega_0} \frac{dI_d^{(s_j)}(t)}{dt} &= R^{(s_j)} I_d^{(s_j)}(t) - \frac{X^{(s_j)}}{\omega_0} \omega^{(s_j)}(t) I_q^{(s_j)}(t) - V_d^{(s_j)}(t) + V_d^{(l_j)}(t), \\
\Phi_q^{(s_j)}(t) &= -X_{q''}^{(s_j)} I_q^{(s_j)}(t) + \frac{X_{q'}^{(s_j)} - X_{q''}^{(s_j)}}{X_{q'}^{(s_j)} - X_k^{(s_j)}} \Phi_{q_2}^{(s_j)}(t) - \frac{X_{q''}^{(s_j)} - X_k^{(s_j)}}{X_{q'}^{(s_j)} - X_k^{(s_j)}} E_{d'}^{(s_j)}(t), \\
\Phi_d^{(s_j)}(t) &= -X_{d''}^{(s_j)} I_d^{(s_j)}(t) + \frac{X_{d'}^{(s_j)} - X_{d''}^{(s_j)}}{X_{d'}^{(s_j)} - X_k^{(s_j)}} \Phi_{d_1}^{(s_j)}(t) + \frac{X_{d''}^{(s_j)} - X_k^{(s_j)}}{X_{d'}^{(s_j)} - X_k^{(s_j)}} E_{q'}^{(s_j)}(t),
\end{aligned}$$

Equations 1.1.2 Stator Windings and Short Transmission Line [2]

1.1.3 EXCITATION SYSTEM MODEL

$$V^{(s_j)} := \sqrt{\left(V_q^{(s_j)}\right)^2 + \left(V_d^{(s_j)}\right)^2}.$$

$$\begin{aligned}
\tau_{d'}^{(s_j)} \frac{dE_{q'}^{(s_j)}(t)}{dt} &= -\left(X_d^{(s_j)} - X_{d'}^{(s_j)}\right) \left(I_d^{(s_j)}(t) - \frac{X_{d'}^{(s_j)} - X_{d''}^{(s_j)}}{\left(X_{d'}^{(s_j)} - X_k^{(s_j)}\right)^2} \left(\Phi_{d_1}^{(s_j)}(t) \right. \right. \\
&\quad \left. \left. + \left(X_{d'}^{(s_j)} - X_k^{(s_j)} \right) I_d^{(s_j)}(t) - E_{q'}^{(s_j)}(t) \right) \right) + V_{Kp}^{(s_j)} E_f^{(s_j)}(t) \\
&\quad + V_{Ki}^{(s_j)} x_f^{(s_j)}(t) - E_{q'}^{(s_j)}(t), \\
\tau_f^{(s_j)} \frac{dE_f^{(s_j)}(t)}{dt} &= -K_f^{(s_j)} E_f^{(s_j)}(t) + U_f^{(s_j)}(t), \\
\frac{dx_f^{(s_j)}(t)}{dt} &= E_f^{(s_j)}(t), \\
\tau_u^{(s_j)} \frac{dU_f^{(s_j)}(t)}{dt} &= K_u^{(s_j)} \bar{U}_f^{(s_j)}(t) - \frac{K_u^{(s_j)} \bar{K}_u^{(s_j)}}{\bar{\tau}_u^{(s_j)}} E_f^{(s_j)}(t) + K_u^{(s_j)} \left(\mathbf{V}_r^{(s_j)} - V^{(s_j)}(t) \right) \\
&\quad - U_f^{(s_j)}(t), \\
\bar{\tau}_u^{(s_j)} \frac{d\bar{U}_f^{(s_j)}(t)}{dt} &= -\bar{U}_f^{(s_j)}(t) + \frac{\bar{K}_u^{(s_j)}}{\bar{\tau}_u^{(s_j)}} E_f^{(s_j)}(t),
\end{aligned}$$

Equations 1.1.3 Excitation System Model [2]

APPENDIX III. SUSTAINABLE DEVELOPMENT GOALS

The Sustainable Development Goals, also known as SDGs, are a group of 17 global goals adopted by all the United Nations members in 2015. These goals have as objectives to end poverty, to protect the planet, and to ensure peace and prosperity by 2030.

These 17 Goals can be divided into 3 dimensions: Biosphere, Society, and Economy. Also, within each goal, there are some specific quantifiable objectives to be reached by 2030.



Figure 1 Sustainable Development Goals

This thesis will have impact in many SDGs but the most important are:

- **Goal 1: No poverty:** Access to energy is a clear factor to determine the prosperity of a region. With the creation of this testbed, the creation of microgrid would be easier and cheaper, and with microgrids, energy could be supplied to places where the grid does not reach. This thesis has a secondary effect on this goal
- **Goal 7: Renewable Energy:** This is thesis has a direct impact on this goal since a microgrid is the only way of properly incorporating DERs into the grid. This Goal will be presented with more details in the following pages.

GOAL 7: AFFORDABLE AND CLEAN ENERGY



Goal 7 of the SDGs is affordable and clean energy, it can be also called “Ensure access to affordable, reliable, sustainable and modern energy for all”. This goal is part of the society dimension. It has some targets for 2030 which are directly taken from the United Nation’s website.

Some of the most relevant are:

- Ensure universal access to affordable, reliable and modern energy services.
- Increase substantially the share of renewable energy in the global energy mix
- double the global rate of improvement in energy efficiency
- Expand infrastructure and upgrade technology for supplying modern and sustainable energy services for all in developing countries, in particular least developed countries, small island developing States, and land-locked developing countries, in accordance with their respective programmes of support

This thesis, as mentioned before will have an impact on all of these objectives. First of all, as microgrids are the way of incorporating DERs into the main grid, by making the cost of microgrid development cheaper, more DERs will be used. Although not all DERs are renewable energy, most of the DERs are clean renewable energy. A microgrid is the way to properly incorporate: Small windmills, Small solar farms, electric vehicles and many others to the grid. All these energy resources mentioned before, are too small to provide regulation services or to be controlled by the grid. So, the creation of new microgrids could have a huge impact on the CO₂ emissions.

Also, even though it is not directly part of this thesis, it is still part of the project that our research group is doing at the University of Illinois. The testbed presented in this thesis plans to be used to test the distributed control architecture developed in the project. This control architecture is more reliable, cheap, and adaptable than the conventional centralized control architecture. Also, it is more adequate for the control of microgrids, since adding or removing DERs from the microgrids does not produce a problem in the control as control nodes can be easily added or removed without this affecting the performance of the control.

The second main relation of this thesis with the goal 7 is that microgrids not only help to incorporate DERs into the grid when working on grid-connected mode but also, microgrids when working on islanded mode can help with the following objectives:

- **Ensuring the continuity in the energy supply:** As microgrids can work either in islanded mode or in grid-connected, they can ensure that the power supply will not stop even if the grid goes out. This is mostly used in places where continuous energy supply is required such as hospitals, military bases...
- **Taking Electricity where the grid is not available to get:** There are some places especially in some parts of Africa where there is not an electrical network to connect to and simply it is cheaper to create an islanded microgrid than bringing the network to that place. Since the overall cost of microgrid development decreases, more microgrids will be developed, this making even cheaper and more reliable microgrids, since more money will be spent in research.

The way to quantify the effect of the creation of new microgrids, can be estimated by using the amount of DERs connected and making some assumptions. For example, not all the DERs are renewable energy resources, but using a correction factor of 0.6 would reflect a much more realistic renewable energy installed capacity. Also, assuming that all of this DERs are connected to the grid through a microgrid, we can estimate the amount of CO₂ that would be produced if this power was generated by carbon-based power plants

QUANTIFIABLE IMPACT

Using figure 1.1 from the thesis introduction, the amount of CO₂ emissions being reduced by the development of microgrids will be estimated. Figure 1.1 shows the exponential growth in DERs just in the USA (for this study just only USA will be taken into consideration) Assuming that 104GW of DERs are connected to the grid, and that from this 104GW 60% are clean zero emissions renewable resources. There are 62.4 GW of 0 emitting DERs. The average emissions of CO₂ by GWh is $4,5 * 10^5 \frac{\text{Kg}}{\text{GWh}}$. Also assuming a capacity factor defined as:

$$\text{Capacity Factor} = \frac{\text{Average Generation(GWh)}}{\text{Instaled Power(GW)} * 8760 \left(\frac{h}{\text{year}}\right)} = 0.5;$$

we have: $62.4(\text{GW}) * 0.5 * 8760 \left(\frac{h}{\text{year}}\right) = 273312\text{GWh}$ per year in US and multiplying by the CO₂ emissions per GWh: $273312 \text{ GWh} * 4,5 * 10^5 \frac{\text{Kg}}{\text{GWh}}$, $1,23 * 10^{11}\text{Kg}$ of CO₂ could be reduced per year.

REFERENCES

- [1] Alejandro D. Dominguez-Garcia. “*Controller Hardware-in-the-Loop Testbed for Distributed Coordination and Control Architectures* “. ECE University of Illinois at Urbana-Champaign.
- [2] Olaoluwapo Ajala “*A hierarchy of microgrid models with some applications*” University of Illinois at Urbana-Champaign, 2018 <http://hdl.handle.net/2142/102828>
- [3] Direct-quadrature-zero transformation Wikipedia https://en.wikipedia.org/wiki/Direct-quadrature-zero_transformation
- [4] About microgrids STRATEGICMICROGRID <https://strategicmicrogrid.com/about-microgrids/>
- [5] Alejandro D. Domínguez-Garcia “Distributed Architectures for Control and Coordination of Distributed Energy Resources in microgrids” Septiembre 2017
- [6] Laaksonen, Hannu. “Stability of microgrid with Different Configurations after Islanding Due to Fault in the Utility Grid.” *ResearchGate*, 2008,
www.researchgate.net/publication/270125448_Stability_of_microgrid_with_Different_Configurations_after_Islanding_Due_to_Fault_in_the_Utility_Grid
- [7] Muyeen, S M. “Design and Implementation of a Nonlinear PI Predictive Controller for a Grid-Tied Photovoltaic Inverter.” *ResearchGate*, 2016,
www.researchgate.net/figure/Control-scheme-of-the-cascaded-structure_fig8_307974105
- [8] Madhavan Jayaraju. “Effect of topography at the proximity of AC electric traction line on the earth fault distance locating algorithm.” *ResearchGate*, 2016,
https://www.researchgate.net/publication/298711125_Effect_of_topography_at_the_proximity_of_AC_electric_traction_line_on_the_earth_fault_distance_locating_algorithm
- [9] Reynaldo Salcedo, “Banshee distribution network benchmark and prototyping platform for hardware-in-the-loop integration of microgrid and device controllers ” IET Journals March 2019
- [10] Typhoon HIL Website <https://www.typhoon-HIL.com/devices/>
- [11] Arangarajan Vinayagam, “*PV Based microgrid with Grid-Support Grid-Forming Inverter Control-(Simulation and Analysis)*” Scientific Research Publishing, 2017.

- [12] Julieta Giraldez “*Phase I Microgrid cost study: Data Collection and analysis of microgrid Costs in the United States*”. NREL October 2018
<https://www.nrel.gov/docs/fy19osti/67821.pdf>
- [13] CarbonTrack Website. “*What is a microgrid? A Quick guide*”
<https://www.carbontrack.com.au/blog/community-microgrid/>
- [14] Ashish Devnani “*What are the different methods of starting synchronous motor?*”
<https://www.quora.com/What-are-the-different-methods-of-starting-synchronous-motor>
- [15] American National Standards institute “*IEEE Recommended Practice for Excitation System Models for Power System Stability Studies*” 2005
<https://www.igmc.ir/Portals/0/bazare%20bargh/darkhast%20sodor%20parvane%20tolid/IEEE%20Std%20421.5-2005.pdf?ver=-xPKmIvaRKGT1bmDMMohvw%3d%3d>
- [16] Neplan “*TURBINE-GOVERNOR MODELS Standard Dynamic Turbine-Governor Systems in NEPLAN Power System Analysis Tool*”
https://www.neplan.ch/wp-content/uploads/2015/08/Nep_TURBINES_GOV.pdf